comptes rendus
palevol
2022 • 21 • 29

Shell histology of the Triassic turtle, *Proterochersis porebensis* Szczygielski & Sulej, 2016, provides novel insights about shell ankylosis

Tomasz SZCZYGIELSKI & Justyna SŁOWIAK

art. 21 (29) — Published on 29 August 2022
www.cr-palevol.fr

PUBLICATIONS SCIENTIFIQUES

Comptes Rendus Palevol est indexé dans / Comptes Rendus Palevol *is indexed by:*
– Cambridge Scientific Abstracts
– Current Contents® Physical
– Chemical, and Earth Sciences®
– ISI Alerting Services®
– Geoabstracts, Geobase, Georef, Inspec, Pascal
– Science Citation Index®, Science Citation Index Expanded®
– Scopus®.

Les articles ainsi que les nouveautés nomenclaturales publiés dans *Comptes Rendus Palevol* sont référencés par / *Articles and nomenclatural novelties published in* Comptes Rendus Palevol *are registered on:*
– ZooBank® (http://zoobank.org)

Comptes Rendus Palevol est une revue en flux continu publiée par les Publications scientifiques du Muséum, Paris et l'Académie des sciences, Paris
Comptes Rendus Palevol *is a fast track journal published by the Museum Science Press, Paris and the Académie des sciences, Paris*

Les Publications scientifiques du Muséum publient aussi / *The Museum Science Press also publish:*
Adansonia, ***Geodiversitas***, ***Zoosystema***, ***Anthropozoologica***, ***European Journal of Taxonomy***, ***Naturae***, ***Cryptogamie*** **sous-sections** ***Algologie***, ***Bryologie***, ***Mycologie***.

L'Académie des sciences publie aussi / *The Académie des sciences also publishes:*
Comptes Rendus Mathématique, Comptes Rendus Physique, Comptes Rendus Mécanique, Comptes Rendus Chimie, Comptes Rendus Géoscience, Comptes Rendus Biologies.

Diffusion – Publications scientifiques Muséum national d'Histoire naturelle
CP 41 – 57 rue Cuvier F-75231 Paris cedex 05 (France)
Tél. : 33 (0)1 40 79 48 05 / Fax : 33 (0)1 40 79 38 40
diff.pub@mnhn.fr / https://sciencepress.mnhn.fr

Académie des sciences, Institut de France, 23 quai de Conti, 75006 Paris.

ISSN (imprimé / *print*) : 1631-0683/ ISSN (électronique / *electronic*) : 1777-571X

Shell histology of the Triassic turtle, *Proterochersis porebensis* Szczygielski & Sulej, 2016, provides novel insights about shell ankylosis

Tomasz SZCZYGIELSKI
Justyna SŁOWIAK
Institute of Paleobiology, Polish Academy of Sciences,
Twarda 51/55, 00-818 Warsaw (Poland)
t.szczygielski@twarda.pan.pl
justyna.slowiak@twarda.pan.pl (corresponding author)

Submitted on 10 March 2021 | Accepted on 10 May 2021 | Published on 29 August 2022

urn:lsid:zoobank.org:pub:771E34F3-2D20-4233-9864-5DBA0A51E021

Szczygielski T. & Słowiak J. 2022. — Shell histology of the Triassic turtle, *Proterochersis porebensis* Szczygielski & Sulej, 2016, provides novel insights about shell ankylosis. *Comptes Rendus Palevol* 21 (29): 619-679. https://doi.org/10.5852/cr-palevol2022v21a29

ABSTRACT
Shell suture obliteration (ankylosis) was exceptionally frequent in the earliest turtles, in contrast to post-Triassic taxa. Since modern turtles grow mostly along sutures, early ankylosis in Triassic taxa is intriguing. The Triassic turtle *Proterochersis porebensis* Szczygielski & Sulej, 2016 is known from numerous specimens, allowing observation of shell microstructure changes during ontogeny. Shell ankylosis occurred seemingly randomly in individuals of variable size, including small and morphologically juvenile, and completely obscured the initial bony composition. We propose that this phenomenon in the Triassic turtles can be an effect of early evolutionary stages of shell histogenesis and physiological mechanisms still used in shell regeneration in modern species. We also describe some parallels between the unusual peripheral microstructure of another Triassic turtle, *Waluchelys cavitesta* Sterli, Martínez, Cerda & Apaldetti, 2020, and *Proterochersis porebensis*. Microstructural changes imply that *Proterochersis porebensis* could change habitat during ontogeny, small individuals appearing more aquatic and larger more terrestrial.

KEY WORDS
Shell histology,
Triassic,
Norian,
turtles,
ankylosis,
shell growth,
sutures,
carapace,
plastron,
Testudinata.

RÉSUMÉ
L'histologie des carapaces de la tortue du Trias, Proterochersis porebensis *Szczygielski & Sulej, 2016, fournit de nouvelles informations sur l'ankylose de la carapace.*
L'oblitération des sutures de carapace (ankylose) était exceptionnellement fréquente chez les premières tortues, contrairement aux taxons post-triasiques. Étant donné que les tortues modernes croissent principalement le long des sutures, l'ankylose précoce chez les taxons du Trias est intrigante. La tortue du Trias *Proterochersis porebensis* Szczygielski & Sulej, 2016 est connue grâce à de nombreux spécimens, ce qui permet l'observation des changements de microstructure de la carapace au cours de l'ontogénie. L'ankylose de la carapace est apparue au hasard chez des individus de taille variable, y compris de petite taille et morphologiquement juvéniles, et a complètement obscurci la composition osseuse initiale. Nous proposons que ce phénomène chez les tortues du Trias peut être un effet des premiers stades évolutifs de l'histogenèse de la carapace et des mécanismes physiologiques encore utilisés dans la régénération de la carapace chez les espèces modernes. Nous décrivons également quelques parallèles entre la microstructure périphérique inhabituelle d'une autre tortue du Trias, *Waluchelys cavitesta* Sterli, Martínez, Cerda & Apaldetti, 2020, et *Proterochersis porebensis*. Les changements microstructuraux impliquent que *Proterochersis porebensis* pourrait changer d'habitat pendant l'ontogénie, les petits individus apparaissant plus aquatiques et les plus grands apparaissant plus terrestres.

MOTS CLÉS
Histologie de la carapace,
Triassique,
Norien,
tortues,
ankylose,
croissance de la carapace,
sutures,
carapace dorsale,
plastron,
Testudinata.

INTRODUCTION

The turtle shell, composed of the dorsal (carapace) and ventral (plastron) parts, is a complex, unique structure optimized for mechanical performance (Scheyer *et al.* 2007; Krauss *et al.* 2009; Zhang *et al.* 2012) and informative in terms of the habitat and phylogenetic relationships (Scheyer & Sander 2007). Although its development and relationships to the rest of the skeleton intrigued scientists for a very long time (Lachmund 1676; Cuvier 1798; Saint-Hilaire 1809; Oken 1823), truly comprehensive comparative histological work concerning the turtle shell began in the 21st century (Scheyer & Sánchez-Villagra 2007; Scheyer & Sander 2007; Scheyer *et al.* 2007, 2008; Witzmann 2009; Delfino *et al.* 2010; Lima *et al.* 2011; Lyson *et al.* 2013; Sterli *et al.* 2021). At the same time, the histology of the oldest known representatives of the turtle lineage gained attention (Scheyer & Sander 2007; Lyson *et al.* 2013; Schoch *et al.* 2019; Sterli *et al.* 2021).

Thus far, despite the long history of research (e.g. von Meyer 1863; Baur 1887; Fraas 1913; Rougier *et al.* 1995), shells of only three species of Late Triassic Testudinata (fully shelled turtles) were studied histologically: *Proterochersis robusta* Fraas, 1913 (Proterochersidae Nopcsa, 1923) and *Proganochelys quenstedti* Baur, 1887 (Proganochelyidae Baur, 1888) from the Norian of Germany (Scheyer & Sander 2007; Lyson *et al.* 2013), and *Waluchelys cavitesta* Sterli, Martinez, Cerda & Apaldetti, 2021 (Australochelyidae Gaffney & Kitching, 1994) from the Norian/Rhaetian of Argentina (Sterli *et al.* 2021). In addition, a single thin section of a costal of *Proterochersis porebensis* Szczygielski & Sulej, 2016 (Proterochersidae) from the Norian of Poland was figured and briefly discussed (Szczygielski & Sulej 2019). Finally, Lichtig & Lucas (2021) provided pictures of polished sections of costals of *Chinlechelys tenertesta* Joyce, Lucas, Scheyer, Heckert & Hunt, 2009 from the Norian of the United States, but did not perform a histological study. These taxa are remarkable not only due to their geological age and basal phylogenetic position, making them important for understanding of the earliest stages of the turtle shell evolution, but also because their shells exhibit unique morphologies unknown in post-Triassic taxa. Unlike other turtles, the peripherals of the australochelyids *Waluchelys cavitesta* and *Palaeochersis talampayensis* Rougier, Fuente & Arcucci, 1995 were found to accommodate internal cavities separated from the surrounding spongiosa by a thick layer of compact bone tissue (de la Fuente *et al.* 2020; Sterli *et al.* 2021). Morphologically different, but similarly positioned cavities (concavities/hollow peripherals) were previously figured in the posterior peripherals of *Proganochelys quenstedti* by Jaekel (1916) and described by Gaffney (1990), but not studied microstructurally, and could be present in *Chinlechelys tenertesta* as well (Szczygielski & Sulej 2019; see below). *Proterochersis* spp., on the other hand, present a mosaic-like pattern of numerous, irregular ossifications partially overlying the costals in the anterior and posterior part of the carapace, which at least in the anterior part of the carapace create a slot-like cavity for the first costal (Szczygielski & Sulej 2019). A mosaic-like shell structure was also discovered in *Chinlechelys tenertesta* (Szczygielski & Sulej 2019; Lichtig & Lucas 2021). Interestingly, both morphologies concern the exclusively dermal component of the carapace and suggest a more complex scenario of the evolution of that component than previously anticipated (Szczygielski & Sulej 2019; Sterli *et al.* 2021). Furthermore, Triassic turtles are unusual in frequent ankylosis, i.e., complete ossification and obliteration of sutures (Pritchard 2008) of their shells, regardless of the individual size (Gaffney 1990; Sterli *et al.* 2007, 2021; Szczygielski & Sulej 2016, 2019; Szczygielski *et al.* 2018). Aside from obscuring the bone layout within the carapace and plastron, this has functional implications, because in extant turtles the shell grows mainly along the sutures, and their mineralization and subsequent obliteration occurs usually in old specimens of sub-terminal body size (Kuchling 1997, 1999; Pritchard 2008).

Since Proterochersidae are among the oldest and basalmost testudinatans (Szczygielski & Sulej 2016, 2019; Szczygielski 2017; Sterli *et al.* 2021), and because the material of *Proterochersis porebensis* is exceptionally rich and includes specimens of varied sizes and, apparently, varied ontogenetic stages (Szczygielski & Sulej 2016; Szczygielski *et al.* 2018), the aim of this work is to expand upon the shell histology of that taxon. In particular, the main objectives are: 1) to check the variability of the shell microstructure between individuals of varied sizes and elements of varied developmental origin (derived from the axial skeleton, gastralia, pectoral girdle, and metaplastic dermal); 2) to look for histological clues providing data about the growth and development of the shell; 3) to investigate the unusual features of the sutural pattern (dermal carapacial mosaic) and ankylosis (e.g. whether the sutures are completely obliterated in small individuals, or if their internal structure is retained and merely obscured by surficial closure or diagenesis); and 4) to compare the observed histological and microstructural characteristics with other Triassic and post-Triassic turtles in order to better understand their diversity, evolution, and potential ecological significance.

MATERIAL AND METHODS

The studied material consists of shell thin sections of 18 specimens of *Proterochersis porebensis* of varied sizes (Table 1; Appendices 1; 2). All specimens come from the Late Triassic (Norian) locality of Poręba, Poland, the locus typicus of *Proterochersis porebensis* which thus far yielded turtle remains attributable only to this single species. The specimens were identified as turtle fragments based on morphology (shape, texture, presence of scute sulci and other typical external features; Szczygielski *et al.* 2018). See Bajdek *et al.* (2019) and references therein for information about the locality.

The thin sections of the specimens ZPAL V. 39/9, ZPAL V. 39/20, ZPAL V. 39/28, and ZPAL V. 39/392 were prepared in 2010 and donated for study by Tomasz Sulej (ZPAL). Their anatomical identification was performed based on photographs taken prior to sectioning and the parts remaining after sectioning. The specimens ZPAL V. 39/2, ZPAL V.

TABLE 1. — Sectioned specimens of *Proterochersis porebensis* Szczygielski & Sulej, 2016. In the case of plastral bones, longitudinal sections follow the antero-posterior axis of the bone, as it was positioned in vivo.

Specimen	Description	Size	References
ZPAL V. 39/2	Part of the carapace, sectioned transversely through the neurals (in two points, including the middorsal ridge) and longitudinally along the costal	Small	Szczygielski *et al.* 2018: fig. S4A, B
ZPAL V. 39/9	?Costal bone, sectioned transversely	Small	–
ZPAL V. 39/20	Posterior costal bone without the overlying osteodermal mosaic, sectioned transversely	Large	Szczygielski & Sulej 2019: figs 12A, B, 13
ZPAL V. 39/28	Right tenth marginal + parts of the third and fourth pleural and eleventh marginal area, sectioned transversely through the costal (and, based on the location, likely the supernumerary dermal ossification; compare with *2*) just above the pleuromarginal sulcus	Middle-sized	–
ZPAL V. 39/61	?Ninth marginal and third supramarginal area (peripheral and costal, possibly supernumerary carapacial ossification), sectioned transversely (longitudinally along the costal)	Large	–
ZPAL V. 39/68	Posterior part of the plastron (anal, intercaudal, and caudal scute areas) sectioned transversely through the caudal and intercaudal ossifications	Middle-sized	Szczygielski & Sulej 2019: fig. 18G, H; Szczygielski *et al.* 2018: fig. 9H
ZPAL V. 39/195	Plastral bone from the bridge region (?right first hyoplastron), sectioned longitudinally	Middle-sized	–
ZPAL V. 39/388	Anterior part of the plastron (gular and extragular projections), sectioned transversely	Small/middle-sized	Szczygielski *et al.* 2018: fig. S7K'–M'
ZPAL V. 39/392	?Posterior peripheral, sectioned obliquely	Large	–
ZPAL V. 39/401	Hyoplastron and posterior process of the entoplastron, sectioned transversely	Large	–
ZPAL V. 39/416	Neural bone, sectioned transversely	Large	Szczygielski & Sulej 2019: fig. 10C, D
ZPAL V. 39/417	Supernumerary carapacial ossification (?third or fourth pleural boss), sectioned obliquely	Middle-sized	Szczygielski & Sulej 2019
ZPAL V. 39/476	Plastral bone from the bridge region (?right hyoplastron), sectioned longitudinally	Small	–
ZPAL V. 39/477	Costal bone, sectioned transversely	Middle-sized(/large)	–
ZPAL V. 39/478	Neural bone, sectioned transversely	Small(/middle-sized)	–
ZPAL V. 39/479	Costal bone, sectioned transversely	Small	–
ZPAL V. 39/480	Costal bone, sectioned transversely (two times) and longitudinally (two times)	Middle-sized(/large)	–
ZPAL V. 39/482	Nuchal region of the carapace, sectioned longitudinally through the nuchal and through dermal ossifications (peripheral and supernumerary osteoderms)	Middle-sized	–

39/61, ZPAL V. 39/68, ZPAL V. 39/195, ZPAL V. 39/388, ZPAL V. 39/392, ZPAL V. 39/401, ZPAL V. 39/416, ZPAL V. 39/417, ZPAL V. 39/476, ZPAL V. 39/477, ZPAL V. 39/478, ZPAL V. 39/479, ZPAL V. 39/480, and ZPAL V. 39/482 were selected and thin-sectioned specifically for this study in the Institute of Paleobiology, Polish Academy of Sciences, and the Faculty of Geology, University of Warsaw. The thin sections were examined and photographed using the polarizing microscope Nikon Eclipse LV100 POL (Faculty of Geology, University of Warsaw). Computed tomography of ZPAL V. 39/480 was performed prior to sectioning using the GE Phoenix v|tome|x s computed tomograph (200 kV, 200 µA, 0.2 mm copper filter, 500 ms exposition time, 1800 projections) housed in the Institute of Biomedical Engineering, University of Silesia, Chorzów, Poland, and visualized using myVGL 3.3.2. Computed tomography of ZPAL V. 39/482 was performed prior to sectioning using Nikon/Metris XT H 225 ST computed tomograph (210 kV, 85 µA, 0.5 mm tin filter, 500 ms exposition time, 1000 projections) housed in the Military University of Technology, Warsaw, Poland, and visualized using VGStudio MAX 2.1. The specimens were provisionally classified to size classes based on comparisons with other, more complete specimens, considering the total known size range of the species (from probable hatchlings measuring merely several centimeters to specimens with carapaces over 70 cm long; see Szczygielski *et al.* 2018) and following convention as explained by Szczygielski *et al.* (2018). Specimens are characterized as small if they come from shells approximately the size of ZPAL V. 39/34 (*c.* 28 cm of carapace length) or smaller, as middle-sized if they are closest in size to ZPAL V. 39/48 (*c.* 42.5 cm of carapace length), and as large if they are closest in size to ZPAL V. 39/49 (*c.* 49 cm of carapace length) or larger. Based on previous research, ZPAL V. 39/34 was identified as a juvenile, ZPAL V. 39/48 as a subadult, and ZPAL V. 39/49 as an adult (Szczygielski & Sulej 2016, 2019; Szczygielski *et al.* 2018). See Table 1 for details on the studied specimens, Appendices 1; 2 for sectioning planes and specimen morphology, and Appendices 3-69 for photographs of thin sections.

The histological nomenclature follows Scheyer & Sander (2007) with the exception of the term "visceral" used instead of "internal" to characterize the surfaces directed towards the

body cavity. This allows using the term "internal" to unambiguously refer to the structures located inside the element (e.g. internal cavities). In the case of peripherals, the term "ventral" will be used to describe the scute-covered surfaces facing ventrally (towards the ground or plastron), to distinguish them from the scute-covered dorsal surfaces exposed in dorsal view and not exposed visceral surfaces.

ABBREVIATIONS

ISF	interwoven structural collagen fibers;
LAGs	lines of arrested growth.

Institutional abbreviations

SMNS	Staatliches Museum für Naturkunde Stuttgart, Stuttgart;
ZPAL	Institute of Paleobiology, Polish Academy of Sciences, Warsaw.

RESULTS

CARAPACE

Microstructural features of costals, neurals, peripherals, and carapacial dermal mosaic elements are mostly undistinguishable. For that reason, and because in ankylosed specimens the limits of particular carapacial elements are not apparent, these elements are described here collectively.

External cortex

The external cortex of the smallest individuals is poorly preserved in the sectioned specimens. The preserved part of the external cortex of the individual ZPAL V. 39/2 shows that it was thin (possibly due to its juvenility; compare with Suzuki 1963), incorporated interwoven structural collagen fibers (ISF) and numerous vascular canals of varying size, circular in cross section (Fig. 1A). In the inner external cortex few secondary osteons can be noticed. Growth marks are well visible. Since at least in most cases these marks take the form of blurry, undulating fronts of discoloration rather than sharp lines, and thus likely represent cyclical changes of crystallite density and/or alignment rather than record of complete growth cessation, they are not identified here as lines of arrested growth (LAGs). The thin section through the middorsal ridge reveals similar microstructure, differing in less visible growth marks. The thickness of the external cortex in the middle-sized ZPAL V. 39/28 is irregular, but in general thinner than the visceral cortex. The external cortex in that specimen incorporates ISF (Fig. 1C). The vascularization is low, with few primary vascular canals sub-circular in cross section. Primary osteons are absent. Possible growth marks are obscured by longitudinally sectioned structural fibers. In contrast, the external cortex of the other middle-sized specimen ZPAL V. 39/477 shows ISF with many primary vascular canals circular in cross section. The specimen ZPAL V. 39/28 was sectioned close to the edges of the overlying scutes, and ZPAL V. 39/477 was sectioned further away from sulci. Both specimens have scattered secondary osteons present close to the gradual transitional zone to the cancellous bone. The middle sized/large costal ZPAL V. 39/480 was sectioned longitudinally (two times) and transversely (proximally and distally, at the level of the striated end exposed from under the rugose dermal ossification; Fig. 2D). All sections show the external cortex being thicker than the visceral. Four growth marks are best visible in the proximal transversal section in the externalmost part of the cortex (Fig. 2G). The inner part of the external cortex incorporates ISF and is well-vascularized. ISF bundles are present in the proximal part of the costal, in the rugose part with better developed dermal ossification (Fig. 2J), and better organized parallel-fibered bone is present in the distal part with recessed, smoother, striated external surface (Fig. 2F, I; compare to the large ZPAL V. 39/20). The external cortex of the latter bears also few primary canals. The specimen bears several undulating, suture-like grooves on its external surface and possible microstructural clues for sutures internally (see sutures below; Fig. 2C). In one of the longitudinal sections a long and narrow canal perforates obliquely (ventrodistally) the external cortex seems to be a residue of the suture (Fig. 2E). In the same section, in the area between the external cortex and the spongiosa, a few long horizontal canals (the longest measuring 6 mm in length) are present between the layer of coarse metaplastic bone and the underlying tissue. The external cortex of the second longitudinal section shows only canals perforating the cortex at acute angles, but no horizontal channels are present (Fig. 2H). This may be caused by poor preservation of the cortex in the contact region of the metaplastic bone and the underlying costal.

Almost avascular external cortex is present in the dermal ossifications (peripheral and supernumerary elements) from the nuchal region and the nuchal bone of the middle sized ZPAL V. 39/482 (Figs 2; 3). Only rare and scattered circular vascular canals are present in the cortex. The cortex incorporates ISF with few growth marks and few secondary osteons are present close to the spongiosa. The external cortex of the supernumerary ossification of the middle-sized individual ZPAL V. 39/417 also incorporates ISF (Fig. 5C), but is well-vascularized, in contrast to the external cortex microstructure of the sectioned costals (ZPAL V. 39/28 and ZPAL V. 39/477). Primary vascular canals in that specimen are circular in cross section ventrally to the pleural boss, and elliptical (oriented latero-dorsally) dorsally to the pleural boss. Growth marks are visible in the external cortex, the secondary osteons are rare in the innermost cortex.

The external cortex in large specimens (ZPAL V. 39/20, ZPAL V. 39/61, ZPAL V. 39/392, ZPAL V. 39/416) also incorporates ISF. Similarly to the distal part of the middle-sized ZPAL V. 39/480, the bundles of the ISF in the sectioned part of ZPAL V. 39/20, which was separated from the externalmost layer of dermis and lacks the typical rugose surface (Szczygielski & Sulej 2019), are expressed weaker compared to most other specimens and mostly externally. The vascularization is high in ZPAL V. 39/416 but low in ZPAL V. 39/20, ZPAL V. 39/61, and ZPAL V. 39/392. In the first mentioned specimen, numerous primary vascular canals approach and open onto the external surface, giving it a wavy relief. A similar waviness of older layers of the cortex is documented by well-expressed growth marks. The canals appear sub-circular to oval in cross

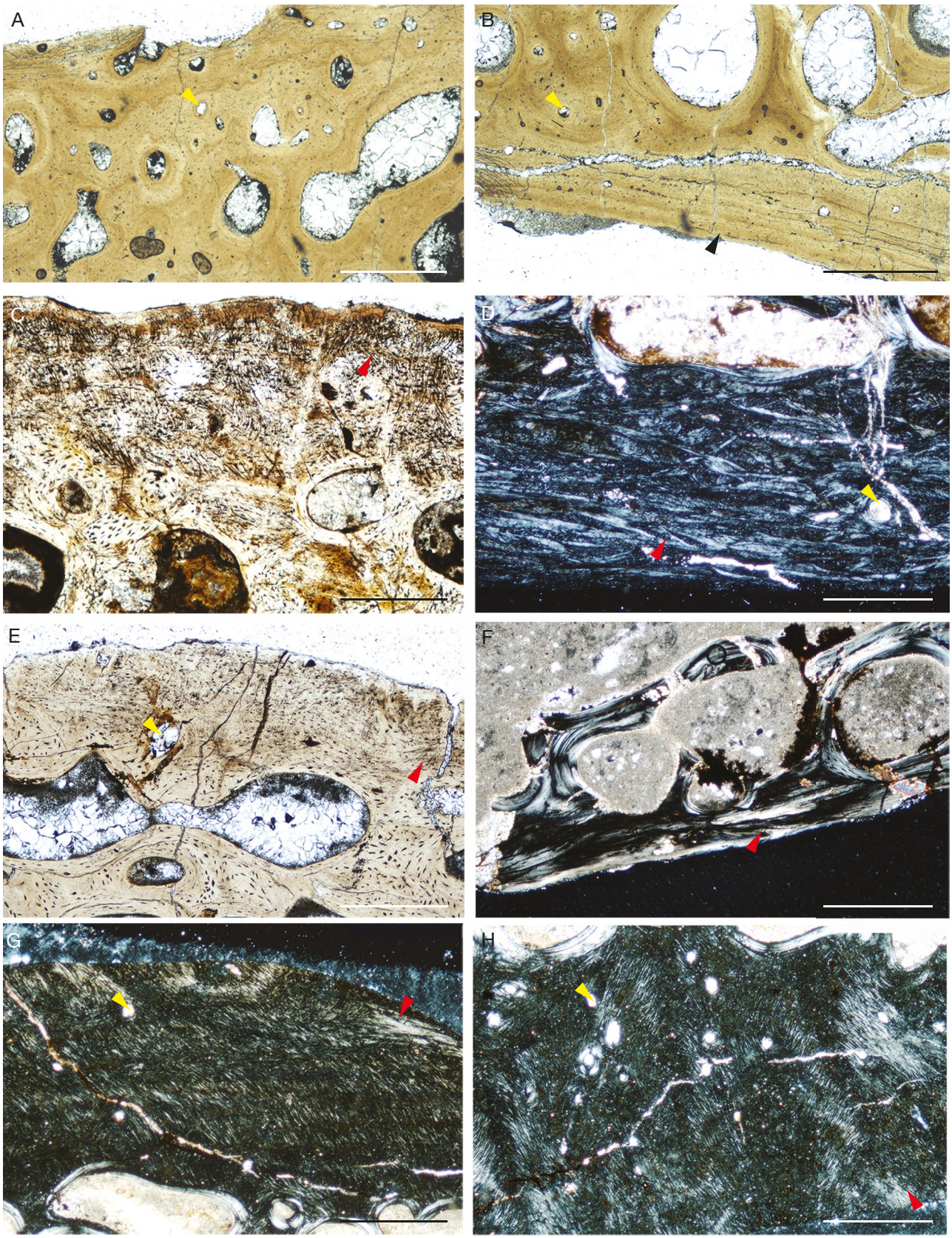

FIG. 1. — The microstructure of the carapace of *Proterochersis porebensis* Szczygielski & Sulej, 2016: **A**, **B**, small specimen ZPAL V. 39/2 cortex in normal transmitted light: **A**, external; **B**, visceral; **C**, **D**, medium-sized specimen ZPAL V. 39/28: **C**, the external cortex in normal transmitted light; **D**, visceral cortex in polarized light; **E**, **F**, large specimen ZPAL V. 39/61: **E**, the external cortex in normal transmitted light; **F**, visceral cortex in polarized light; **G**, **H**, large specimen ZPAL V. 39/20 cortex in polarized light: **G**, external: **H**, visceral. Arrowheads: **red**, ISF; **yellow**, primary canals; **black**, growth marks. Scale bars: 0.5 mm.

section and locally in the lateral parts of ZPAL V. 39/416 exhibit a slightly oblique inclination relative to the surface. Secondary osteons are absent in the whole external cortex. In ZPAL V. 39/20, ZPAL V. 39/61, and ZPAL V. 39/392 the external cortex shows much less numerous and smaller primary vascular canals circular in cross section (Figs 1E, G; 5A, B). Growth marks are barely noticeable and capture a smoother, only gently wavy relief similar to the external surface of the external cortex. The secondary osteons are rare in the innermost external cortex of the specimens ZPAL V. 39/20 and ZPAL V. 39/61. In the large peripheral, ZPAL V. 39/392, the innermost part of the cortex shows numerous secondary osteons, which mark the beginning of the spongiosa. The external cortex on the dorsal surface differs in its microstructure to the external cortex on the ventral surface. The external cortex of the latter shows intensive remodeling.

Spongiosa

In all sampled specimens, the spongiosa is composed of predominantly secondary trabeculae with local remnants of primary interstitial bone. The ratio of the primary to secondary bone shows larger local variations within some single sections than between some specimens.

In the small specimen ZPAL V. 39/2, the trabeculae are thick and short, with small, mainly circular vascular canals (Fig. 6C). Between the marrow cavities, primary canals and secondary osteons are present. The small specimen ZPAL V. 39/9 and larger ZPAL V. 39/478 (small/middle sized individual) show spongiosa with slenderer and longer bony trabeculae, and larger and irregular marrow cavities (Fig. 6D). Their trabeculae also lack secondary osteons and primary canals, in contrast to ZPAL V. 39/2. Finally, in ZPAL V. 39/479 the trabeculae are the longest and slendermost, so the marrow cavities are large.

The bony trabeculae pattern in the spongiosa of the middle-sized individuals ZPAL V. 39/28, ZPAL V. 39/417, ZPAL V. 39/477, ZPAL V. 39/482, and ZPAL V. 39/480 varies between the specimens. In ZPAL V. 39/477 the trabeculae are thick and usually short, so the marrow cavities are generally small. In ZPAL V. 39/28, ZPAL V. 39/417, ZPAL V. 39/482, and ZPAL V. 39/480 the trabeculae are longer and slender, the marrow cavities are comparatively larger (Figs 2E-H; 6A).

The spongiosa is similar between all four sampled large specimens (ZPAL V. 39/20, ZPAL V. 39/61, ZPAL V. 39/392, and ZPAL V. 39/416). The trabeculae are mainly thick and short, and the marrow cavities mostly small, as in the whole spongiosa of ZPAL V. 39/20, ZPAL V. 39/416, and ZPAL V. 39/392 (Fig. 6B, F). However, it is restricted to the areas close to the external and visceral cortex, while internally the marrow cavities are larger and surrounded by slender trabeculae. In ZPAL V. 39/416 primary vascular canals are also present in the interstitial bone of the spongiosa, between the lamellar bone-lined marrow cavities. Particularly, the spongiosa in ZPAL V. 39/61 gives an osteoporotic appearance but seems to be at least partially exaggerated by taphonomic damage and wear, reflected in numerous cracks and breaks along the trabeculae (Fig. 6G).

Visceral cortex

Among small specimens, the visceral cortex is best preserved in ZPAL V. 39/2, in which it is thin and less vascularized than the external cortex, only with rare small circumferential canals (Fig. 1B). It is predominantly composed of ISF-incorporating tissue, although it superficially attains a more ordered, parallel-fibered organization, most notable at the transition of the neural spine into the neural bone and in the proximal part of the costal. This structure is locally crossed by coarse bundles of fibers sub-perpendicular to the visceral surface or aligned ventromedially. The part of the visceral cortex preserved in ZPAL V. 39/479 is poorly vascularized and seems to have a parallel-fibered organization. As in ZPAL V. 39/2, this may be caused by the relatively proximal position of the section along the costal.

In contrast to the gradual transition towards the external cortex, the spongiosa is well distinguished from the visceral cortex in ZPAL V. 39/28. The cortex maintains a homogenous thickness along the section and incorporates ISF with some bundles of more ordered fibers running at acute angles to the visceral surface (Fig. 1D). The tissue is less vascularized than the external cortex with few primary vascular canals of small circumference. However, a few large canals ovoid in outline are also present in the visceral cortex. Few scattered secondary osteons are present close to the transitional zone. The visceral cortex of ZPAL V. 39/417 has a similar microstructure as in ZPAL V. 39/28, however, it is slightly better vascularized (Fig. 5D). The visceral (perimedullary) cortex of two supernumerary ossifications and peripheral of ZPAL V. 39/482 surrounds an internal cavity (Fig. 4G), which likely accommodated the cranial edge of the first costal (compare with ZPAL V. 39/22 in Szczygielski & Sulej 2019), although the peripheral region of which seems to be partially separated by a prominent thickening of the visceral cortex. The microstructure varies along the cortex, mostly it is thick and incorporates ISF, but thinner layers of parallel-fibered bone prevail around the dorsodistal and ventral part of the cavity. The parallel-fibered cortex has smoother relief and is less vascularized than the parts incorporating the ISF. The coarse roughness of the metaplastic surface lining the embayment for the first costal is visible macroscopically (Fig. 4D-G), also in ZPAL V. 39/22 (Szczygielski & Sulej 2019). At least six growth marks are visible in the section, secondary osteons are absent. The thin visceral cortex of the nuchal bone of ZPAL V. 39/482 shows ordered parallel-fibered bone (Fig. 4B). In the preserved part, the vascular canals are common. Growth marks and secondary osteons are absent. The visceral cortex is poorly preserved and mostly missing in the middle-sized individual ZPAL V. 39/477 (Appendices 49-51). It is also incomplete in ZPAL V. 39/480, which mostly lacks the visceralmost part of the cortex. The visceral cortex incorporates ISF and scattered secondary osteons.

The visceral cortex of all the analyzed large specimens (ZPAL V. 39/20, ZPAL V. 39/61, and ZPAL V. 39/416; Fig. 1F, H) incorporates ISF. In ZPAL V. 39/61, ZPAL V. 39/461 it is less vascularized than the external cortex (Appendices 37-39),

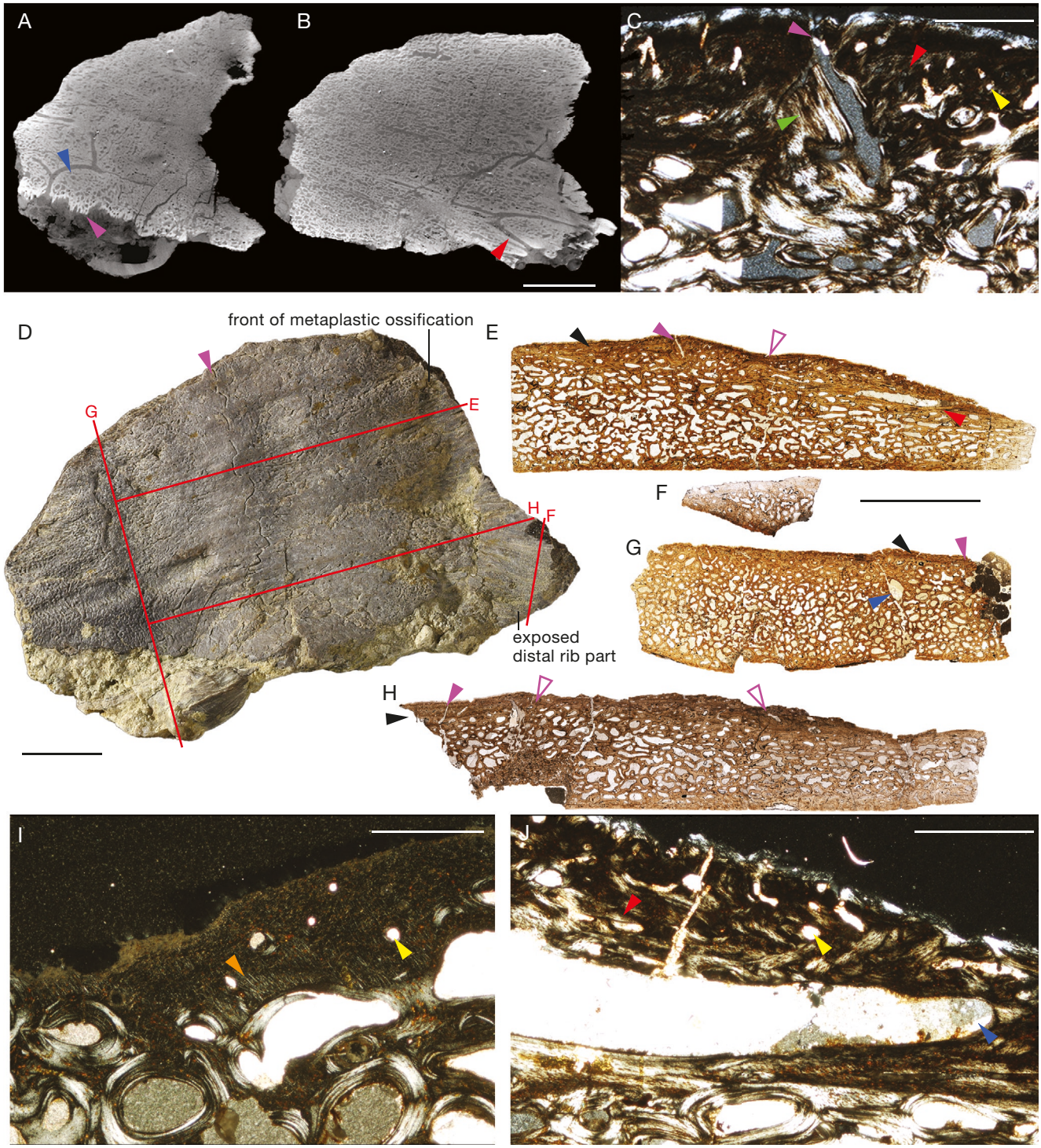

Fig. 2. — *Proterochersis porebensis* Szczygielski & Sulej, 2016 ZPAL V. 39/480, costal with the front of coarse metaplastic ossification revealing the underlying distal part: **A**, **B**, coronal CT scans of the specimen (closer and further away from the exterior) showing a large vascular canal at the interface between the costal bone and overlying coarse dermal ossification; **C**, closeup of a canal associated with externally visible suture-like groove in polarized light; **D**, the specimen in external view with marked sectioning lines; **E**, longitudinal section of the costal showing a possible semiankylosed suture and the large vascular canal; **F**, cross section of the distal part of the rib; **G**, cross section of the proximal part with open intercostal suture; **H**, longitudinal section showing possible remnants of sutures; **I**, the external cortex of the distal part (section **F**) in polarized light; **J**, close up to the large vascular canal in polarized light, showing the tissues surrounding the canal. Arrowheads: **red**, ISF; **yellow**, primary canals; **black**, growth marks; **dark blue**, large vascular canal between the dermal ossification and the underlying costal; **orange**, parallel-fibered bone; **purple**, sutures; **purple outlines**, areas where sutures could be present as suggested by the bone microstructure. Distal in **A**-**E**, **H**, and **J,** towards the right; **E**-**H**, in normal transmitted light with the external cortex towards the top of the page. See text for discussion. Scale bars: A, B, D-H, 1 cm; C, J, 1 mm; I, 0.5 mm.

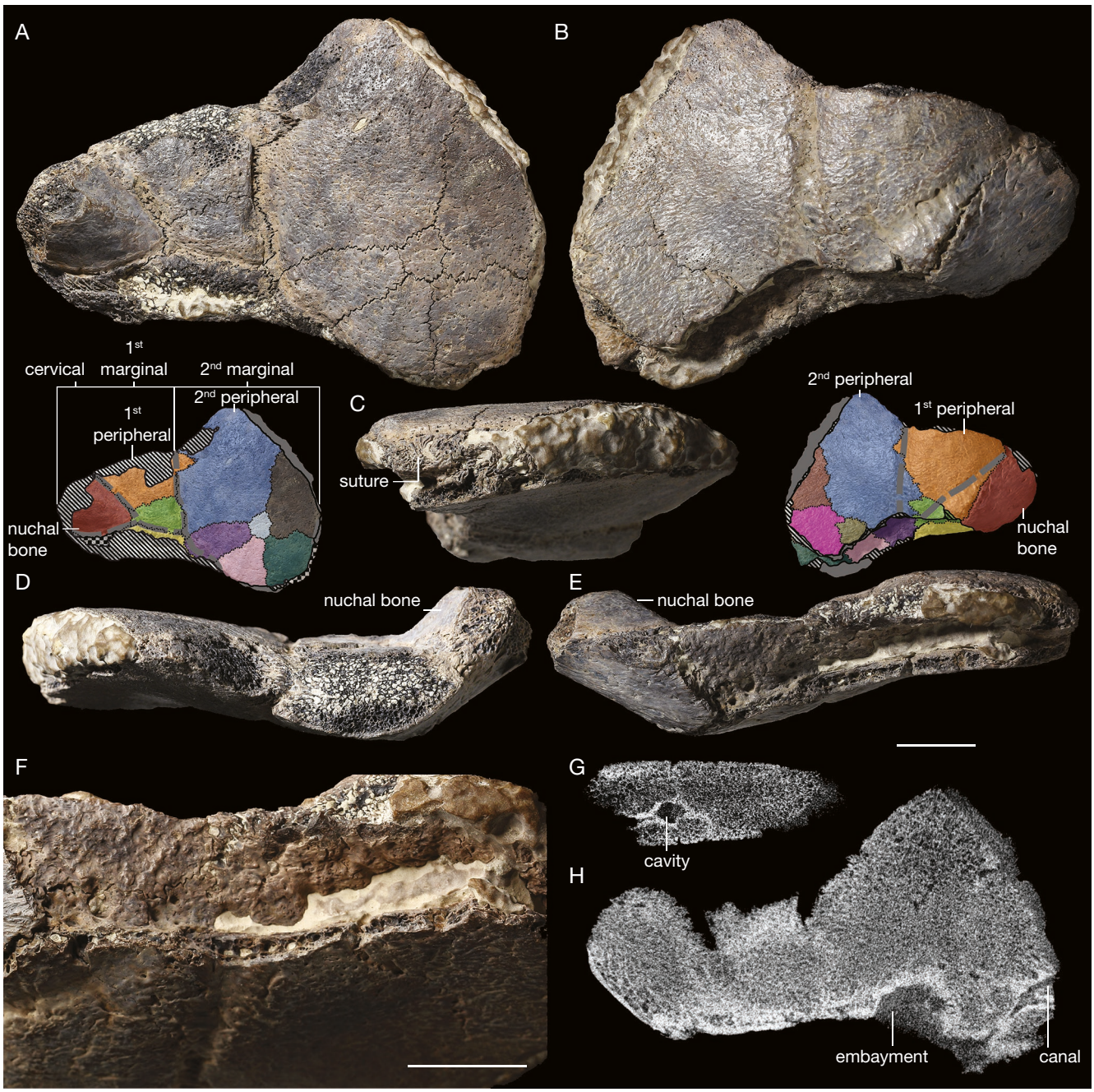

Fig. 3. — *Proterochersis porebensis* Szczygielski & Sulej, 2016 ZPAL V. 39/482, a nuchal fragment of the carapace, composed of the nuchal bone, peripherals, and supernumerary carapacial ossifications, before thin sectioning: **A**, dorsal view; **B**, ventral view; **C**, lateral view; **D**, anterior view; **E**; posterior view; **F**, close-up of the posterior embayment for the first costal in posteroventral view; **G**, longitudinal CT section through the lateral part of the specimen revealing a small cavity surrounded by the peripheral and supernumerary ossifications. Distal towards the right; **H**, coronal CT section showing a branching, canal-like structure continuing from the embayment between the bones. In the explanatory drawing for **A** and **B**: **dotted lines**, sutures; **thick dashed gray line**, scute sulci; **hatching**, broken and damaged surfaces; **checkerboard**, exposed sutural surfaces; **gray**, matrix. Scale bars: 1 cm.

but in ZPAL V. 39/20 the vascularization of both cortices is similar (Fig. 1E, H). In the innermost visceral cortex, scattered secondary osteons are present. In the section of ZPAL V. 39/20 a relatively large vascular trough is present opening onto the visceral surface of the element (Fig. 6B). Its gradual drift is captured by the asymmetrically deposited bone lamellae. The cut surface of the remainder of the specimen shows that slightly more proximally the same vascular space is fully encased in the cortex.

Plastron

External cortex

The plastral bone of the small individual (ZPAL V. 39/476) shows well-vascularized, thick external cortex incorporating ISF (Fig. 7A). The vascularization follows the long (i.e., mediolateral) axis of the bone and is unusually ordered, locally (close to the natural edge of the element) attaining a nearly fibrolamellar-like (Fig. 7B) organization, with the primary canals arranged in rows separated by thin layers of bone.

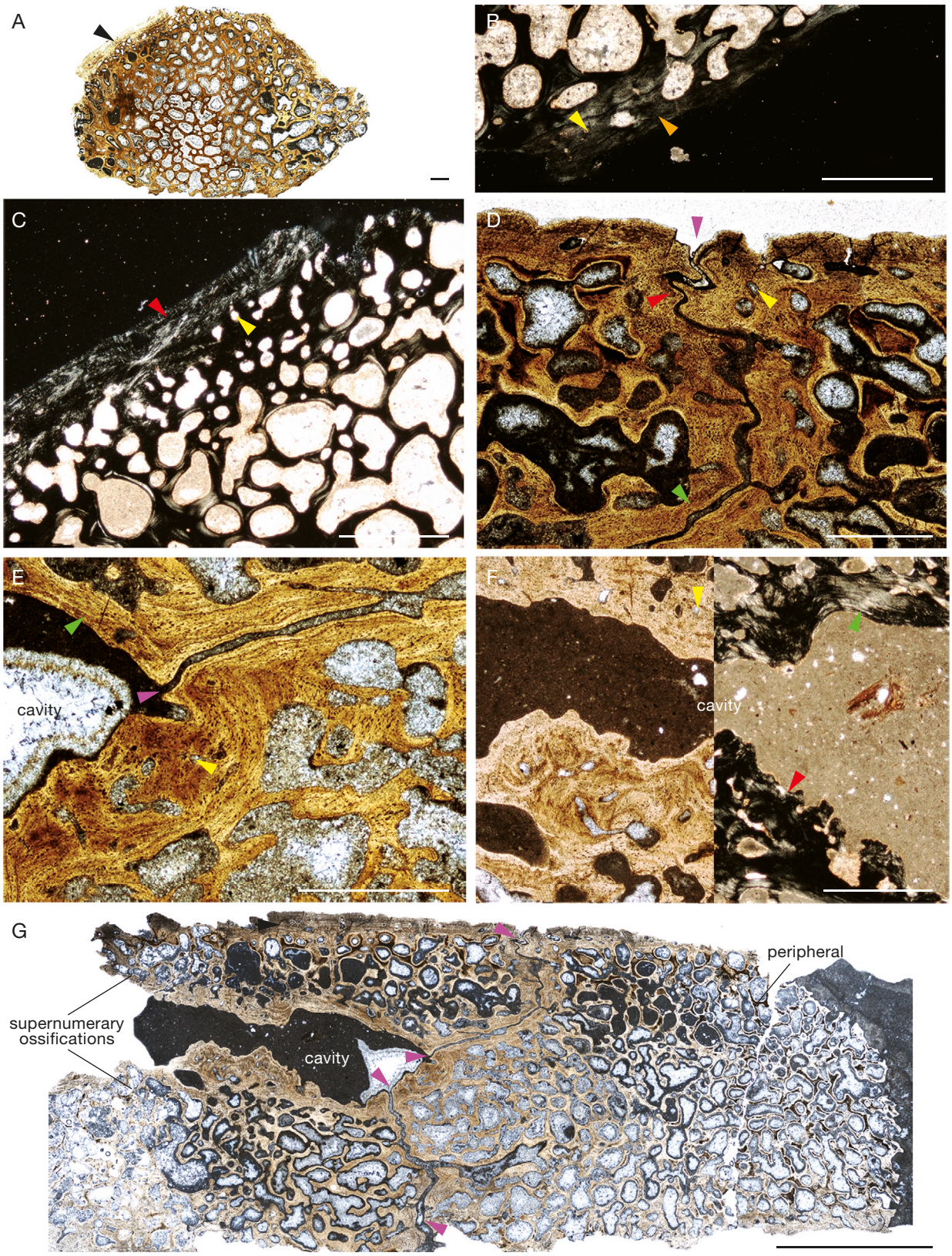

FIG. 4. — Microstructure of the nuchal, supernumerary ossifications, and peripheral of the middle-sized *Proterochersis porebensis* Szczygielski & Sulej, 2016 ZPAL V. 39/482: **A**, anteroposterior section through the nuchal bone in normal transmitted light; **B**, **C**, cortex of the nuchal in polarized light: **B**, visceral; **C**, external (**C**); **D**-**G**, supernumerary ossifications and peripheral histology; **D**, **E**, cortex of a suture between a supernumerary ossification and peripheral, close to the external (**D**) and visceral (**E**) cortex in normal transmitted light; **F**, visceral (perimedullary) cortex of two supernumerary ossifications surrounding a cavity in normal transmitted and polarized light. Posteriorly, the cavity was partially filled and enclosed by the first costal bone; **G**, anteroposterior section through the supernumerary ossifications and peripheral. Note the well-visible sutures. Arrowheads: **red**, ISF; **yellow**, primary canals; **black**, growth marks; **green**, lamellar bone; **purple**, sutures; **orange**, parallel-fibered bone. Scale bars: A-F, 1 mm; G, 5 mm.

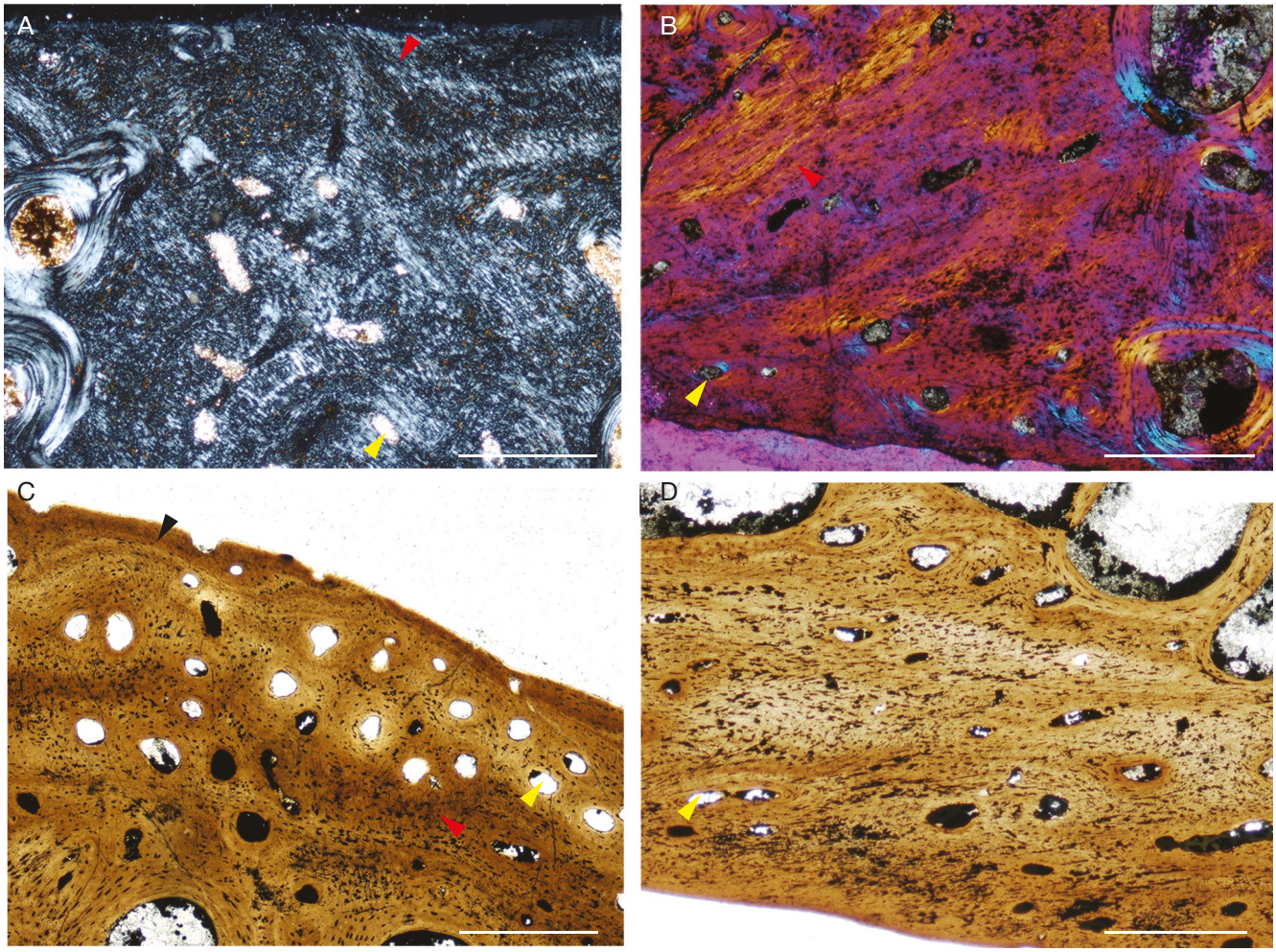

Fig. 5. — Microstructure of a peripheral (A, B; ZPAL V. 39/392) and supernumerary carapacial ossification (C, D; ZPAL V. 39/417) of *Proterochersis porebensis* Szczygielski & Sulej, 2016: **A**, the external cortex of the peripheral in polarized; **B**, polarized light with quartz wedge; **C**, **D**, cortex of the supernumerary carapacial ossification in normal transmitted light: **C**, external; **D**, visceral. Arrowheads: **red**, ISF; **yellow**, primary canals; **black**, growth marks. Scale bars: 0.5 mm.

In this more ordered area, in a row extending along the middle part of the external cortex thickness and close to the sutural edge, the circumferences of the vascular canals are noticeably larger than in the outer and inner parts. The canals become smaller and more randomly scattered towards the central part of the bone. The transition between the external cortex and the spongiosa is sharp.

The middle-sized individual (ZPAL V. 39/195) has a much thicker external cortex compared to the visceral. It incorporates ISF, is well vascularized, with few growth marks (Fig. 7C). The vascularization pattern and density changes along the section, with the vasculature becoming externally denser and oriented subvertically or obliquely closer to the edge of the bone. Few secondary osteons are limited to the innermost cortex. The external cortex surrounding the gular and extragular projection (ZPAL V. 39/388) is weakly vascularized and incorporates ISF (Fig. 8A, B). Few growth marks can be noticed in the cortex, mostly cumulated in the externalmost cortex. The secondary osteons are rare, mostly positioned close to the spongiosa. The external cortex of the caudal and intercaudal scute areas of ZPAL V. 39/68 is weakly preserved. It is avascular with ISF, but lacking secondary osteons (Fig. 8D, E).

The section of the biggest plastron sample analyzed herein (ZPAL V. 39/401) has the outer layer of external cortex slightly abraded, but the preserved parts show that it incorporated ISF and that the rich vascularization closely approached and opened onto the external bone surface (Fig. 7E). No growth marks can be noticed (although this may be a result of a low thickness of the sample). The inner layers show a highly vascularized tissue with primary canals and secondary osteons. The transition between the spongiosa and the external cortex is gradual.

Spongiosa

The cancellous bone in the plastron of a small individual (ZPAL V. 39/476) is composed of mainly long and slender bony trabeculae, and the marrow cavities predominantly take form of small sub-circular to large irregular spaces. Remains of scattered secondary osteons are recorded within bony trabeculae.

The spongiosa in the middle-sized ZPAL V. 39/195 is composed of thick, and mostly short secondarily remodeled trabeculae (Appendices 24-26). The marrow cavities are mostly small and sub-circular, large and irregular spaces are

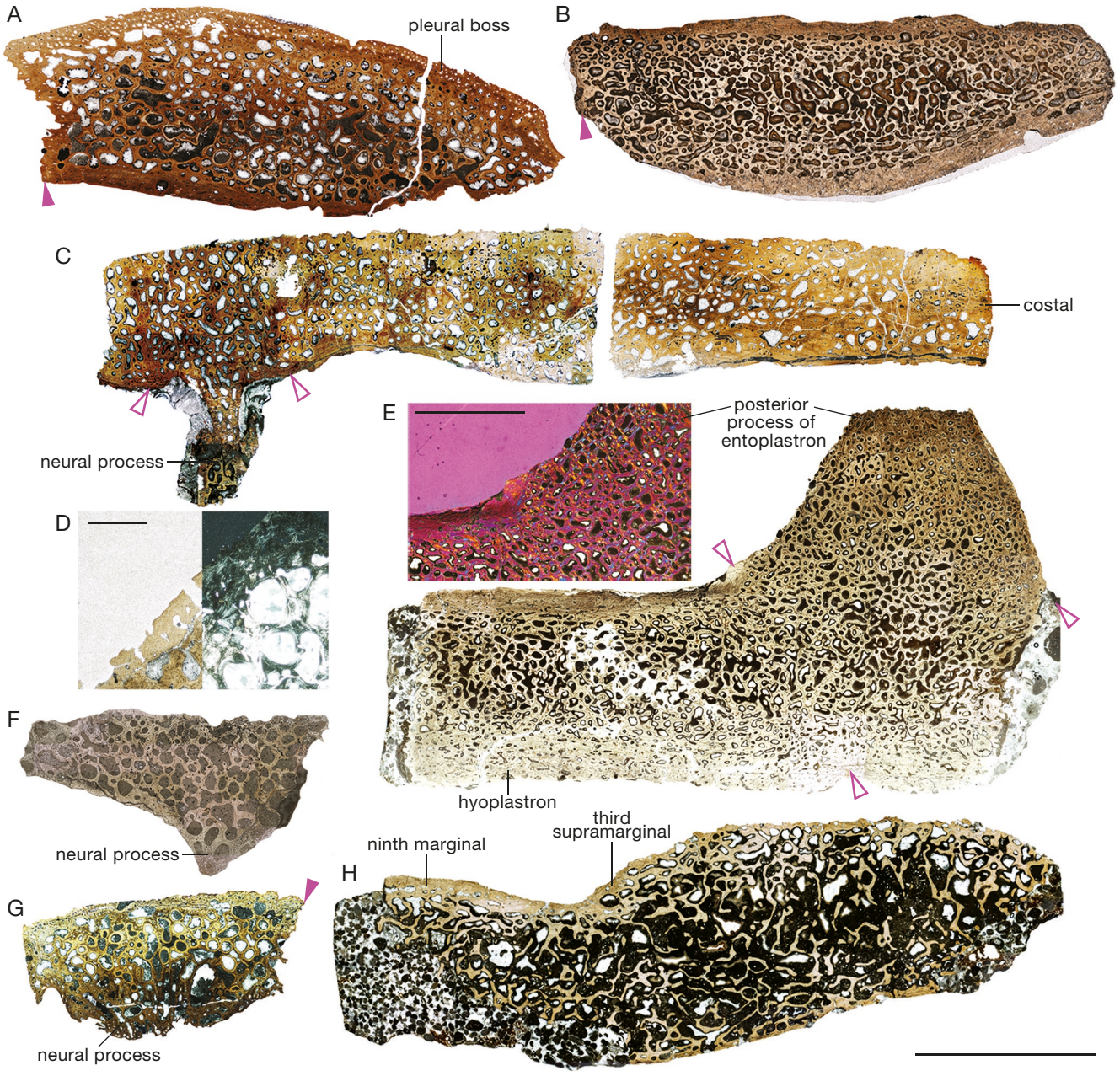

Fig. 6. — Full scans of the thin sections of *Proterochersis porebensis* Szczygielski & Sulej, 2016: **A**, a supernumerary carapacial ossification of the middle-sized specimen ZPAL V. 39/417 showing an open suture; **B**, posterior costal of the large individual ZPAL V. 39/20; **C**, neural and costal of the small individual ZPAL V. 39/2 showing disappearing costoneural sutures; **D**, close-up of the external cortex of the middorsal ridge of the neural ZPAL V. 39/2 in normal and polarized light; **E**, hyoplastra and entoplastron of the large individual ZPAL V. 39/401, close up of the area where the suture would be expected in polarized light with quartz wedge; **F**, neural of the small specimen ZPAL V. 39/478; **G**, neural of the large specimen ZPAL V. 39/416 with open costoneural suture; **H**, carapace fragment of the large individual ZPAL V. 39/61 with obliterated sutures. Arrowheads: **Purple**, sutures; **purple outlines**, areas where sutures are expected based on topology and comparisons with other turtles (not indicated in **H**). External cortices of carapacial elements (**A**-**D**, **F**-**H**) towards the top of the page, external cortex of the plastron (**E**) towards the bottom of the page. Scale bars: A-C, F-H, 1 cm; D, 1 mm; E, 5 mm.

rare in the section. Secondary osteons within the spongiosa are more numerous in comparison to the smaller ZPAL V. 39/476 (Appendices 46-48). The spongiosa of the posterior part of the plastron (ZPAL V. 39/68) is less remodeled, with marrow cavities diverse in shape and generally thick trabeculae varying in length (Fig. 8F). No obvious borders between the bony elements forming that region, i.e., ischia, intercaudal, and caudal ossifications (Szczygielski & Sulej 2019), can be observed, including the suture between the contralateral ischia.

The cancellous bone of the large ZPAL V. 39/401 surrounds numerous small to medium-sized, mostly irregular intertrabecular spaces (Fig. 6E). The trabeculae are thick and short. The secondary osteons are present in the spongiosa, similar as in ZPAL V. 39/ 68 and ZPAL V. 39/195.

Visceral cortex

The visceral cortex is poorly preserved in ZPAL V. 39/476 (Fig. 7B). It is similar in thickness to the external cortex, but

much less vascularized. The vascular canals are sub-circular in cross section and small. The visceralmost cortex is not preserved in the section, but the deeper part shows ISF. No growth marks or secondary osteons can be noticed in the visceral cortex of the specimen.

The middle-sized individual (ZPAL V. 39/195) has the visceral cortex much thinner than the external. It is also less vascularized, incorporates ISF in the deeper part and is composed of parallel-fibered bone in the surficial part of the cortex (Fig. 7D). The transition between the spongiosa and the visceral cortex in the middle-sized ZPAL V. 39/195 is sharp (Appendices 24-26). Few circular cross sections of vascular canals of small circumference can be noticed in the innermost visceral cortex. Locally, the canals become more parallel to the plane of the cross section, either running anteroposteriorly through the bone or obliquely towards the external surface, their morphology is, however, different from those described in *Proterochersis robusta* and their diameter is larger (Scheyer & Sander 2007). In the section, the structure of the visceral cortex is weakly preserved, however it shows horizontal organization, indicating parallel-fibered bone. One possible growth mark can be noticed. Scattered secondary osteons are present in the innermost cortex. In ZPAL V. 39/68, a short segment of the internal cortex of the caudal process is preserved bilaterally between the edges covered by the caudal scutes and the attachment of the ischia. It is, however, completely secondarily remodeled (Fig. 8F).

The transitional zone between the visceral cortex and the spongiosa of the large ZPAL V. 39/401 is sharp, with few secondary osteons (Fig. 6E). The visceral cortex incorporates ISF in the deeper cortex and parallel-fibered bone in the surficial part (Fig. 7F). The mainly small and sub-circular vascular canals are present, but rare. Several (seven-eight) growth marks are visible in the section. The closely spaced growth marks close to the outermost part of the visceral layer indicate that the specimen was fully-grown.

Unlike in *Proterochersis robusta*, a network of thin branching primary vascular canals (Scheyer & Sander 2007) is not apparent in the visceral cortex of any sectioned plastral element of *Prot. porebensis*. Although some canals could potentially be obscured by cracking, close inspection of the thin sections suggest rather a completely taphonomic origin of the observed cracks.

Sutures

Well-defined, unankylosed sutures are preserved in ZPAL V. 39/20 (intercostal sutures; Fig. 6B), ZPAL V. 39/416 (costoneural suture; Fig. 6F), ZPAL V. 39/417 (sutures around the dermal ossification; Fig. 6A), ZPAL V. 39/482 (sutures between the peripheral and supernumerary ossifications; Figs 3; 4D-G), and in the transverse section of the specimen ZPAL V. 39/480 (intercostal suture; Fig. 2C-H). In these specimens, the compact bone of the sutures is generally primary, poorly vascularized, close to avascular, incorporates ISF, and is overall histologically indistinguishable from the cortices of the same specimens. Only in the specimen ZPAL V. 39/482 the ISF are present along the suture, but disappear further away from the external and internal bone surfaces, where the microstructure of the tissue surrounding the suture becomes more organized (Fig. 4D-F). In some specimens (particularly ZPAL V. 39/480 and ZPAL V. 39/482; Figs 2E, G; 4G) the shape of the sutural surfaces is reflected in the layout of the underlying growth marks, but in others (ZPAL V. 39/20, ZPAL V. 39/416, ZPAL V. 39/417; Fig. 6A, B, G) the growth marks are absent or inconspicuous. Overall, the open suture morphology is reminiscent of that in the Early Jurassic aquatic turtle *Condorchelys antiqua* Sterli, 2008 (Cerda *et al.* 2015).

Very similar structurally are the ankylosed costoneural and (in distal part) intercostal sutures in the small ZPAL V. 39/2 (Fig. 6C; Appendices 6; 7). The sutures in that specimen are not detectable macroscopically and histologically they are represented as areas of primary bone with ISF and a system of roughly evenly spaced, small primary vascular canals with very few larger cavities – effectively a local continuation of the cortices throughout the whole thickness of the bone. In ZPAL V. 39/478 the costoneural suture is nearly completely obliterated (Fig. 6D). Its initial position, aside from topological clues (e.g. the proximity of the neural arch), may be only arbitrarily estimated based on a sub-vertical band of comparatively thicker trabeculae. Similar thickened trabeculae are, however, also present seemingly randomly elsewhere in the same section, proving that the patterns within the cancellous bone are not a reliable indicator of initial bone layout. This is further supported by ZPAL V. 39/61 (carapace fragment incorporating – based on topological comparisons with other specimens – a costal, a peripheral, and, likely, a supernumerary carapacial ossification; Fig. 6G), ZPAL V. 39/68 (a plastron fragment with caudal and intercaudal ossifications and attached ischia; Fig. 8F), ZPAL V. 39/388 (a plastron fragment composed of epiplastron and the extragular ossification; Fig. 8C); and ZPAL V. 39/401 (a plastron fragment composed of two contralateral hyoplastra and the posterior entoplastral process; Fig. 6E). Neither of these four specimens preserves any definitive histological clues about sutures or initial number and layout of contributing bones, either in the cortices or spongiosa.

A set of microstructures in the external cortex, possibly representing semiankylosed and ankylosed sutures related to the presence of the dermal carapacial mosaic external to the costal (Szczygielski & Sulej 2019) is visible in the longitudinal sections of the specimen ZPAL V. 39/480 (Fig. 2E, H). The position of the almost closed suture discernable in the thin section corresponds with closed, suture-like groove visible on the external surface of the specimen (Fig. 2D). This groove is associated with a long and narrow canal in the external cortex positioned at an acute ventrodistal angle to the bone surface. Similar to the sutures of other specimens described above, it is surrounded by avascular bone with ISF (Figs 2J; 4D, E). On the proximal side of the canal, in its deeper part, the tissue is better organized (lamellar) than distally. A few narrower canals branch obliquely from the main canal – the longest close to the external opening of the canal, and several shorter deeper into the cortex (Fig. 2C). Internally, presumed remains of an ankylosed suture can be

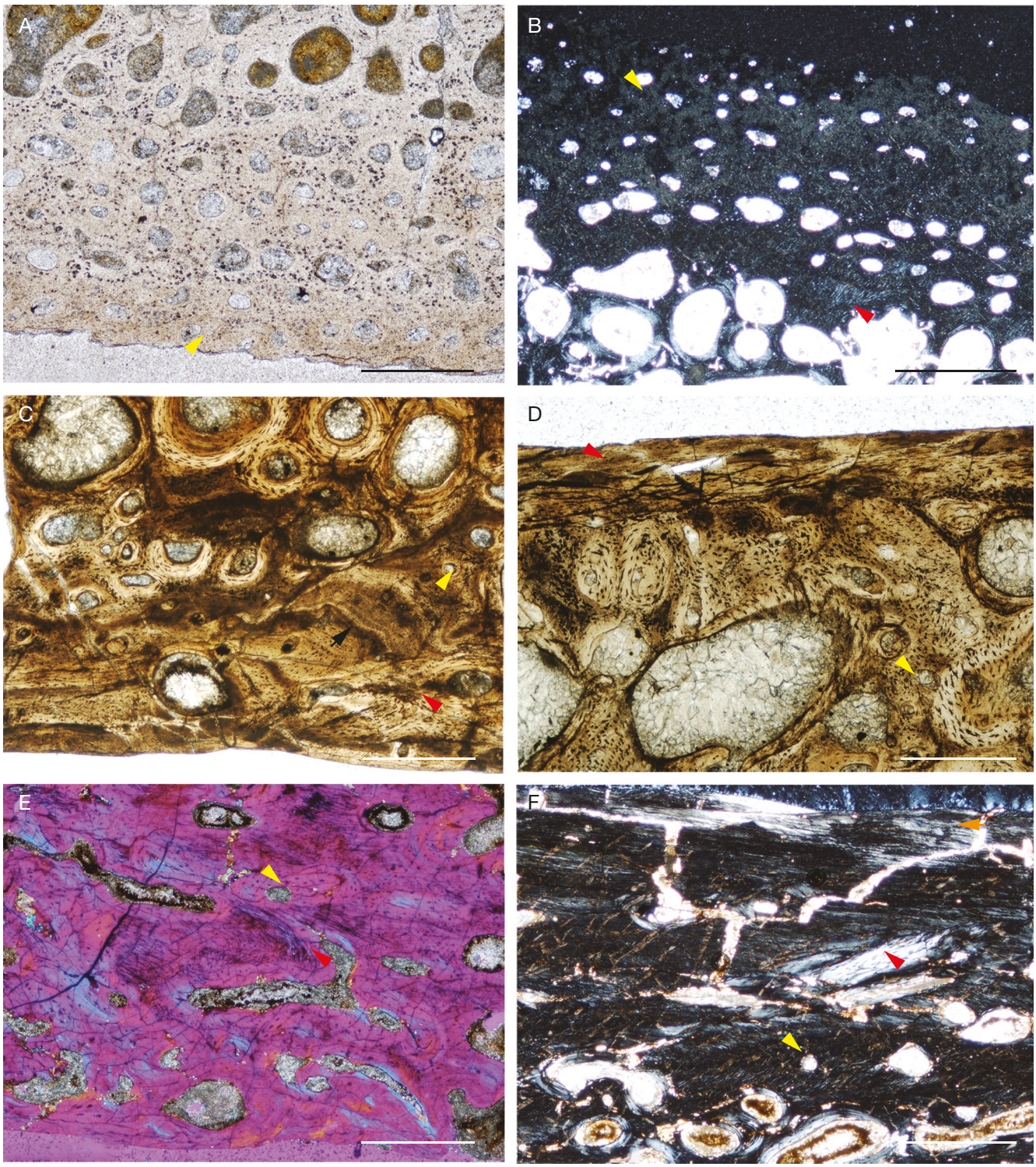

Fig. 7. — Microstructure of plastral bones of *Proterochersis porebensis* Szczygielski & Sulej, 2016: **A**, **B**, small individual ZPAL V. 39/476: **A**, external cortex in normal transmitted light; **B**, visceral cortex in polarized light; **C**, **D**, medium specimen ZPAL V. 39/195 cortex in normal transmitted light: **C**, external; **D**, visceral; **E**, **F**, large individual ZPALV. 39/401: **E**, external cortex in polarized light with quartz wedge; **F**, visceral cortex in polarized light. Arrowheads: **red**, ISF; **yellow**, primary canals; **orange**, parallel-fibered bone. Scale bars: 0.5 mm.

observed: a zigzag structure formed of primary bone tissue with suture-like layout of growth marks crossing the external half of the spongiosa (Fig. 2E). The layout of the growth marks and general structure of the bone correspond in these places to the unankylosed intercostal suture in the same specimen and sutures in other specimens (e.g. ZPAL V. 39/482; Fig. 4G), as well as to the described sutures of *Condorchelys antiqua* (see Cerda *et al.* 2015). Below, the visceral cortex and the visceral half of the spongiosa show no signs of a suture. Another possible remainder of a suture is visible distally to

the one described above. It is marked by a shallow hole in the bone surface, and below it a primary bone oriented in a zigzag manner and entering the spongiosa is present.

The second longitudinal section (Fig. 2H) crosses the same suture visible macroscopically as the first longitudinal section described above, but there is no canal crossing the external cortex (although this may be caused by the crushing of the external cortex). A putative zigzag structure with suture-like layout of growth marks corresponding to the suture visible on the bone surface is present in the spongiosa in the form of three oval openings arranged in one row, one below another. This identification is further supported by the fact that those openings are surrounded by primary bone tissue. There is a second possible suture in the section, further distally, preserved as a canal running at an acute angle to the front of metaplastic ossification on the external bone surface (i.e., parallel to the long axis of the costal, around the interface of the predominantly metaplastic tissue and the striated costal exposed more distally; Fig. 2H, J) in the external cortex. The terminal part of the canal is already closed, but a hole is preserved on the bone surface, which corresponds to the canal. Based on the CT images, the canal is sub-circular in cross-section and part of a continuous, sparsely branching, primarily longitudinal network restricted to the external part of the bone (Fig. 2A, B). It differs from typical vascular canals observed in this and other sectioned specimens in its greater circumference. It is furthermore floored by parallel-fibered bone and roofed by primary bone tissue with coarse ISF, which distinguishes it from the surrounding intertrabecular spaces and secondary canals, which are lined by lamellar bone. A comparable large, sublongitudinal vascular canal is also observed at the interface between the carapacial dermal mosaic and the underlying costal in ZPAL V. 39/20 (Szczygielski & Sulej 2019) and on the visceral surface of the supernumerary carapacial ossification ZPAL V. 39/417, as well as between the dermal ossifications of ZPAL V. 39/482 (Fig. 3H). In some isolated costals (ZPAL V. 39/19, ZPAL V. 39/239) similar vascularization is visible externally, but this may result from surficial damage or erosion and is exceedingly rare, based on the sample of over 100 collected isolated costals and costal-including shell fragments of *Proterochersis porebensis*. Comparable large, pipe-like canals (vascular spaces) are also present in peripherals and other carapacial bones of the Late Cretaceous meiolaniform turtle, *Trapalcochelys sulcata* Sterli, Fuente & Cerda, 2013, but are apparently absent or very uncommon in other species (Sterli *et al.* 2013). The spongiosa below the canal is not preserved well enough to detect any possible zigzag structure. In the section there are also present at least two conspicuous microstructural patterns relatable to closed sutures, in the middle part of the sectioned area, as indicated by the zigzag organization of the tissue and acute to perpendicular to the bone surface canals already closed in the external cortex.

The CT images of ZPAL V. 39/480 (Fig. 2A, B) reveal that the abovementioned structures observed histologically are not continuous along most of the specimen and much of the interior of the bone is remodeled into secondary spongiosa – a process also responsible for obliteration of typical shell sutures. This makes their interpretation difficult, as they may either represent microstructural cues concerning the presence of the carapacial mosaic (compare with Szczygielski & Sulej 2019) or they may represent peculiarities of shell histogenesis at its early evolutionary stages. As stated above, the identification of initial positions of sutures based on microstructural features is extremally difficult in *Proterochersis porebensis*, and thus the interpretation presented here requires caution, although the structures observed in ZPAL V. 39/480 are comparatively prominent in their uniqueness.

To check the relative incidence of ankylosis, a sample of shells and shell fragments of *Proterochersis porebensis* of varied sizes identifiable as carapaces and/or plastra was examined. Out of 364 specimens identifiable as carapaces or carapace fragments, 93 preserve sutures, 101 are clearly ankylosed, and 170 are too fragmentary to confirm whether sutures were retained or not. In the sample of 93 plastra or plastral fragments, 35 specimens are fully ankylosed, two show what appears to be closed but not fully obliterated sutures, 17 have sutures present, and 39 are too fragmentary to tell. In the case of the too fragmentary, "ambiguous" group, most specimens may, however, be still relatively safely speculated to be parts of ankylosed individuals due to their significant thickness and breaks occurring close to the places, where the sutures would be expected inferred from topology. Based on observations of suture retaining specimens from Poręba as well as other turtle fossils, during decomposition the shells tend to fail along the suture lines rather than right next to them. Although the taphonomic characteristics of the Poręba site led to many specimens being broken regardless of sutures, in general the suture retaining elements do not show extensive edge damage resembling that observed in the "ambiguous" specimens. Despite the smaller sample size, the trend towards ankylosis is even more pronounced in *Proterochersis robusta*: out of 24 carapace specimens ("*Chelytherium obscurum*" Meyer, 1863 specimens counted individually, see Szczygielski 2020), 11 are completely ankylosed, two exhibit not ankylosed or only partially ankylosed but closed sutures (traceable under magnification due to different color of mineralization or microstructural cues, in some cases only if the external cortex is damaged, but not three-dimensional), three retain open sutures, and ten are too fragmentary to tell. Out of 12 plastral specimens, seven are completely ankylosed, three exhibit not ankylosed or only partially ankylosed but closed sutures, and five retain open sutures. SMNS 16442, SMNS 17755, and SMNS 18440 are classified into two groups (SMNS 16442 both for carapace and plastron, SMNS 17755, and SMNS 18440 only for the plastron), because they present both closed but unankylosed and open sutures externally and viscerally, respectively (Szczygielski & Sulej 2019). Note that also in *Proganochelys quenstedti* the plastron seems to retain sutures more frequently than the carapace (Gaffney 1990).

Scute sulci

Scute sulci are cross-sectioned in ZPAL V. 39/28, ZPAL V. 39/61, ZPAL V. 39/68, ZPAL V. 39/392, ZPAL V. 39/401, and ZPAL V. 39/479. The tissue in their proximity is a normally

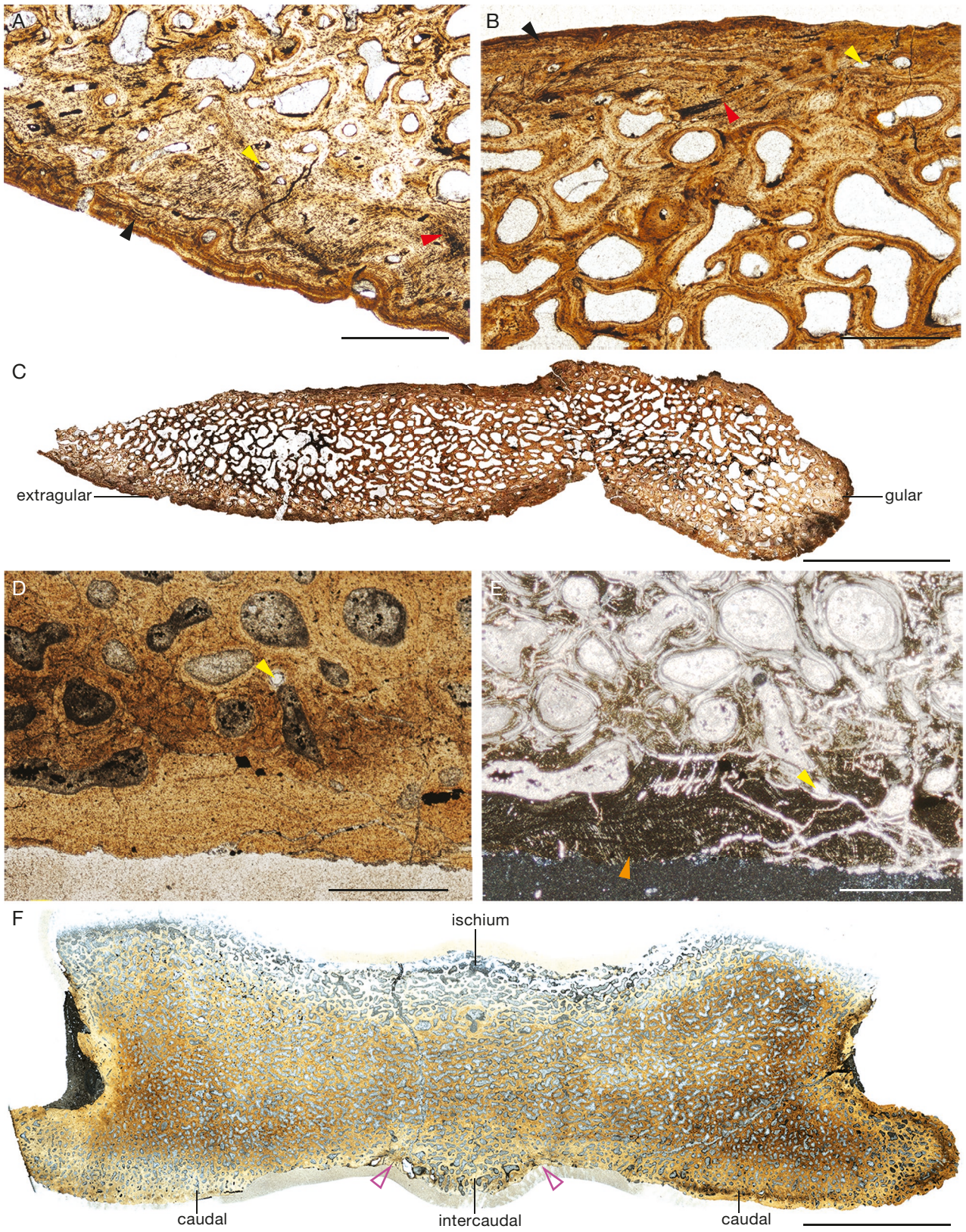

FIG. 8. — Microstructure of the gular and caudal plastral elements of middle-sized individuals of *Proterochersis porebensis* Szczygielski & Sulej, 2016: **A**, **B**, external cortex of the gular (epiplastron) and extragular projections (extragular ossification) of ZPAL V. 39/388 in normal transmitted light; **C**, bone microstructure of the whole anterior plastron fragment ZPAL V. 39/388 composed (right to left) of the entoplastron, epiplastron, and extragular ossification; **D**, **E**, the external cortex of the caudal ossification of ZPAL V. 39/68: **D**, in normal transmitted light; **E**, polarized light; **F**, bone microstructure of the whole posterior plastron fragment ZPAL V. 39/68 composed of the ischia (dorsally), caudal (ventrolaterally) and intercaudal (ventromesially) ossifications in normal transmitted light. Note the complete absence of sutures in **C** and **F**. Arrowheads: **red**, ISF; **yellow**, primary canals; **black**, growth marks; **orange**, parallel-fibered bone; **purple outlines**, areas where sutures are expected based on topology and comparisons with other turtles. Scale bars: A, B, 1 mm; C, F, 1 cm; D, E, 0.5 mm.

structured primary dermal bone with ISF, homogenous with the remainder of the cortex, and shows no marks of a drift or other clear forms of remodeling.

Aberrant partitioning

Although most isolated elements identifiable as parts of the dermal carapacial mosaic give little clue about their initial position within the shell and their exact development is uncertain, at least one specimen, ZPAL V. 39/493 (Fig. 9), appears to be an abnormally transversely partitioned costal plate with protruding distal part of the rib. This specimen presents a typical external and visceral texture, and bears a sinuous (undulating) sulcus characteristic for *Proterochersis* spp. (Szczygielski *et al.* 2018), leaving little doubt concerning its taxonomic provenance. Based on personal examination of most Triassic turtle specimens in the world, including all the osteological material of Proterochersidae, despite an unusual sutural alignment, we cannot find a better morphological fit for that specimen than a distal part of a costal. The plate has sutural edges all around, the sutures are easily distinguishable morphologically from damaged parts of its perimeter and a transverse break crossing the middle of the specimen. Both the plate and the rib-like ridge on the visceral surface end in a well-developed sutural surface bearing a reticular pattern of thin bony lamellae perforated by small vascular canals (Fig. 9E). The morphology of the sutures is relatively uniform around the specimen, with locally more parallel organization of the lamellar-shaped protrusions, consistent with typical morphologies observed in shell sutures of *Proterochersis porebensis* and other turtles (Szczygielski & Sulej 2019). The spacing between the protrusions is smaller than between the trabeculae exposed in the broken part of the plate. The plate is relatively wide (4.7 cm), so if its identification as a costal is correct, it would likely originate from a middle-sized individual.

DISCUSSION

Mode of life

The studies of the shell bone histology of turtles reveal that the shell microstructure is, to an extent, correlated with the environment in which they live, although it is also impacted by other factors and thus any inferences based on the correspondence between the microstructure and habitat must be treated with caution (Scheyer & Sander 2007; Scheyer *et al.* 2014; Janello *et al.* 2020). The shells of modern terrestrial turtles usually show diploe structure (cancellous bone), well-defined cortexes, low vascularization of the external and visceral cortex, ISF in the external and parallel-fibered bone in the visceral cortex, and short and thick bone trabeculae of the cancellous bone (Scheyer & Sander 2007; Janello *et al.* 2020). Aquatic turtles commonly present two types of shell bone microstructure, regarding their pelagic or neritic occurrence (Scheyer *et al.* 2014; Janello *et al.* 2020). The shell bones of semi-aquatic, mainly aquatic, or freshwater species have the diploe structure framed by thick external and thin visceral cortex, well-vascularized external cortex with ISF, parallel-fibered bone in the visceral cortex vascularized by primary vascular canals, and the cancellous bone built of bony trabeculae of variable thickness and length, with interstitial ISF in non-remodeled areas of branching (Scheyer *et al.* 2014; Janello *et al.* 2020). Finally, the pelagic species have a homogeneous shell bone microstructure. The cortices are greatly reduced or absent, the external and visceral cortex (if present) strongly vascularized, composed of bone tissue with ISF and parallel-fibered bone, respectively. Their cancellous bone is usually composed of long and slender bony trabeculae (Scheyer & Sander 2007; Houssaye 2013; Scheyer *et al.* 2014; Janello *et al.* 2020). The earliest (Middle Jurassic) uncontroversial aquatic turtles (*Eileanchelys waldmani* Anquetin, Barrett, Jones, Moore-Faye & Evans, 2009 and *Heckerochelys romani* Sukhanov, 2006) show shell bone microstructure like the neritic species, but their external and visceral cortices are of comparable thickness, similar as in tortoises (Scheyer *et al.* 2014).

The microstructure of the plastron of the Late Triassic *Proterochersis robusta* was described to have a diploe structure with short and robust bony trabeculae in the cancellous bone and cortices comparable in thickness and poorly vascularized (Scheyer & Sander 2007). It was considered indicative that *Proterochersis robusta* was a terrestrial turtle, together with other Late Triassic (*Proganochelys quenstedti*, *Palaeochersis talampayensis*) and Early Jurassic (*Australochelys africanus* Gaffney & Kitching, 1994, *Kayentachelys aprix* Gaffney, Hutchison, Jenkins & Meeker, 1987) species (Jaekel 1916; Gaffney 1990; Joyce & Gauthier 2004; Scheyer & Sander 2007; Scheyer *et al.* 2014; Lichtig & Lucas 2017; Lautenschlager *et al.* 2018; Dziomber *et al.* 2020); nonetheless some ambiguity and possible semi-aquatic or aquatic signal was noted for *Proterochersis robusta* (Benson *et al.* 2011; Lichtig & Lucas 2017; Dziomber *et al.* 2020). The published photographs of polished transverse sections through costals of *Chinlechelys tenertesta* appear to be dense and compact (Lichtig & Lucas 2021), but without proper histological approach any interpretations of shell microstructure of that turtle are dubious.

In contrast to the turtles sampled so far, the costals of *Proterochersis porebensis* do not share the same structure with the plastral bones. Aside from the fragments located deep relative to dermis, which formed attachments for muscles and/or body wall structures (proximal parts of costals, visceral surface of the nuchal bone), both the external and the visceral cortices of the carapacial bones are of similar thickness and incorporate ISF. This contrasts with parallel-fibered bone in the visceral cortex of the plastron. Moreover, the spongiosa of the carapace is composed of less compacted trabeculae, longer and slenderer than the trabeculae building the spongiosa of the plastral bones. The presence of ISF in both the external and visceral cortex was found also in the costals of the Miocene pleurodire *Stupendemys geographicus* Wood, 1976 and the Cretaceous meiolaniform *Trapalcochelys sulcata*, as well as in the neurals and, variably, peripherals (but not costals) of a Jurassic stem turtle *Condorchelys antiqua* (see Scheyer & Sánchez-Villagra 2007; Sterli *et al.* 2013; Cerda *et al.* 2015). Although the inclusion of the ISF within the visceral cortex is indicative of an unusual thickness of the integument, which

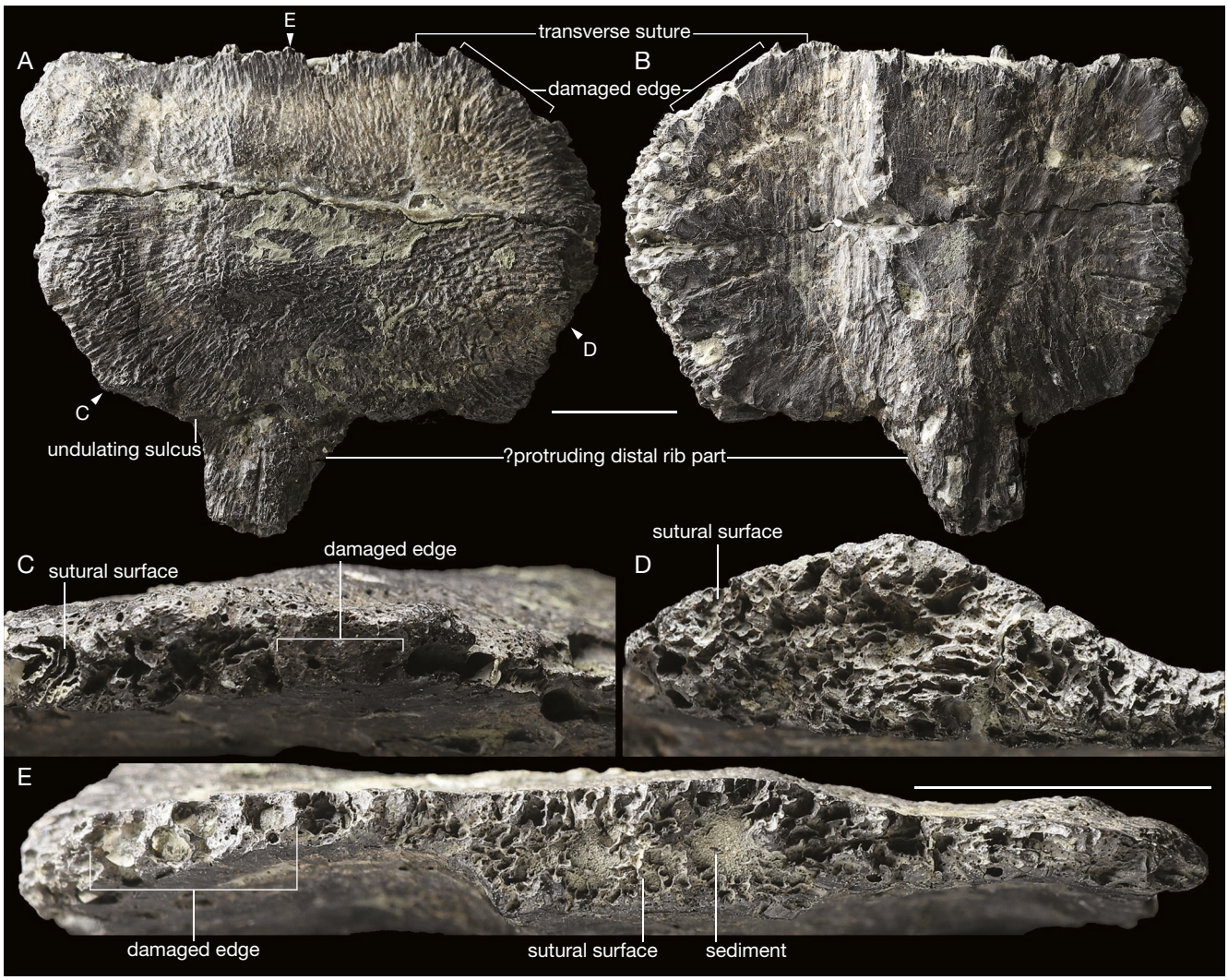

Fig. 9. — *Proterochersis porebensis* Szczygielski & Sulej, 2016 ZPAL V. 39/493, a carapacial element possibly representing a transversely partitioned costal: **A**, external view; **B**, visceral view; **C**-**E**, close-ups of the edges indicated by letters in **A**. Scale bars: 1 cm.

completely embedded these elements, little is known about its correspondence with lifestyle or function of these animals. The differences in the carapace microstructure of *Prot. porebensis* compared to terrestrial turtles support the semi-aquatic lifestyle as indicated by supposed turtle bromalites found in Poręba, the type locality of that species (Bajdek *et al.* 2019). It is unknown whether the visceral carapacial cortex incorporated ISF in *Prot. robusta* as well, because the only carapacial fragment sampled thus far is a peripheral which lacked the visceral surface (Scheyer & Sander 2007).

The structure of the plastral bones in the large individuals of both *Proterochersis porebensis* and *Prot. robusta* (see Scheyer & Sander 2007) is similar as in terrestrial turtles. However, in the small individuals of *Prot. porebensis*, the external cortex is highly vascularized, and the cancellous bone is built of bony trabeculae of variable thickness. The same changes in the external cortex vascularization and slenderness of the bony trabeculae in the cancellous bone between large and small individuals of *Prot. porebensis* can be noticed also in the costals. However even in large individuals, the cancellous bone is not so dense as in the plastral bones of *Prot. porebensis* and the shells of the terrestrial turtles. Thus, because the structure of the shell of the small specimens of *Prot. porebensis* share the porosity with the earliest aquatic turtles (compare with Scheyer *et al.* 2014), it is possible that they lived in similar aquatic environment. More mature individuals appear to be more terrestrial, as indicated by the lower vascularization and denser cancellous bone. This change in ontogeny suggests that the observed microstructural patterns are not constrained by the early evolutionary stage of carapacial bone histogenesis in proterochersids (e.g. inability to form a denser, less vascularized dermal tissue due to phylogenetic ancestry), but indeed reflects the environmental adaptations, although obviously some other than environmental factors cannot be completely refuted. Even though the functionally-driven microstructural characteristics tend to overcome the systematic patterns in the shell microstructure of stem turtles (e.g. Scheyer *et al.* 2014; Janello *et al.* 2020), exceptions do exist and additional data should accompany and inform any microstructure-based ecological inferences (Janello *et al.* 2020, Sterli *et al.* 2021).

Histology in relation to element homology

The sections in general reveal no striking differences in histology and microstructure dependent on the morphogenetic origin and homologies of the elements (for detailes review of shell element homology see Szczygielski & Sulej 2019 and references therein). The costals and neurals ossifying in connection to endoskeletal elements are histologically no different from presumably osteodermal elements (peripherals, supernumerary ossifications) and homologues of the pectoral girdle (epiplastra, nuchal bone). Some differences were observed mostly in the gastralia-derived plastron (more pronounced remodeling, limited inclusion of ISF in the visceralmost layers (Fig. 7B, D, F), thicker bony trabeculae of the spongiosa, differences in vascular pattern) but overall, the varying characteristics (e.g. degree of vascularization of the external cortex, general density, presence of ISF in the visceral cortex) seem to be mostly dependent on either topology, ontogenetic stage, or vary seemingly randomly between individuals; some other factors, such as sex or seasonal variability cannot be refuted. Any potential differences may be obscured by remodeling and incorporation of the cortices into the spongiosa. For example , the ischium in ZPAL V. 39/68 is nearly completely remodeled, so its exact boundaries cannot be deduced even from the primary matrix (Fig. 8F).

Some differences of the length and density of the ISF are observed in the external cortices of the sectioned costals (Figs 1; 2). These differences may partially result different location within the carapace or ontogeny, but also seem to be correlated with different planes of sectioning (transverse versus longitudinal), and possibly with the position of these planes along the particular costals. The transverse sections of ZPAL V. 39/20, ZPAL V. 39/477, and ZPAL V. 39/480 (Figs 1F; 2E, H) show relatively few short and angled fibers while the longitudinal sections of ZPAL V. 39/2 and ZPAL V. 39/480 (Figs 1A; 2F, G) have more pronounced, interweaving fibers. In addition, the sections through distal parts of costals ZPAL V. 39/20 (transverse) and ZPAL V. 39/480 (both transverse and longitudinal) with smoother or longitudinally striated external sculpture present less abundant and more organized, sub-parallel fibers than the portions with normal, rugose external sculpturing (including the proximal parts of ZPAL V. 39/480 – both transverse and longitudinal sections). Although the structural fiber direction somewhat varies, it seems to be to a large extent sub-longitudinal (at low angles relative to the long axis of the bone), and at least in the distalmost part of ZPAL V. 39/480 the tissue is best classified as parallel-fibered bone, without or with minimal dermal metaplastic contribution (Ignacio Cerda 2021, pers. comm.; Fig. 2I). In that respect it is similar to the short and angled fibers documented in transversely sectioned *Pappochelys rosinae* Schoch & Sues, 2015 ribs (Schoch *et al.* 2019). It was proposed that those fibers in the latter species may represent an initial stage of metaplastic ossification and fibrous connections between neighboring ribs (Schoch *et al.* 2019). However, a similar image of the external cortex is also at least locally present in the transverse sections of *Proterochersis porebensis* costals despite the firm sutural connections between them and evident metaplastic ossification in most specimens. Ribs in *Pap. rosinae* and the distal end of ZPAL V. 39/480 exhibit external ornamentation (particularly in large individuals) which may be indicative of some dermal (metaplastic) contribution (Schoch & Sues 2015, 2017). In addition, at least in some stem turtles, such as *Condorchelys antiqua*, the tissue of the external cortex locally exhibits features intermediate between the metaplastic, ISF-incorporating dermal bone and parallel-fibered bone, or even more resembling the latter, making distinction difficult (Cerda *et al.* 2015; Ignacio Cerda 2021, pers. comm.). Given this difficulty and the differences noticed in *Prot. porebensis*, the observed morphology of the fibers in *Pap. rosinae* may thus not necessarily demonstrate the complete lack of metaplastic ossification in that animal, but instead be an effect of visual underrepresentation of the structural fibers caused by the transverse sectioning plane. Longitudinal thin sectioning, therefore, would be advised. On the other hand, if correctly interpreted, the lack of metaplastic contribution in the wide, distal end of the costal ZPAL V. 39/480 would be incongruent with the interpretation of Lichtig & Lucas (2021), who consider the costal plates completely metaplastic and homologically separate from the underlying narrow rib shafts.

Remodeling of the middorsal ridge

A peculiarity of *Proterochersis* spp. is the presence of a well-defined, middorsal ridge surrounded by lateral troughs, which disappeared later in life, in supposedly juvenile individuals (Szczygielski *et al.* 2018). This structure is covered by a histologically normal external cortex in the supposed juvenile ZPAL V. 39/2. Given the mode of ossification observed in *Proterochersis porebensis* and other turtles, with new layers of cortex deposited externally, and older layers resorbed and turned into spongiosa internally, the lateral troughs seem to be simply filled with bone tissue during ontogeny. Unfortunately, no information can be inferred about the shape of the overlying scutes. Based on the rugose external surface of the middorsal ridge and associated structures, the same as on the remaining surface of the carapace, Szczygielski *et al.* (2018) suggested that the vertebral scutes in juveniles of *Proterochersis* spp. reflected the shape of the underlying neurals, i.e., that the ridge and troughs were expressed externally, and gradually leveled out during ontogeny due to periodic decornification or scute shedding. The middorsal ridge lacks Sharpey's fibers that could confirm close association with the scutes, but the sectioned specimen lacks Sharpey's fibers anywhere on its costals and neurals. These scenarios thus cannot be unambiguously confirmed nor refuted based on available data.

Suture morphology, ankylosis, and shell growth

One of the most unusual characteristics of the Triassic turtles is the frequent ankylosis (Pritchard 2008). This was documented by Gaffney (1990) for all but the smallest (supposedly youngest) specimen of *Proganochelys quenstedti* (even including the probable subadult), by Sterli *et al.* (2007, 2021) for the australochelyids *Palaeochersis talampayensis* and *Waluchelys cavitesta*, and by Szczygielski (2020), Szczygielski & Sulej

TABLE 2. — Comparison of the cavitated peripheral structures in australochelyids (represented by *Waluchelys cavitesta* as documented by Sterli *et al.* (2021)) and proterochersids (represented by *Proterochersis porebensis* Szczygielski & Sulej, 2016 ZPAL V. 39/482).

		Waluchelys cavitesta Sterli, Martínez, Cerda & Apaldetti, 2020	***Proterochersis porebensis*** Szczygielski & Sulej, 2016
Internal peripheral cavity		Present	Present
Diploe-structured bone		Present	Present
External cortex	Interwoven structural fibers	Present	Present
	Vascularization	Poor to avascular	Poor
	Growth marks	Present	Present
Spongiosa thicker than the cortices		Present	Present
Perimedullary cortex	Interwoven structural fibers	Present	Present
	Structural stratification	Local	Local
	Vascularization near the spongiosa	Poor to avascular	Poor to avascular
	Vascularization near the medullary cavity	Better than in the external cortex	Better than in the external cortex
	Growth marks	Close to the spongiosa	Present
Sutures		Absent	Present
Tendency for complete shell ankylosis		Yes	Yes

(2016, 2019), and Szczygielski *et al.* (2018) for the proterochersids *Proterochersis robusta*, *Prot. porebensis*, and *Keuperotesta limendorsa* Szczygielski & Sulej, 2016. Interestingly, however, the sutures are present in some specimens of these taxa, which revealed a very unconventional, mosaic-like shell composition in the latter group carapaces. This study further documents that the sutures commonly ankylosed early, in small and morphologically juvenile specimens of *Prot. porebensis*, such as ZPAL V. 39/2 (Szczygielski *et al.* 2018), leaving no clues about the initial composition of the shell, but are also clearly present in some larger specimens. The process of the obliteration of sutures is relatively easily explained by their complete ossification and subsequent resorption of the compacta and formation of spongiosa in its place, as this process typically occurs in tetrapods (Bailleul *et al.* 2016; Nikolova *et al.* 2017). The ankylosis in individuals of varied sizes, including the small supposed juveniles, is nonetheless problematic from the developmental point of view, as the sutures are the main areas of shell growth in modern turtles, and their obliteration effectively ends the growth stage of the animal (Pritchard 1979, 2008; Kuchling 1999; Legler & Vogt 2013). Given the apparently thick dermis, as indicated by the presence of ISF within both the external and visceral cortices, nearly complete lack of secondary osteons in the externalmost and visceralmost layers of the external and visceral cortices, and low observable number of growth marks even in large carapacial fragments, it seems likely that the typical process of constant, concurrent bone apposition on the surfaces and internal resorption was the main mode of carapacial bone development in *Proterochersis porebensis*. Based on that assumption, the shell could hypothetically, albeit with limited efficiency, grow and keep its geometry after the ankylosis mainly by means of remodeling with little evidence observable in the cortices, thanks to the intensive incorporation of their older, inner layers into the spongiosa and the retained layers of the cortices being at most a few seasons old. Secondary remodeling is evident in large specimens of *Stupendemys geographicus*, which shares with *Proterochersis porebensis* and *Trapacochelys sulcata* the presence of interwoven structural fibers in the visceral cortex of carapacial bones (Scheyer & Sánchez-Villagra 2007; Sterli *et al.* 2013) and tendency for ankylosis of some (albeit not all, even in the largest specimens) sutures (Wood 1976; Cadena *et al.* 2013). In contrast, however, the presence of sutures in other, middle-sized and large specimens can only be explained either by large intraspecific variation of adult size (including sexual dimorphism), extremely varied suture retention throughout life, or their reformation during life as a result of localized shell decalcification (both with no direct analogues in modern turtles and thus debatable) or as a response to common shell damage (but see below).

Sexual dimorphism expressed as size differences between the males and females is common in turtles (e.g. Berry & Shine 1980; Pritchard 2008; Leuteritz & Gantz 2013; Cordero 2018). It was also discussed previously for *Proterochersis* spp. as a possible explanation for the unusual pattern of shell ankylosis, but since the ankylosis is expressed by individuals representing nearly the full spectrum of sizes (including some of the smallest individuals) rather than distributed bimodally (signifying terminal sizes for each of the sexes), this hypothesis appears unsatisfactory (Szczygielski *et al.* 2018; Szczygielski & Sulej 2019). Furthermore, two forms of potentially dimorphic characters of the plastron (long and spiky versus short and rounded caudal processes) lack correspondence with the presence or absence of ankylosis (Szczygielski *et al.* 2018). A more generalized, non-sexually dimorphic variability of adult sizes is another possibility. In such a case, ankylosed individuals would always be adults, regardless of their size, which could vary widely, e.g. as an effect of developmental plasticity, with no bimodal distribution. This hypothesis, however, is refuted by the fact that the smallest ankylosed individuals exhibit a number of characteristics interpreted as juvenile, such as the lack of protruding anterior marginals, gulars, extragulars, and caudals, a different morphology of scute sulci, or the presence of the middorsal carapacial ridge (Szczygielski & Sulej 2016; Szczygielski *et al.* 2018). This small, morphologically different morphotype cannot be considered a form of sexual

dimorphism due to its uncommonness compared to larger, adult- or subadult-like morphotype (in contrast to the ratio approaching 1 : one expected for sexual morphs) and the record of intermediate morphologies between the morphotypes best interpreted as gradual ontogenetic changes (Szczygielski & Sulej 2016; Szczygielski *et al.* 2018). Finally, ankylosed individuals interpreted as subadults based on their morphology are known for both *Proterochersis porebensis* and *Proganochelys quenstedti* (see Gaffney 1990; Szczygielski & Sulej 2016). In summary, not all of the ankylosed individuals can be considered adults and represent advanced developmental stages for which the ankylosis would be expected.

While some sutures can ankylose prematurely in extant turtles, this is an abnormality usually leading to shell malformations, and complete ankylosis occurs physiologically only in mature specimens of some species, with most taxa retaining sutures throughout life (Pritchard 1979, 2008; Kuchling 1997; Rothschild *et al.* 2013). Very few species, such as the American box turtles, ankylose relatively early, although in those species the early ankylosis seems to be regular and heterochronic rather than result from unusually varied timing, and occurs normally around or after maturation (Pritchard 1979, 2008; Kuchling 1997). At least in some taxa this can be explained as an adaptation protecting against forms of damage common in their environment (e.g. trampling), as a trade-off between the shell rigidity and growth capabilities (Kuchling 1997, 1999).

Aside from programed suture obliteration at maturity and physiological disorders, a premature partial or complete ankylosis can occur in modern turtles due to damage, as an effect of imperfect, but extraordinary shell regeneration potential observed in these animals (Gadow 1886; Danini 1946; Woodbury & Hardy 1948; Smith 1958; Legler 1960; Rose 1986; Kuchling 1997, 1999; Martínez-Silvestre & Soler-Massana 2000). In cases of superficial damage, the keratinous scutes are shed, the necrotic and damaged bone tissue around the wound is separated via localized osteoclastic bone resorption across the spongiosa, a new keratinous layer is formed below the sequestrum, and finally the bone is reconstructed (Legler 1960; Kuchling 1997, 1999). In those cases the remaining visceral parts of the elements (and, indirectly, the connections to the axial skeleton) seem to organize and dictate the pattern of re-ossification, so the layout of bony elements remains generally the same (with possible minor aberrations), and in most species the layout of scutes is completely reconstructed (although some additional intercalary scutes may appear; Kuchling 1997, 1999). Deeper damage, leading to complete necrosis of carapacial bones, causes the same general reaction, but whole bony elements are ejected by the new corneous and bony layers developing underneath, and eventually lost, usually after several months, but in some cases after several years (Gadow 1886; Smith 1958; Legler 1960; Rose 1986; Kuchling 1997, 1999; Martínez-Silvestre & Soler-Massana 2000). In extreme cases, such as wildfires, even a complete new carapace may be reformed inside of the older, necrotic one (Rose 1986). This reconstruction is less perfect than in the case of more superficial damage: the visceral layer of the carapace is ankylosed, with normal sutural pattern only present in the proximal part of the costals, the external layer partitioned into numerous irregular ossifications (Rose 1986), and the keratinous scute pattern lost; instead, the whole shell is covered by a continuous keratinous layer (Rose 1986; Kuchling 1997, 1999). The shed necrotic bones even in cases of severe burns were reported to be externally indistinguishable from unaffected bones of dry specimens, albeit they may in time become smooth and shiny as a result of their prolonged exposure to wear and weathering (Legler 1960). According to Rose (1986), their visceral surface is rough and pitted due to the exposure of the spongiosa and loss of contact with the ribs and vertebrae; possibly, the morphology differs depending on the damage. Interestingly, this general mechanism appears in turtles to be an universal response to damage caused by mechanical (predation, falls, crushing, scratching), thermal (fire, cold), chemical, and biological (fungal and bacterial infections) factors, and possibly malnutrition or metabolic disorders (Gadow 1886; Kuchling 1997; Martínez-Silvestre & Soler-Massana 2000; Nevarez *et al.* 2008), and widely scalable depending on the severity of injury. Unfortunately, the details of that process are poorly understood, the only histological studies thus far, severely limited in scope, being that of Gadow (1886) and Danini (1946) who observed regeneration of mechanically damaged carapaces.

According to Kuchling (1997), the extraordinary regenerative potential may be plesiomorphic for Testudinata. The selection pressure for development of such regeneration mechanisms during the Late Triassic seems high and may be closely linked to the pressure towards consolidation of incipient non-testudinate pantestudinate shells into solid, study constructions. The Late Triassic was the time of migration of largely aquatic pantestudinates (Li *et al.* 2008, 2018; Schoch & Sues 2015; Schoch *et al.* 2019) into a semi-aquatic or more terrestrial setting (Joyce & Gauthier 2004; Scheyer & Sander 2007; Lichtig & Lucas 2017; Lautenschlager *et al.* 2018; Bajdek *et al.* 2019; Dziomber *et al.* 2020), in which they were likely less mobile and more vulnerable. At the same time happened the evolutionary radiation of dinosaurs and other archosauromorphs, including large carnivorous species. These forms cooccurred with the earliest turtles and their remains are also found in Poręba (the locus typicus of *Proterochersis porebensis*) and Kocury (where the same or closely related turtle species lived; Sulej *et al.* 2012; Niedźwiedzki *et al.* 2014; Skawiński *et al.* 2017; Bajdek *et al.* 2019; Czepiński *et al.* 2021). In addition, the Late Triassic was the time of increased incidence of wildfires compared to the Early and Middle Triassic, and the charcoal finds document not only surface, but even crown fires in the areas around the Poręba's paleonvironment (Kubik *et al.* 2015). Modern tortoises and semiaquatic turtles are susceptible to fires, which may affect large parts of their population, and despite high death rates many individuals are able to survive, often with extensive injuries to the shells, sometimes right next to the scars from previous seasons (Babbitt & Babbitt 1951; Kuchling 1997; Harris *et al.* 2020). The ability to regenerate is thus pivotal, particularly for long-living animals.

Therefore, it seems likely that similar regeneration mechanisms were already present (or developing) in the Triassic, and that programmed shell ankylosis could occur early in life (or even variably, due to imprecision of early developmental pathways or spotty distribution of their variants within the populations at those early stages of evolution) as a countermeasure against, e.g. predation. Several observations, however, are not completely congruent with this view. Firstly, given the uneven growth rate of ankylosed and non-ankylosed individuals, a significant variation of the time of shell ankylosis within the population should logically lead to widely varied body sizes of individuals exhibiting comparable ontogenetic stages of development (i.e., decoupling of the individual size and morphological characteristics, such as scute prominence, ossification advancements of limbs and girdles, etc.), which is not the case in the observed samples (Gaffney 1990; Szczygielski *et al.* 2018). On the contrary, many specimens of *Proterochersis* spp. with preserved sutures can be classified as middle-sized or small, and thus are not generally larger, nor differ significantly in morphology from similarly sized ankylosed individuals (Szczygielski *et al.* 2018). Secondly, there are not many signs of predation or other damage on the known specimens of *Proterochersis* spp. Thirdly, there is no evidence of only partial shell ankylosis which should be common in cases of localized damage. Although fragmentary specimens give limited insight, virtually always the sutures are either observable or seem completely absent and no specimen composed of several fused bones but with sutural edges around them was found. The only partial exception are *Proterochersis robusta* SMNS 16442, SMNS 17755, and SMNS 18440, in which the carapacial and/or plastral sutures are closed (but not obliterated) externally, but some of them are open viscerally (Szczygielski & Sulej 2019). This, however, may reflect the normal process of sutural closure progressing viscerally from the exterior. As already noted, the sutures are also more frequently retained in the plastron than in the carapace (Szczygielski & Sulej 2019). A more common retention of plastral and interperipheral sutures compared to other carapacial sutures was also noted in *Proganochelys quenstedti*, but this as well appears to document a natural progression of suture obliteration rather than an effect of local damage (Gaffney 1990). Fourthly, extensive damage to the shell which results in its complete ankylosis in modern turtles and could lead to the reconstruction of shell surface, possibly obliterating surficial traces, involves scute destruction and loss of their normal pattern (Rose 1986; Kuchling 1997, 1999). This is not observed in any representative of *Proterochersis* spp. (Szczygielski *et al.* 2018).

Considering these observations, a hypothetical mechanism of suture reformation in already ankylosed shells is intriguing, if only speculative. If the mechanisms of bone resorption and regeneration, which are utilized to reform shells in injured and burned extant turtles, were indeed already present or evolving in the Triassic, when the turtle shell developed, then hypothetically they could be co-opted or, perhaps, even plesiomorphically utilized to periodically reform already ankylosed sutures, explaining their varied occurrence in specimens of various sizes and ontogenetic stages, and allowing a normal growth. General mechanisms that allow localized and coordinated resorption of already deposited bone are present in turtles and other vertebrates, and although they usually follow the pre-existing sutures, their application to already ankylosed shells is worth discussing.

Seasonal, reproduction-related local de-ossification of the plastron (Pritchard 1979, 2008) in males (aiding mounting the convex carapaces of females and copulation) and annual demineralization of the femur (mostly trabeculae and, to a lesser extent, the cortex; Suzuki 1963) occur in some modern turtles, but not in the carapaces. Noteworthy in that context is the observation that in some of our sectioned specimens, such as the large ZPAL V. 39/61, the trabeculae within the carapace are particularly slender, presenting a nearly osteoporotic appearance, hypothetically suggesting that on the earliest stages of shell evolution it could also serve as a calcium reservoir for eggshell formation. Furthermore, the process of localized demineralization is exhibited, in some cases seasonally, by several turtle taxa during development of shell kinesis (Pritchard 2008; Legler & Vogt 2013; Cordero *et al.* 2018). Selective resorption of specific already ossified ribs and neural arches with retention of periosteal sheath and concurrent development of costal plates occurs in *Malacochersus tornieri* (Siebenrock, 1903) normally during ontogeny (Procter 1922). Mautner *et al.* (2017) furthermore noted a better development of some costals in smaller than in larger individuals of that species, although it is unknown whether this results from their resorption during ontogeny or simply intraspecific variation. Appearance of additional ossifications in carapaces of *Graptemys* spp. was reported by Newman (1906) and explained by partial resorption of bone due to starvation. Development of similar additional ossifications in shells of *Chelus fimbriatus* (Schneider, 1783) during ontogeny, in some cases connecting to the underlying bone in suture-like fashion, in others described as partially fused or resorbed, was noticed by Hay (1922, 1929). Although Szczygielski & Sulej (2019) noted differences in shape, layout, number and interaction with the normal bones of the shell between these ossifications and the dermal carapacial mosaic present in *Proterochersis* spp., some underlying developmental mechanisms may be homologous. Sterli *et al.* (2021) recently proposed a mechanism of cavitation of peripheral bones via localized resorption of already deposited dermal bone. Finally, osteoclastic separation of a bone layer surrounding injury occurs routinely in carapace regeneration (Gadow 1886; Danini 1946; Kuchling 1999; Martínez-Silvestre & Soler-Massana 2000).

The reformation of sutures between fused and subsequently separated bony elements is poorly documented in vertebrates but does occur. Studies on surgical removal of cranial synostoses in mammals document that at least in some cases the bone redeposition after the procedure leads to reformation of anatomically correct sutures in place of the obliterated or fused ones. Moreover, in many cases additional sutures may appear in the process, either temporarily, to be obliterated soon after, with retention of the normal layout (e.g. Mabbutt *et al.* 1979; Mossaz & Kokich 1981), or permanently (e.g.

Shillito 1973). The success in those cases, however, is dependent on the activity of dura mater (which is absent in turtle shell) and other, unrecognized factors (Shillito 1973; Mabbutt *et al.* 1979; Mossaz & Kokich 1981; Agrawal *et al.* 2006). Contrarily, the regeneration capability of the calvarium seems to be still lesser compared to that of the turtle shell, which is able to eject whole bones and reform a completely new bony layer (see above), and the predominant histogenesis of these structures is different (membrane vs metaplastic ossification). As mentioned above, regeneration of mild damage to the shell in turtles allows reformation of normal or slightly abnormal suture layouts (Kuchling 1997, 1999), and more severe incidents lead to development of ankylosed bony layer with local abnormal partitioning (Rose 1986). Physiologically or externally induced osteoclastic partitioning with subsequent re-ossification of the carapace and reformation of sutures could therefore hypothetically lead to recreation of normal or creation of semi-random, or even random patterns. This could possibly solve the problem of erratic ankylosis or lack thereof in Triassic turtles, and potentially even explain the appearance of the asymmetric carapacial mosaic in *Proterochersis* spp. (Szczygielski & Sulej 2019) and aberrant partitioning of ZPAL V. 39/493 (Fig. 9). Some studies concerning abnormal additional ossifications in the shells of modern turtles reveal that the frequency of abnormal suture layouts is positively correlated with the size of the specimen (McEwan 1982), possibly hinting at rare development of additional sutures during the life of the animal, either spontaneously or due to the extrinsic factors such as trauma. It must be kept in mind that populational observations of changes in bony shell structure over time are practically unfeasible, so other factors, such as stochastic variability, cannot be excluded. Information on that topic is extremely scarce and the cases described are not entirely comparable to the condition in *Proterochersis* spp., so this explanation remains purely speculative and highlights a potential direction for future studies.

Peripheral cavities

Sterli *et al.* (2021) and de la Fuente *et al.* (2020) described an unusual morphology of the peripherals of *Waluchelys cavitesta* and *Palaeochersis talampayensis*. They noted the presence of cavities lined with (and, in some cases, partially filled by) a layer of compact perimedullary (visceral) cortex and concluded that this unique microstructure may document an unexpected complexity of shell development and evolution. Posterior peripheral cavitation is also present in *Proganochelys quenstedti* (see Jaekel 1916; Gaffney 1990). It was thus far only studied macroscopically, and therefore the histology, microstructure, and, consequently, the precise nature of these structures is impossible to compare with those of the australochelyids. Their gross morphology (e.g. the visceral exposition of cavities in *Proganochelys quenstedti* vs lack of exposition in the Australochelyidae), however, differs and may indicate a different origin (Juliana Sterli 2021, pers. comm.). Gaffney (1990) observed that at least some of the peripheral cavities in *Proganochelys quenstedti* are more prominent in the adult than in the supposed subadult specimen, implying their deepening during ontogeny. He also noted that while some of them appear to be restricted to individual peripherals, others seem to be created at the junction of the interperipheral and costoperipheral sutures; due to ankylosis of the shells and, thus, obliteration of the sutures, he highlighted however that this interpretation must be treated as speculative. Szczygielski & Sulej (2019) hypothesized that these non-perforating, externally roofed openings between the bones forming the posterior edge of the carapace may be an indirect evidence of an external layer of supernumerary dermal ossifications comparable to those in *Proterochersis* spp. The third taxon of a Triassic turtle with possibly cavitated carapacial rim is *Chinlechelys tenertesta*. The most characteristic element attributed to that taxon comprises of a spiky, hollowed out structure composed of numerous osteoderms, which were proposed to be a part of a neck spine (Lucas *et al.* 2000; Joyce *et al.* 2009), but may in fact represent a part of the posterior edge of the carapace (Lucas *et al.* 2000; Lucas & Lichtig 2018; Szczygielski & Sulej 2019; Lichtig & Lucas 2021). If the latter is correct, the cavities in the posterior edge of the carapace of *Chinlechelys tenertesta* could resemble those in *Proganochelys quenstedti*, although the specimen is too incomplete to determine whether they were open proximally or completely enclosed by the dermal ossifications.

Herein, we presented the histology and microstructure of the nuchal region of the carapace of the fourth taxon, *Proterochersis porebensis*, which presents yet another form of peripheral cavities, presenting similarities in some aspects to those described in the Australochelyidae, but also some important differences (Table 2). In both cases the empty space (cavity) is shielded dorsally and ventrally by a diploe-structured bone and both cortices comparatively thin and incorporating interwoven structural fibers, the external cortex nearly or completely avascular, and the visceral (perimedullary) cortex of locally ordered structure and vascularization gradually increasing towards the cavity. Aside from these resemblances, there are also some differences. Firstly, Sterli *et al.* (2021) interpreted the medullary cavities of *Waluchelys cavitesta* as being resorptive in nature, with the internal cortex composed of primary tissue, while in *Proterochersis porebensis* the growth marks mostly follow the visceral surface of the visceral cortex, thus the perimedullary cortex is identical with the visceral cortex of contributing dermal ossifications. Given the dynamic resorption and new deposition of cortices observed elsewhere in *Proterochersis porebensis*, however, resorption of the walls of the cavity in later stages of its development may be plausible. Secondly, Sterli *et al.* (2021) found the cavities of *Waluchelys cavitesta* completely confined to the interior of the peripheral series. Although their complete proximal enclosure is not exactly apparent from the published material, it is corroborated by more complete specimens of *Palaeochersis talampayensis* (Juliana Sterli 2021, pers. comm.). The internal cavity of *Proterochersis porebensis* ZPAL V. 39/482 preserves a prominent opening proximally (viscerally), although its peripheral region is partially enclosed laterally by a thickening of the visceral cortex with complete posterior enclosure of a small section more laterally (Fig. 3G) which continues further anterolaterally as a branching canal separating the dermal ossifications (Fig. 3H).

At least the proximal cavity was filled in life by the first costal which is disarticulated and thus apparently did not reach into the partially enclosed region. Therefore, the cavity was likely completely surrounded by the costal, peripherals, and supernumerary dermal ossifications. The main difference between the peripheral cavities in *Waluchelys cavistesta* and *Proterochersis porebensis* ZPAL V. 39/482 is the presence of sutures in the latter, which prove that the structure is complex in nature, composed of several separate ossifications. Most specimens of *Proterochersis porebensis*, however, lack discernible sutures in the nuchal region (Szczygielski & Sulej 2016, 2019; Szczygielski *et al.* 2018), as does *Waluchelys cavitesta* and most other Triassic turtle specimens (Gaffney 1990; Sterli *et al.* 2007, 2021). Furthermore, the data presented herein indicate that at least in *Proterochersis porebensis* the shell ankylosis tends to completely remove any evidence of initial sutural layout at the microstructural level, and that the tissue bridging the suture and connecting both elements is not distinguishable from cortical primary tissue, making histological sections an unreliable tool for determination of the original shell composition in ankylosed specimens. For that reason, the cavities in *Proterochersis porebensis* at some stage of development could potentially take form very similar to those observed in *Waluchelys cavitesta* and *Palaeochersis talampayensis*, regardless of their supposedly different nature. Despite any similarities, current evidence does not corroborate the presence of the carapacial mosaic and complex (multipartite) peripheral elements surrounding them, but rather supports their development within the already formed peripherals (Ignacio Cerda 2021, pers. comm.). Note, however, that since neither of the known australochelyid specimens preserves any identifiable carapacial sutures, the exact boundaries of particular elements are difficult to trace, until non-ankylosed specimens are found. Nonetheless, regardless if the cavities in the Australochelyidae were formed by peripherals alone, the general morphogenetic pattern of the shell periphery based on dermal ossification might have been common for the Triassic taxa, with differences between them less severe and homology more straightforward than assumed by Sterli *et al.* (2021), but still substantially different than in more derived turtles. Otherwise, the similarities would have to arise independently, though the adaptive value of such a structure is unclear. There is no evidence of peripheral cavities in the posterior part of the carapace in *Proterochersis* spp., unlike in *Waluchelys cavitesta, Proganochelys quenstedti*, and *Chinlechelys tenertesta*, which suggests that their distribution along the peripheral series and/or retention throughout the life of the animal was different, even if the underlying mechanisms were shared between the taxa.

CONCLUSIONS

All the shell-building elements of *Proterochersis porebensis* are histologically homogenous. Some variability is observed but seems to mostly result from the locations of particular thin sections within the shell, ontogeny, and possibly intraspecific differences and/or sexual dimorphism.

The unusual dermal carapacial mosaic of proterochersids is composed of elements histologically indistinguishable from the remaining bony shell components and separated by true, well-developed sutures. Therefore, it cannot be interpreted as an artifact caused by breakage.

The integument of *Proterochersis porebensis* seems to have been unusually thick, as the interwoven structural fibers of the dermis are commonly found in the visceral cortices of carapacial elements.

After several seasons from deposition, the deep cortices of *Proterochersis porebensis* were readily incorporated into the spongiosa, resulting in relatively few growth marks even in large specimens. Remodeling of the externalmost and visceralmost cortices is, however, rare.

True shell ankylosis with complete suture ossification and subsequent complete obliteration is confirmed in *Proterochersis porebensis*, unusually common, and occurs even in some small and morphologically juvenile specimens. The macroscopic lack of sutures is, therefore, not a taphonomic or diagenetic artifact, or an effect of only superficial (cortical) co-ossification with retention of internal suture morphology. Because of that, thin sectioning is not a reliable method for evaluation of the initial layout and number of shell-building elements in Triassic turtles.

The closure of shell sutures seems to have first happened exteriorly and progress towards the visceral surface of the shell.

Not ankylosed sutures are, nonetheless, present in some middle-sized and large specimens. This may be either explained by extremally varied time of ankylosis (although no expected side effects, such as varied tempo of growth dependent on the retention or obliteration of sutures relative to morphological development, are observed in the sample) or (speculatively) as an effect of local (possibly seasonal) reformation of sutures. Considering the shell regeneration mechanisms present in extant turtles, which in some cases lead to random or semi-random layout of reformed sutures, the latter scenario could potentially explain the presence of dermal carapacial mosaic in the Proterochersidae. More data (both from fossil and extant taxa) are necessary to evaluate this hypothesis.

Some microstructural similarities with the peculiar peripheral morphology of australochelyids are observed, which may indicate that the development of dermal peripheral components of the carapace in proterochersids might have utilized the same basic developmental pathways.

The microstructural changes dependent on the specimen size suggest that *Proterochersis porebensis* could change its habitat during ontogeny, with smaller individuals being more aquatic and larger more terrestrial.

Acknowledgements
We thank Grzegorz Widlicki (Faculty of Geology, University of Warsaw, Poland) and Adam Zaremba (ZPAL) for preparation of the thin sections used for the study, Tomasz Sulej (ZPAL) and Robert Bronowicz for the access to the previously sectioned specimens (ZPAL V. 39/9, ZPAL V. 39/20, ZPAL V. 39/28, and ZPAL V. 39/392), and Marian Dziewiński (ZPAL) for their photographs. We also thank Michał Surowski (Faculty of

Geology, University of Warsaw) for photography of the thin sections, Piotr Duda (Institute of Biomedical Engineering, University of Silesia, Chorzów, Poland) for CT scanning of ZPAL V. 39/480, Szymon Łukasiewicz (Military University of Technology, Warsaw, Poland) for CT scanning of ZPAL V. 39/482, and Dorota Kołbuk (ZPAL) for checking the French abstract and keywords. We also thank the editor, Juliana Sterli, as well as the reviewers, Ignacio Cerda and an anonymous reviewer, for their helpful comments. This study was funded by the National Science Centre (Narodowe Centrum Nauki), Poland grant no. 2016/23/N/NZ8/01823 awarded to Tomasz Szczygielski.

REFERENCES

Agrawal D., Steinbok P. & Cochrane D. 2006. — Reformation of the sagittal suture following surgery for isolated sagittal craniosynostosis. *Journal of Neurosurgery* 105 (2): 115-117. https://doi.org/10.3171/ped.2006.105.2.115

Anquetin J., Barrett P. M., Jones M. E. H., Moore-Fay S. & Evans S. E. 2009. — A new stem turtle from the Middle Jurassic of Scotland: new insights into the evolution and palaeoecology of basal turtles. *Proceedings of the Royal Society B* 276 (1658): 879-886. https://doi.org/10.1098/rspb.2008.1429

Babbitt L. H. & Babbitt C. H. 1951. — A herpetological study of burned-over areas in Dade County, Florida. *Copeia* 1: 79.

Bailleul A. M., Scannella J. B., Horner J. R. & Evans D. C. 2016. — Fusion patterns in the skulls of modern archosaurs reveal that sutures are ambiguous maturity indicators for the Dinosauria. *PLoS ONE* 11 (2): e0147687. https://doi.org/10.1371/journal.pone.0147687

Bajdek P., Szczygielski T., Kapuścińska A. & Sulej T. 2019. — Bromalites from a turtle-dominated fossil assemblage from the Triassic of Poland. *Palaeogeography, Palaeoclimatology, Palaeoecology* 520: 214-228. https://doi.org/10.1016/j.palaeo.2019.02.002

Baur G. 1887. — Ueber den Ursprung der Extremitäten der Ichthyopterygia. *Berichte über de Versammlungen des Oberrheinischen Vereines* 20: 17-20.

Benson R. B. J., Domokos G., Várkonyi P. L. & Reisz R. R. 2011. — Shell geometry and habitat determination in extinct and extant turtles (Reptilia: Testudinata). *Paleobiology* 37 (4): 547-562. https://doi.org/10.1666/10052.1

Berry J. F. & Shine R. 1980. — Sexual size dimorphism and sexual selection in turtles (order Testudines). *Oecologia* 44: 185-191. https://doi.org/10.1007/BF00572678

Cadena E. A., Jaramillo C. A. & Bloch J. I. 2013. — New material of the platychelyid turtle *Notoemys zapatocaensis* from the Early Cretaceous of Colombia; Implications for understanding Pleurodira evolution, *in* Brinkman D. B., Holroyd P. A. & Gardner J. D. (eds), *Morphology and Evolution of Turtles*. Springer Science+Business Media, Dordrecht: 105-120.

Cerda I. A., Sterli J. & Scheyer T. M. 2015. — Bone shell microstructure of *Condorchelys antiqua* Sterli, 2008, a stem turtle from the Jurassic of Patagonia. *Comptes Rendus Palevol* 15 (1-2): 128-141. https://doi.org/10.1016/j.crpv.2015.01.004

Cordero G. A. 2018. — Is the pelvis sexually dimorphic in turtles?. *The Anatomical Record* 301 (8): 1-22. https://doi.org/10.1002/ar.23831

Cordero G. A., Quinteros K. & Janzen F. J. 2018. — Delayed trait development and the convergent evolution of shell kinesis in turtles. *Proceedings of the Royal Society B* 285 (1888): 20181585. https://doi.org/10.1098/rspb.2018.1585

Cuvier G. 1798. — *Tableau élémentaire de l'histoire naturelle des animaux*. Imprimeur du Corps législatif et de l'Institut national, Paris, 770 p. https://gallica.bnf.fr/ark:/12148/bpt6k64769551

Czepiński Ł., Dróżdż D., Szczygielski T., Tałanda M., Pawlak W., Lewczuk A., Rytel A. & Sulej T. 2021. — An Upper Triassic terrestrial vertebrate assemblage from the forgotten Kocury locality in southern Poland with a new aetosaur taxon. *Journal of Vertebrate Paleontology* 41 (1): e1898977. https://doi.org/10.1080/02724634.2021.1898977

Danini E. S. 1946. — Histological processes as observed in the regeneration of the carapace of the tortoise *Emys orbicularis* L. *Izvestiya Akademii Nauk SSSR* 5: 581-594.

de la Fuente M. S., Sterli J. & Krapovickas V. 2020. — Triassic turtles from Pangea: The legacy from South America. *Journal of South American Earth Sciences* 105: 102910. https://doi.org/10.1016/j.jsames.2020.102910

Delfino M., Scheyer T. M., Fritz U. & Sánchez-Villagra M. R. 2010. — An integrative approach to examining a homology question: Shell structures in soft-shell turtles. *Biological Journal of the Linnean Society* 99 (2): 462-476. https://doi.org/10.1111/j.1095-8312.2009.01356.x

Dziomber L., Joyce W. G. & Foth C. 2020. — The ecomorphology of the shell of extant turtles and its applications for fossil turtles. *PeerJ* 8: e10490. https://doi.org/10.7717/peerj.10490

Fraas E. 1913. — *Proterochersis*, eine pleurodire Schildkröte aus dem Keuper. *Jahreshefte des Vereins für Vaterlandische Naturkunde in Württemberg* 69: 13-30.

Gadow H. 1886. — On the reproduction of the carapax in tortoises. *Journal of Anatomy and Physiology* 20: 220-224.

Gaffney E. S. 1990. — The comparative osteology of the Triassic turtle *Proganochelys*. *Bulletin of the American Museum of Natural History* 194: 1-263. http://hdl.handle.net/2246/884

Gaffney E. S. & Kitching J. W. 1994. — The most ancient African turtle. *Nature* 369: 55-58. https://doi.org/10.1038/369055a0

Gaffney E. S., Hutchison J. H., Jenkins F. A. & Meeker L. J. 1987. — Modern turtle origins: The oldest known cryptodire. *Science* 237 (4812): 289-291. https://doi.org/10.1126/science.237.4812.289

Harris K. A., Clark J. D., Elmore R. D. & Harper C. A. 2020. — Direct and indirect effects of fire on eastern box turtles. *Journal of Wildlife Management* 84 (7): 1384-1395. https://doi.org/10.1002/jwmg.21920

Hay O. P. 1922. — On the phylogeny of the shell of the Testudinata and the relationships of *Dermochelys*. *Journal of Morphology* 36 (3): 421-445. https://doi.org/10.1002/jmor.1050360304

Hay O. P. 1929. — Further consideration of the shell of *Chelys* and of the constitution of the armor of turtles in general. *Proceedings of the United States National Museum* 73 (2724): 1-12. https://doi.org/10.5479/si.00963801.73-2724.1

Houssaye A. 2013. — Bone histology of aquatic reptiles: What does it tell us about secondary adaptation to an aquatic life? *Biological Journal of the Linnean Society* 108 (1): 3-21. https://doi.org/10.1111/j.1095-8312.2012.02002.x

Jaekel O. 1916. — Die Wirbeltierfunde aus dem Keuper von Halberstadt. Serie II. Testudinata. *Palaeontologische Zeitschrift* 2: 88-214. https://doi.org/10.1007/BF03160328

Janello J. M., Cerda I. A. & de la Fuente M. S. 2020. — The relationship between bone shell microanatomy and palaeoecology in Testudinata from South America. *Palaeogeography, Palaeoclimatology, Palaeoecology* 537: 109412. https://doi.org/10.1016/j.palaeo.2019.109412

Joyce W. G. & Gauthier J. A. 2004. — Palaeoecology of Triassic stem turtles sheds new light on turtle origins. *Proceedings of the Royal Society of London B: Biological Sciences* 271 (1534): 1-5. https://doi.org/10.1098/rspb.2003.2523

Joyce W. G., Lucas S. G., Scheyer T. M., Heckert A. B. & Hunt A. P. 2009. — A thin-shelled reptile from the Late Triassic of North America and the origin of the turtle shell. *Proceedings of the Royal Society of London B: Biological Sciences* 276 (1656): 507-513. https://doi.org/10.1098/rspb.2008.1196

KRAUSS S., MONSONEGO-ORNAN E., ZELZER E., FRATZL P. & SHAHAR R. 2009. — Mechanical function of a complex three-dimensional suture joining the bony elements in the shell of the red-eared slider turtle. *Advanced Materials* 21: 407-412. https://doi.org/10.1002/adma.200801256

KUBIK R., UHL D. & MARYNOWSKI L. 2015. — Evidence of wildfires during deposition of the Upper Silesian Keuper succession, southern Poland. *Annales Societatis Geologorum Poloniae* 85 (4): 685-696. https://doi.org/10.14241/asgp.2014.009

KUCHLING G. 1997. — Restoration of epidermal scute patterns during regeneration of the chelonian carapace. *Chelonian Conservation and Biology* 2: 500-506.

KUCHLING G. 1999. — *The reproductive biology of the Chelonia*. Springer, Berlin, Heidelberg, New York, Barcelona, Hong Kong, London, Milan, Paris, Singapore, Tokyo, 223 p. https://doi.org/10.1007/978-3-642-80414-4

LACHMUND D. F. 1676. — Testudo ex suo scuto, ut vulgus putat, exire non potest. *Miscellanea Curiosa Medico-Physica Academiae Naturae Curiosorum, sive Ephemeridum Medico-Physicarum Germanicarum* 4-5: 240.

LAUTENSCHLAGER S., FERREIRA G. S. & WERNEBURG I. 2018. — Sensory evolution and ecology of early turtles revealed by digital endocranial reconstructions. *Frontiers in Ecology and Evolution* 6: 7. https://doi.org/10.3389/fevo.2018.00007

LEGLER J. M. 1960. — Natural history of the ornate box turtle, *Terrapene ornata ornata* Agassiz. *University of Kansas Publications, Museum of Natural History* 11: 527-669.

LEGLER J. M. & VOGT R. C. 2013. — *The turtles of Mexico. Land and freshwater forms*. University of California Press, Berkeley, Los Angeles, London, 416 p.

LEUTERITZ T. E. J. & GANTZ D. T. 2013. — Sexual Dimorphism in Radiated Tortoises (*Astrochelys radiata*). *Chelonian Research Monographs* 6: 105-112.

LI C., WU X., RIEPPEL O., WANG L. & ZHAO L. 2008. — An ancestral turtle from the Late Triassic of southwestern China. *Nature* 456: 497-501. https://doi.org/10.1038/nature07533

LI C., FRASER N. C., RIEPPEL O. C. & XIAO-CHUN W. 2018. — A Triassic stem turtle with an edentulous beak. *Nature* 560: 476-479. https://doi.org/10.1038/s41586-018-0419-1

LICHTIG A. J. & LUCAS S. G. 2017. — A simple method for inferring habitats of extinct turtles. *Palaeoworld* 26 (3): 1-8. https://doi.org/10.1016/j.palwor.2017.02.001

LICHTIG A. J. & LUCAS S. G. 2021. — *Chinlechelys* from the Upper Triassic of New Mexico, USA, and the origin of turtles. *Palaeontologia Electronica* 24: a13.

LIMA F. C., SANTOS A. L. Q., VIEIRA L. G., DA SILVA-JUNIOR L. M., ROMÃO M. F., DE SIMONE S. B. S., HIRANO L. Q. L., SILVA J. M. M., MONTELO K. M. & MALVÁSIO A. 2011. — Ontogeny of the shell bones of embryos of *Podocnemis unifilis* (Troschel, 1848) (Testudines, Podocnemididae). *Anatomical Record* 294 (4): 621-632. https://doi.org/10.1002/ar.21359

LUCAS S. G. & LICHTIG A. J. 2018. — New morphology of *Chinlechelys*, a Late Triassic turtle from New Mexico, U.S.A. *Society of Vertebrate Paleontology Meeting Program and Abstracts*: 171.

LUCAS S. G., HECKERT A. B. & HUNT A. P. 2000. — Probable turtle from the Upper Triassic of east-central New Mexico. *Neues Jahrbuch für Geologie und Paläontologie – Monatshefte* 5: 287-300. https://doi.org/10.1127/njgpm/2000/2000/287

LYSON T. R., BEVER G. S., SCHEYER T. M., HSIANG A. Y. & GAUTHIER J. A. 2013. — Evolutionary origin of the turtle shell. *Current Biology* 23 (12): 1113-1119. Elsevier Ltd. https://doi.org/10.1016/j.cub.2013.05.003

MABBUTT L. W., KOKICH V. G., MOFFETT B. C. & LOESER J. D. 1979. — Subtotal neonatal calvariectomy. A radiographic and histological evaluation of calvarial and sutural redevelopment in rabbits. *Journal of Neurosurgery* 51 (5): 691-696. https://doi.org/10.3171/jns.1979.51.5.0691

MARTÍNEZ-SILVESTRE A. & SOLER-MASSANA J. 2000. — Regeneración del caparazón en *Testudo hermanni hermanni* después de un incendio forestal. *Boletín de la Asociación Herpetológica Española* 11: 90-92.

MAUTNER A.-K., LATIMER A. E., FRITZ U. & SCHEYER T. M. 2017. — An updated description of the osteology of the pancake tortoise *Malacochersus tornieri* (Testudines: Testudinidae) with special focus on intraspecific variation. *Journal of Morphology* 278 (3): 321-333. https://doi.org/10.1002/jmor.20640

MCEWAN B. 1982. — Bone anomalies in the shell of *Gopherus polyphemus*. *Florida Scientist* 45 (3): 189-195. https://www.jstor.org/stable/24320245

VON MEYER H. 1863. — Mittheilung an Professor H. B. Geinitz. *Neues Jahrbuch für Mineralogie, Geologie und Palaeontologie* 1863: 444-450.

MOSSAZ C. F. & KOKICH V. G. 1981. — Redevelopment of the calvaria after partial craniectomy in growing rabbits: the effect of altering dural continuity. *Acta Anatomica* 109: 321-331. https://doi.org/10.1159/000145398

NEVAREZ J. G., RADEMACHER N. & SHAW S. 2008. — Carapace sequestrum in an African spurred tortoise, *Geochelone sulcata*. *Journal of Herpetological Medicine and Surgery* 18 (2): 45-51. https://doi.org/10.5818/1529-9651.18.2.45

NEWMAN H. H. 1906. — The significance of scute and plate 'abnormalities' in Chelonia. A contribution to the evolutionary history of the chelonian carapace and plastron. Part II. *Biological Bulletin* 10 (3): 99-114. https://doi.org/10.2307/1535756

NIEDŹWIEDZKI G., BRUSATTE S. L., SULEJ T. & BUTLER R. J. 2014. — Basal dinosauriform and theropod dinosaurs from the mid-late Norian (Late Triassic) of Poland: Implications for Triassic dinosaur evolution and distribution. *Palaeontology* 57 (6): 1121-1142. https://doi.org/10.1111/pala.12107

NIKOLOVA S., TONEVA D., GEORGIEV I., HARIZANOV S., ZLATAREVA D., HADJIDEKOV V. & LAZAROV N. 2017. — A CT-study of the cranial suture morphology and its reorganization during the obliteration. *Collegium Antropologicum* 41: 125-131.

OKEN L. 1823. — Litterarischer Anzeiger. *Isis von Oken* 12-13: 442-469.

PRITCHARD P. C. H. 1979. — *Encyclopedia of turtles*. T.F.H. Publications, Surrey, 895 p.

PRITCHARD P. C. H. 2008. — Evolution and structure of the turtle shell, *in* WYNEKEN J., GODFREY M. H. & BELS V., *Biology of Turtles*. CRC Press, Boca Raton, London, New York: 46-83.

PROCTER J. B. 1922. — A study of the remarkable tortoise, *Testudo loveridgii* Blgr., and the morphogeny of the chelonian carapace. *Proceedings of the General Metings for Scientific Business of the Zoological Society of London* 92 (3): 483-526. https://doi.org/10.1111/j.1096-3642.1922.tb02155.x

ROSE F. L. 1986. — Carapace regeneration in *Terrapene* (Chelonia: Testudinidae). *The Southwestern Naturalist* 31 (1): 131-134. https://doi.org/10.2307/3670981

ROTHSCHILD B. M., SCHULTZE H.-P. & PELLEGRINI R. 2013. — Osseous and other hard tissue pathologies in turtles and abnormalities of mineral deposition, *in* BRINKMAN D. B., HOLROYD P. A. & GARDNER J. D., *Morphology and Evolution of Turtles*. Springer Science+Business Media, Dordrecht: 501-534. https://doi.org/10.1007/978-94-007-4309-0_27

ROUGIER G. W., DE LA FUENTE M. S. & ARCUCCI A. B. 1995. — Late Triassic turtles from South America. *Science* 268 (5212): 855-858. https://doi.org/10.1126/science.268.5212.855

SAINT-HILAIRE G. 1809. — Sur les tortues molles, nouveau genre sous le nom de *Trionyx*, et sur la formation des carapaces. *Annales du Muséum national d'Histoire naturelle* 14: 1-20. https://www.biodiversitylibrary.org/page/3498619

SCHEYER T. M. & SÁNCHEZ-VILLAGRA M. R. 2007. — Carapace bone histology in the giant pleurodiran turtle *Stupendemys geographicus*: Phylogeny and function. *Acta Palaeontologica Polonica* 52: 137-154.

Scheyer T. M. & Sander P. M. 2007. — Shell bone histology indicates terrestrial palaeoecology of basal turtles. *Proceedings of the Royal Society of London B: Biological Sciences* 274 (1620): 1885-1893. https://doi.org/10.1098/rspb.2007.0499

Scheyer T. M., Sander P. M., Joyce W. G., Böhme W. & Witzel U. 2007. — A plywood structure in the shell of fossil and living soft-shelled turtles (Trionychidae) and its evolutionary implications. *Organisms, Diversity & Evolution* 7 (2): 136-144. https://doi.org/10.1016/j.ode.2006.03.002

Scheyer T. M., Brüllmann B. & Sánchez-Villagra M. R. 2008. — The ontogeny of the shell in side-necked turtles, with emphasis on the homologies of costal and neural bones. *Journal of Morphology* 269 (8): 1008-1021. https://doi.org/10.1002/jmor.10637

Scheyer T. M., Danilov I. G., Sukhanov V. B. & Syromyatnikova E. V 2014. — The shell bone histology of fossil and extant marine turtles revisited. *Biological Journal of the Linnean Society* 112 (4): 701-718. https://doi.org/10.1111/bij.12265

Schneider J. G. 1783. — *Allgemeine Naturgeschichte der Schildkröten: Nebst einem systemischen Verzeichnisse der einzelnen Arten und zwey Kupfern*. J. G. Müller, Leipzig, 32 p. https://www.biodiversitylibrary.org/page/4787806

Schoch R. R. & Sues H.-D. 2015. — A Middle Triassic stem-turtle and the evolution of the turtle body plan. *Nature* 523: 584-587. https://doi.org/10.1038/nature14472

Schoch R. R. & Sues H.-D. 2017. — Osteology of the Middle Triassic stem-turtle *Pappochelys rosinae* and the early evolution of the turtle skeleton. *Journal of Systematic Palaeontology* 16 (11): 1-39. https://doi.org/10.1080/14772019.2017.1354936

Schoch R. R., Klein N., Scheyer T. M. & Sues H.-D. 2019. — Microanatomy of the stem-turtle *Pappochelys rosinae* indicates a predominantly fossorial mode of life and clarifies early steps in the evolution of the shell. *Scientific Reports* 9: 10430. https://doi.org/10.1038/s41598-019-46762-z

Shillito J. 1973. — A new cranial suture appearing in the site of craniectomy for synostosis. *Radiology* 107 (1): 83-88. https://doi.org/10.1148/107.1.83

Siebenrock F. 1903. — Über zwei seltene und eine neue Schildkröte des Berliner Museums. *Sitzungsberichte der Mathematisch-Naturwissenschaftlichen Klasse der kaiserlichen Akademie der Wissenschaften* 112: 439-445.

Skawiński T., Ziegler M., Czepiński Ł., Szermański M., Tałanda M., Surmik D. & Niedźwiedzki G. 2017. — A re-evaluation of the historical 'dinosaur' remains from the Middle-Upper Triassic of Poland. *Historical Biology* 29 (4): 442-472. https://doi.org/10.1080/08912963.2016.1188385

Smith H. M. 1958. — Total regeneration of the carapace in a box turtle. *Turtox News* 36: 234-237.

Sterli J. 2008. — A new, nearly complete stem turtle from the Jurassic of South America with implications for turtle evolution. *Biology Letters* 4 (3): 286-289. https://doi.org/10.1098/rsbl.2008.0022

Sterli J., de la Fuente M. S. & Rougier G. W. 2007. — Anatomy and relationships of *Palaeochersis talampayensis*, a Late Triassic turtle from Argentina. *Palaeontographica Abteilung A* 281 (1-3): 1-61. https://doi.org/10.1127/pala/281/2007/1

Sterli J., de la Fuente M. S. & Cerda I. A. 2013. — A new species of meiolaniform turtle and a revision of the late cretaceous meiolaniformes of South America. *Ameghiniana* 50 (2): 240-256. https://doi.org/10.5710/AMGH.16.01.2013.582

Sterli J., Martínez R. N., Cerda I. A. & Apaldetti C. 2021. — Appearances can be deceptive: Bizarre shell microanatomy and histology in a new Triassic turtle (Testudinata) from Argentina at the dawn of turtles. *Papers in Palaeontology* 7 (2): 1097-1132. https://doi.org/10.1002/spp2.1334

Sukhanov V. B. 2006. — An archaic turtle, *Heckerochelys romani* gen. et sp. nov., from the Middle Jurassic of Moscow Region, Russia. *Fossil Turtle Research* 1: 112-118.

Sulej T., Niedźwiedzki G. & Bronowicz R. 2012. — A new Late Triassic vertebrate fauna from Poland with turtles, aetosaurs, and coelophysoid dinosaurs. *Journal of Vertebrate Paleontology* 32 (5): 1033-1041. https://doi.org/10.1080/02724634.2012.694384

Suzuki H. K. 1963. — Studies on the osseous system of the slider turtle. *Annals of the New York Academy of Sciences* 109 (1): 351-410. https://doi.org/10.1111/j.1749-6632.1963.tb13476.x

Szczygielski T. 2017. — Homeotic shift at the dawn of the turtle evolution. *Royal Society Open Science* 4 (4): 160933. https://doi.org/10.1098/rsos.160933

Szczygielski T. 2020. — Obscure by name: solving the enigma of *Chelytherium obscurum*, the first described Triassic turtle. *Zoological Journal of the Linnean Society* 192 (4): 1111-1112. https://doi.org/10.1093/zoolinnean/zlaa139

Szczygielski T. & Sulej T. 2016. — Revision of the Triassic European turtles *Proterochersis* and *Murrhardtia* (Reptilia, Testudinata, Proterochersidae), with the description of new taxa from Poland and Germany. *Zoological Journal of the Linnean Society* 177 (2): 395-427. https://doi.org/10.1111/zoj.12374

Szczygielski T. & Sulej T. 2019. — The early composition and evolution of the turtle shell (Reptilia, Testudinata). *Palaeontology* 62 (3): 375-415. https://doi.org/10.1111/pala.12403

Szczygielski T., Słowiak J. & Dróżdż D. 2018. — Shell variability in the stem turtles *Proterochersis* spp. *PeerJ* 6: e6134. https://doi.org/10.7717/peerj.6134

Witzmann F. 2009. — Comparative histology of sculptured dermal bones in basal tetrapods, and the implications for the soft tissue dermis. *Palaeodiversity* 2: 233-270.

Wood R. C. 1976. — *Stupendemys geographicus*, the world's largest turtle. *Breviora* 436: 1-31.

Woodbury A. M. & Hardy R. 1948. — Studies of the desert tortoise, *Gopherus agassizii*. *Ecological Monographs* 18 (2): 145-200. https://doi.org/10.2307/1948638

Zhang W., Wu C., Zhang C. & Chen Z. 2012. — Numerical study of the mechanical response of turtle shell. *Journal of Bionic Engineering* 9: 330-335. https://doi.org/10.1016/S1672-6529(11)60129-7

Submitted on 10 March 2021;
accepted on 10 May 2021;
published on 29 August 2022.

APPENDICES

APPENDIX 1. — Sectioned carapace specimens of *Proterochersis porebensis* Szczygielski & Sulej, 2016: **A**, ZPAL V. 39/2, carapace fragment in external view; **B**, ZPAL V. 39/9, costal fragment in external view; **C**, ZPAL V. 39/20, costal fragment in external view, **D**, **E**, ZPAL V. 39/28, carapace fragment in external (**D**) and visceral (**E**) view; **F**, ZPAL V. 39/61, carapace fragment in external view; **G**, ZPAL V. 39/392, peripheral fragment of the carapace in visceral view; **H**, ZPAL V. 39/416, neural in external view; **I**, **J**, ZPAL V. 39/417, supernumerary carapacial ossification in external (**I**) and visceral (**J**) view; **K**, ZPAL V. 39/477, costal in external view; **L**, ZPAL V. 39/478, neural in external view. M, ZPAL V. 39/479, costal in visceral view; **N**, ZPAL V. 39/482, nuchal fragment of the carapace in dorsal view. **Red**, sectioning lines. Scale bar: 1 cm.

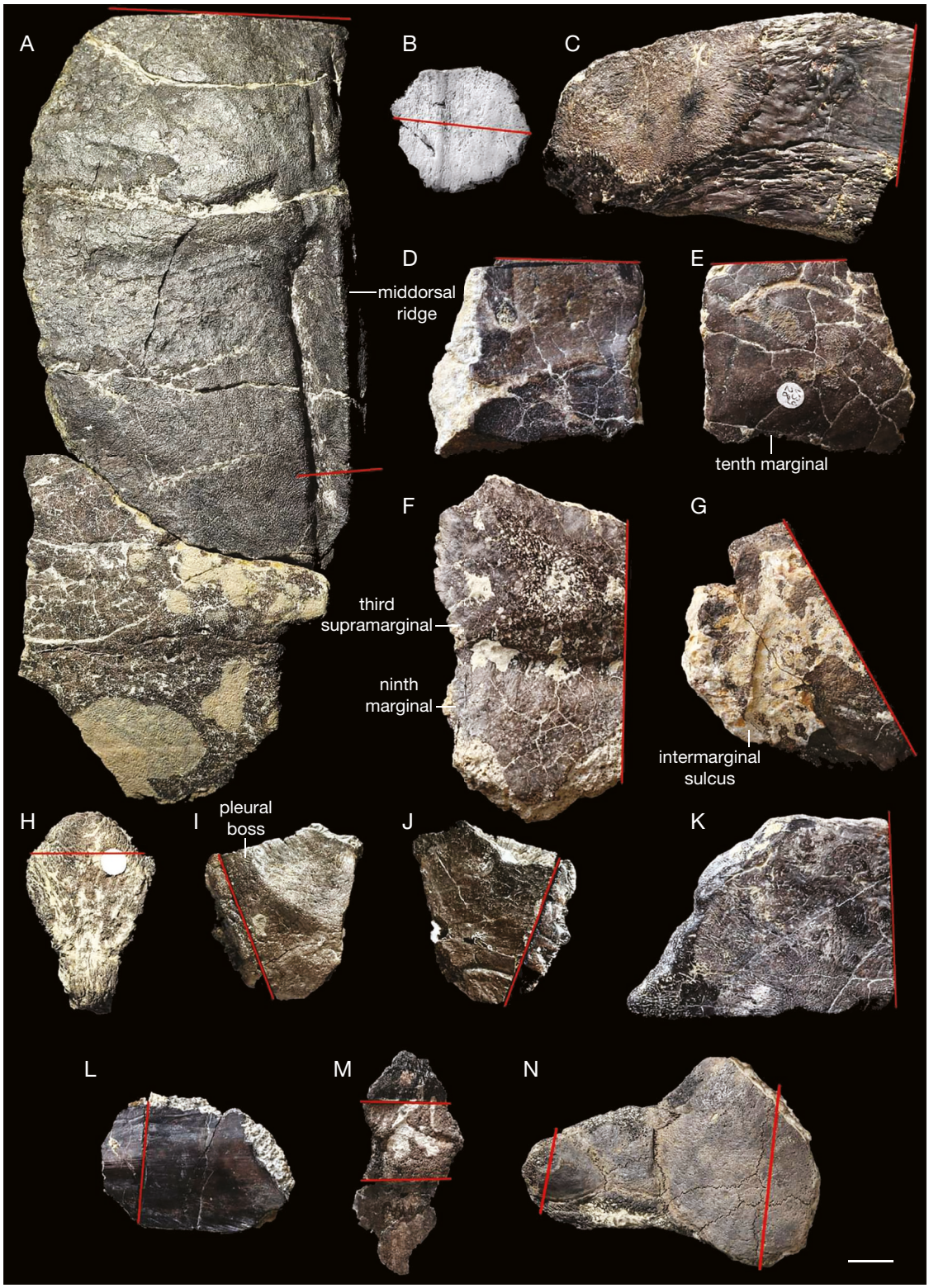

Appendix 2. — Sectioned plastral specimens of *Proterochersis porebensis* Szczygielski & Sulej, 2016: **A**, ZPAL V. 39/68, posterior plastral fragment in external view; **B**, ZPAL V. 39/195, ?hyoplastron in external view; **C**, ZPAL V. 39/388, gular fragment in ventral view; **D**, ZPAL V. 39/401, anterior plastral fragment in external view; **E**, ZPAL V. 39/476, ?hyoplastron in external view. **Red**, sectioning lines. Scale bar: 1 cm.

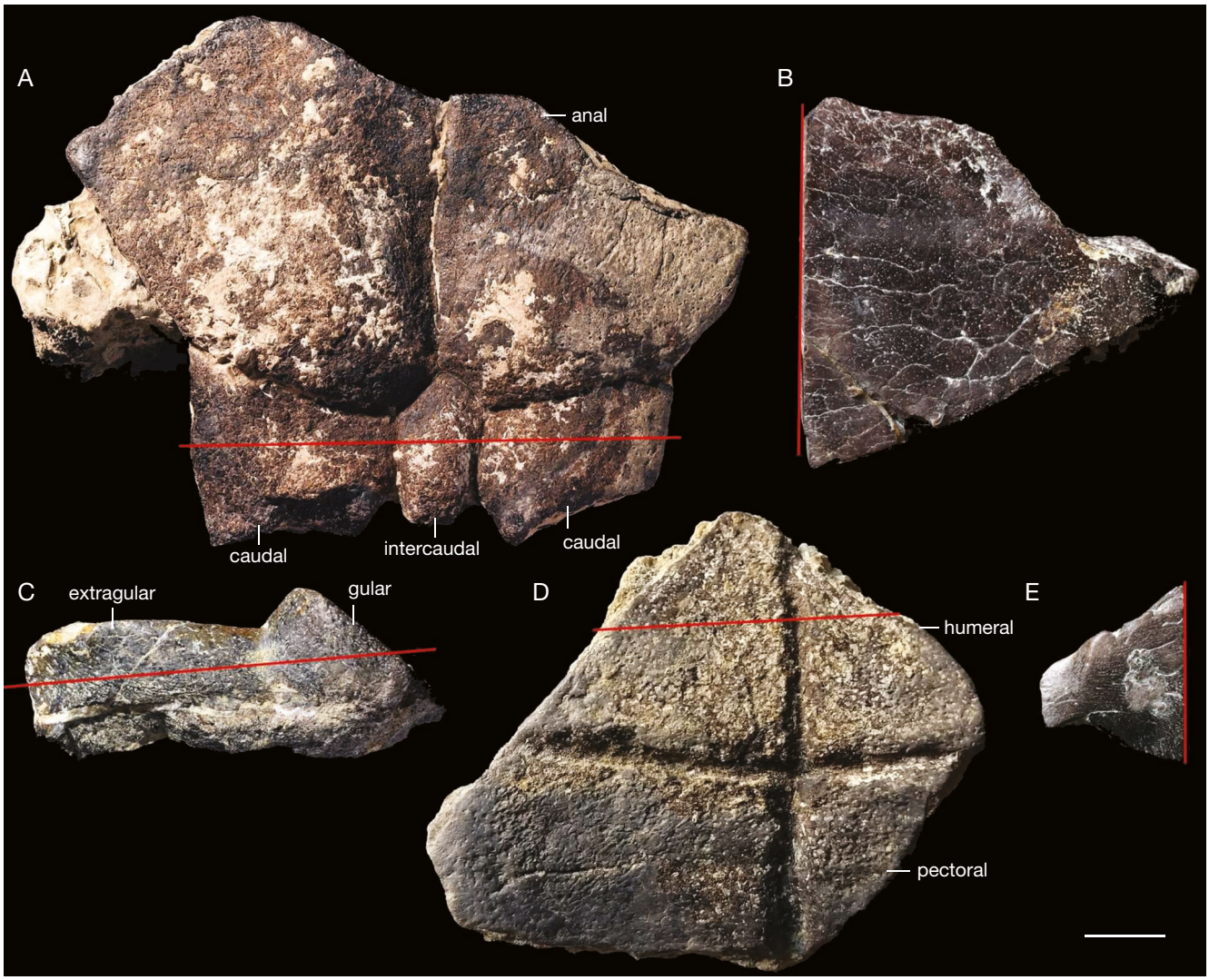

Appendix 3. — ZPAL V. 39/2. Carapace sectioned transversely through the neural and longitudinally along the costal in normal light. Scale bar: 5 mm.

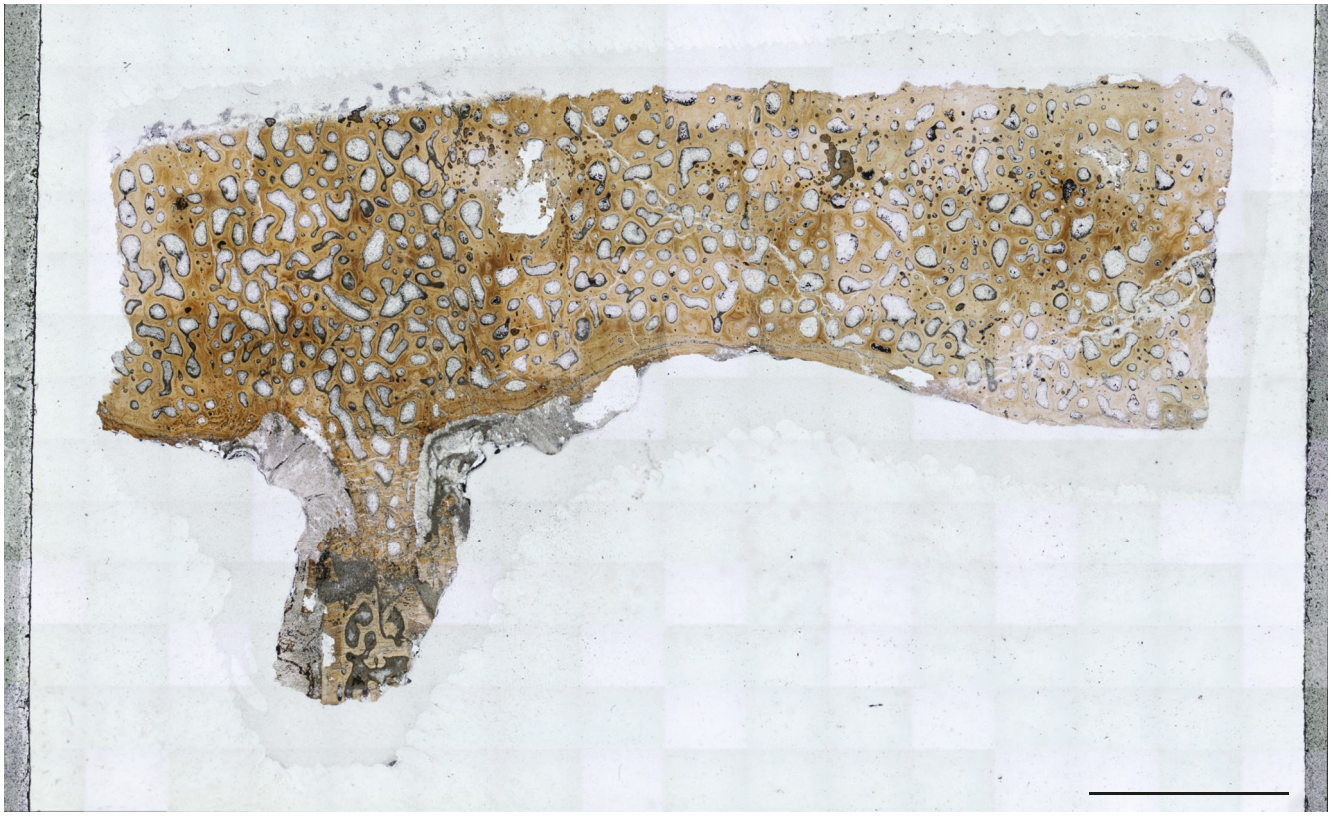

Appendix 4. — ZPAL V. 39/2. Carapace sectioned transversely through the neural and longitudinally along the costal in polarized light with quartz wedge. Scale bar: 5 mm.

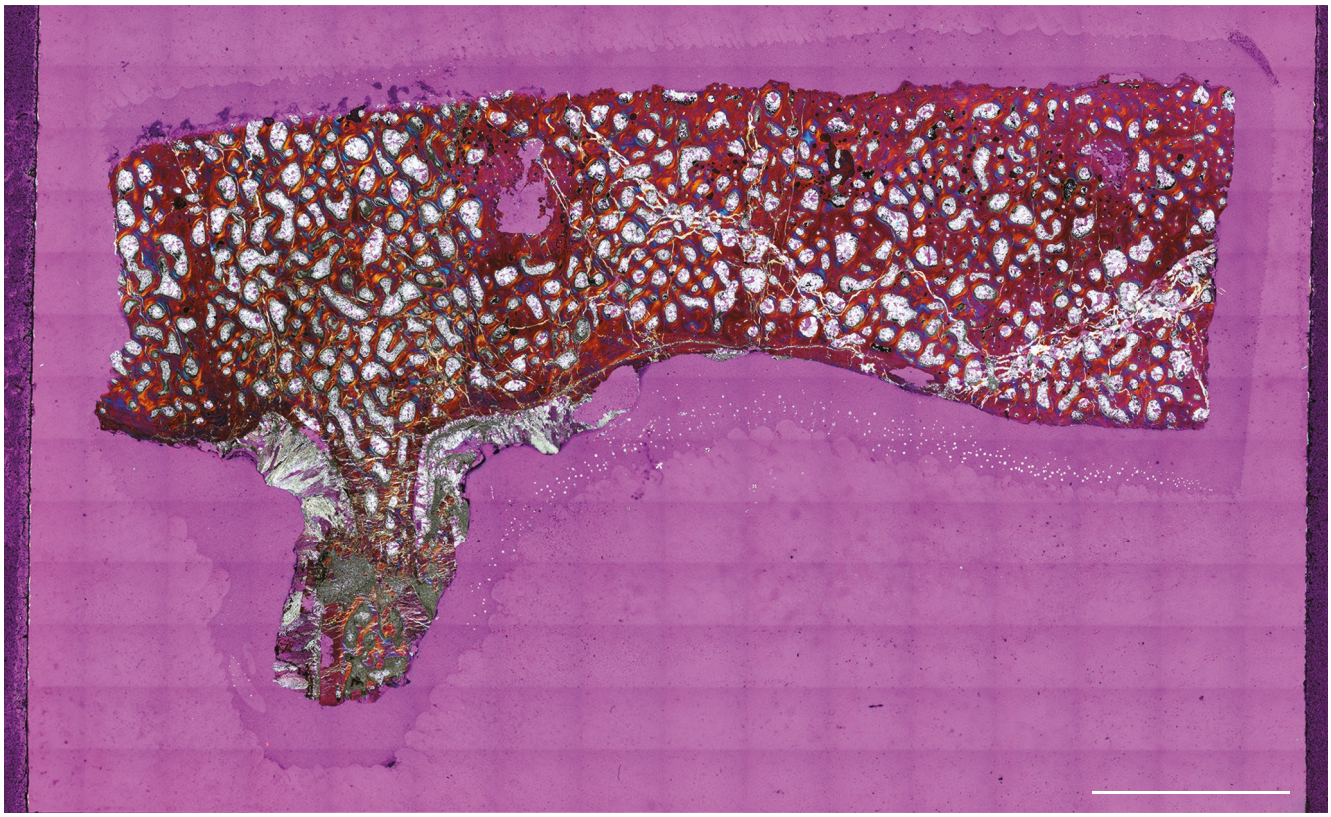

APPENDIX 5. — ZPAL V. 39/2. Carapace sectioned transversely through the neural and longitudinally along the costal in polarized light. Scale bar: 5 mm.

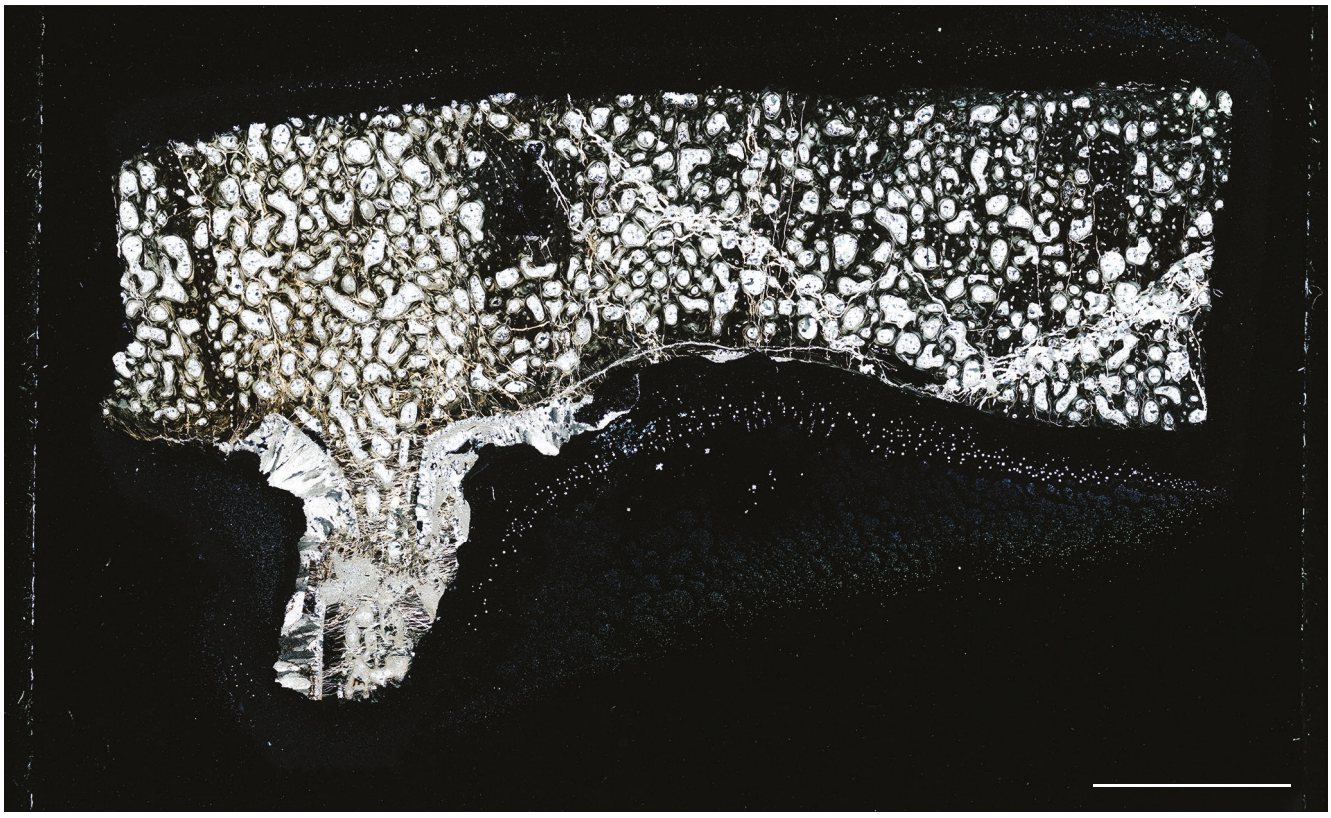

Appendix 6. — ZPAL V. 39/2. Close-up of ossified costoneural suture, external part, in polarized light. Scale bar: 1 mm.

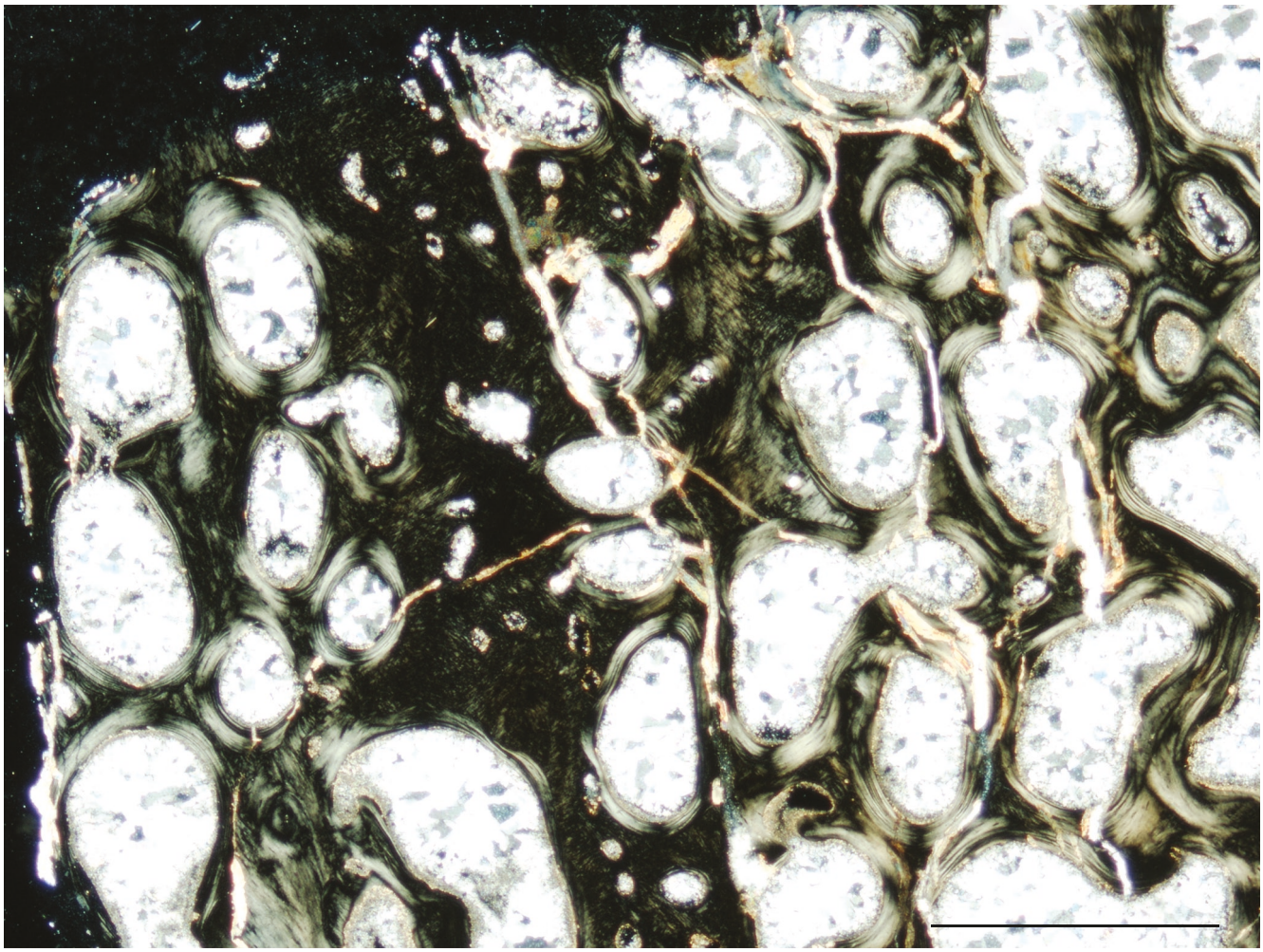

Appendix 7. — ZPAL V. 39/2. Close-up of ossified costoneural suture, visceral part, in polarized light. Scale bar: 1 mm.

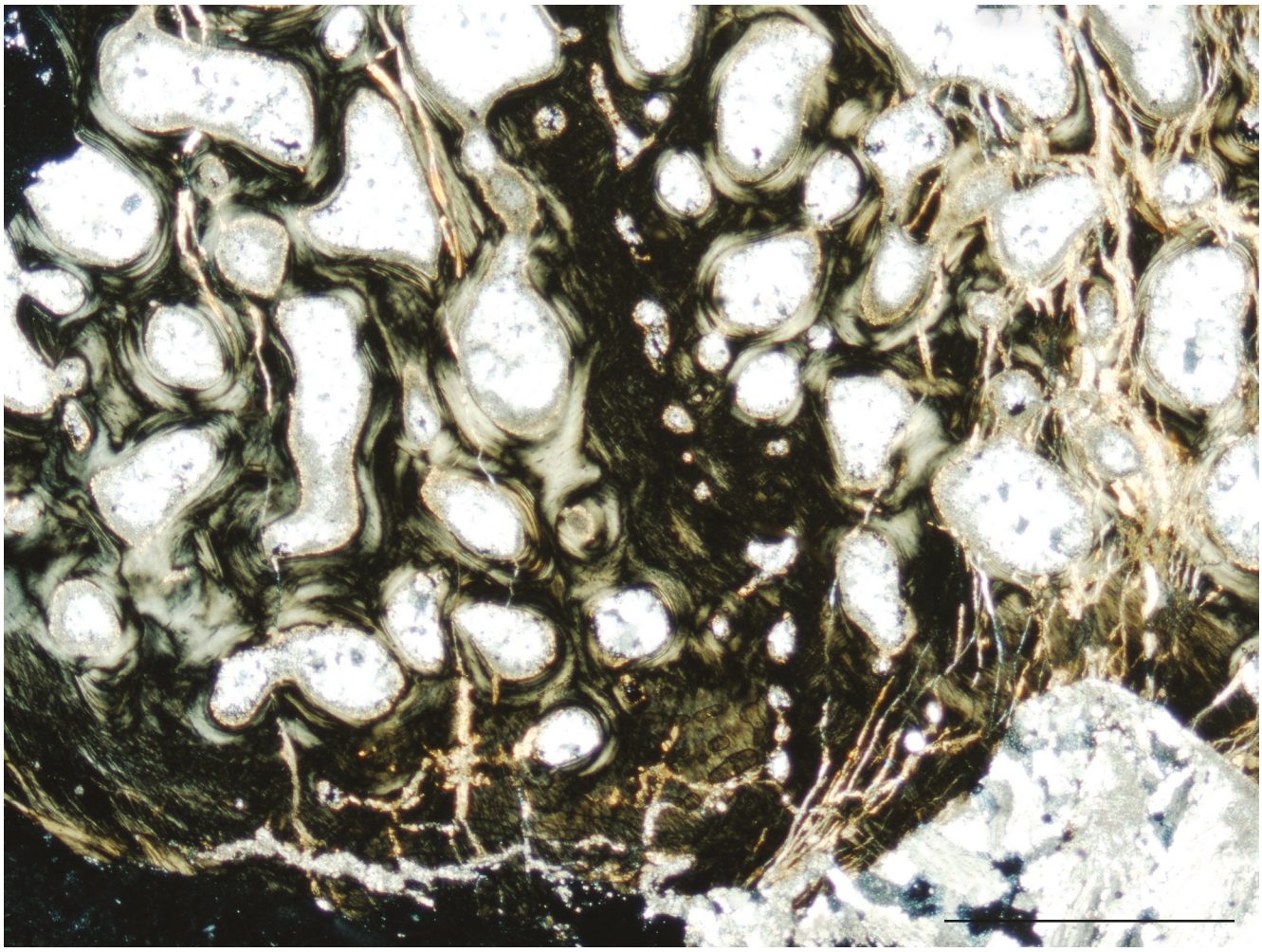

APPENDIX 8. — ZPAL V. 39/2. Carapace sectioned longitudinally along the costal in normal light. Scale bar: 5 mm.

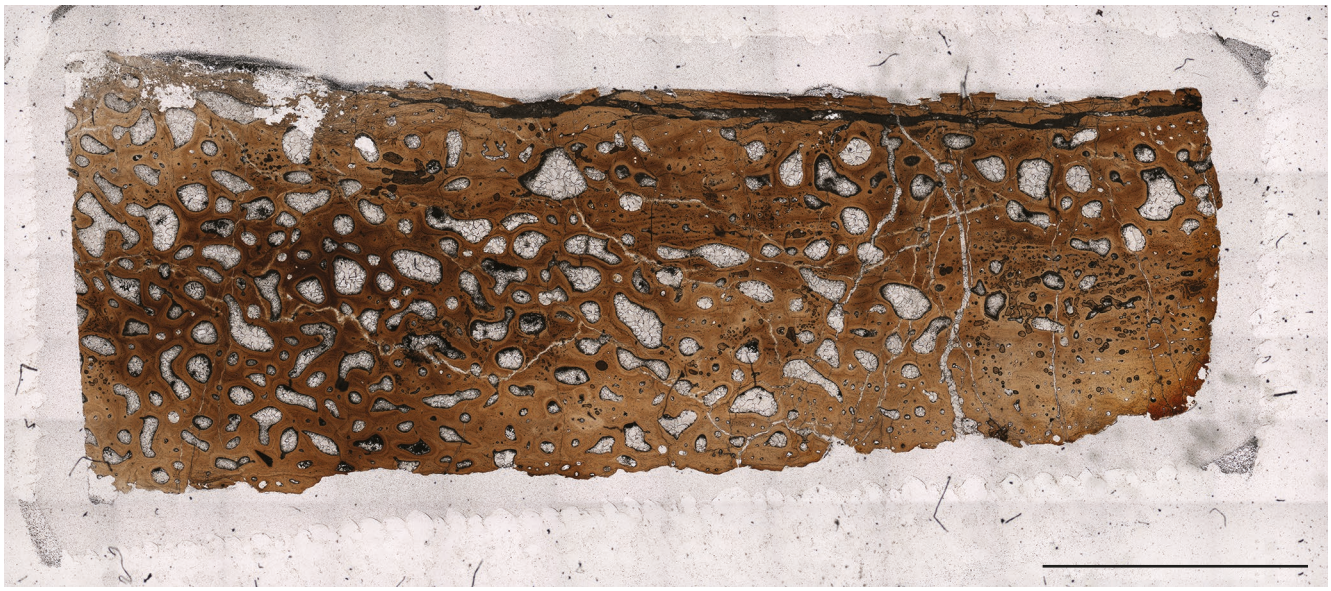

APPENDIX 9. — ZPAL V. 39/2. Carapace sectioned longitudinally along the costal in polarized light with quartz wedge. Scale bar: 5 mm.

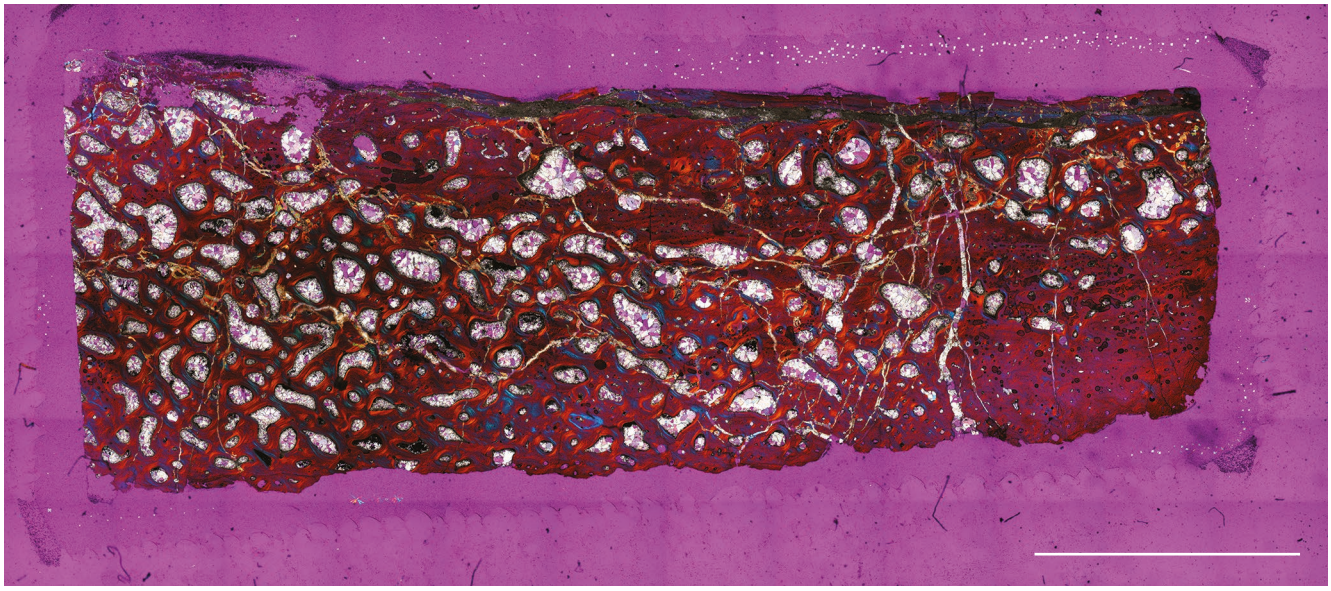

Appendix 10. — ZPAL V. 39/2. Carapace sectioned longitudinally along the costal in polarized light. Scale bar: 5 mm.

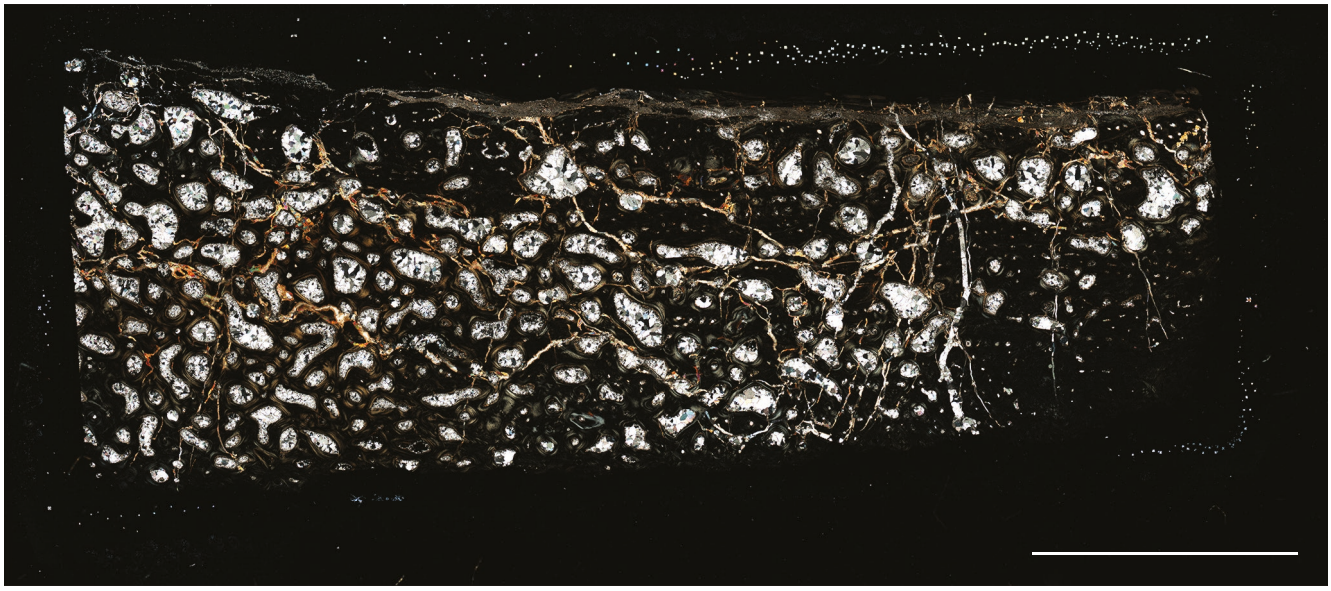

Appendix 11. — ZPAL V. 39/9. ?Costal bone, sectioned transversely in normal light. Scale bar: 1 mm.

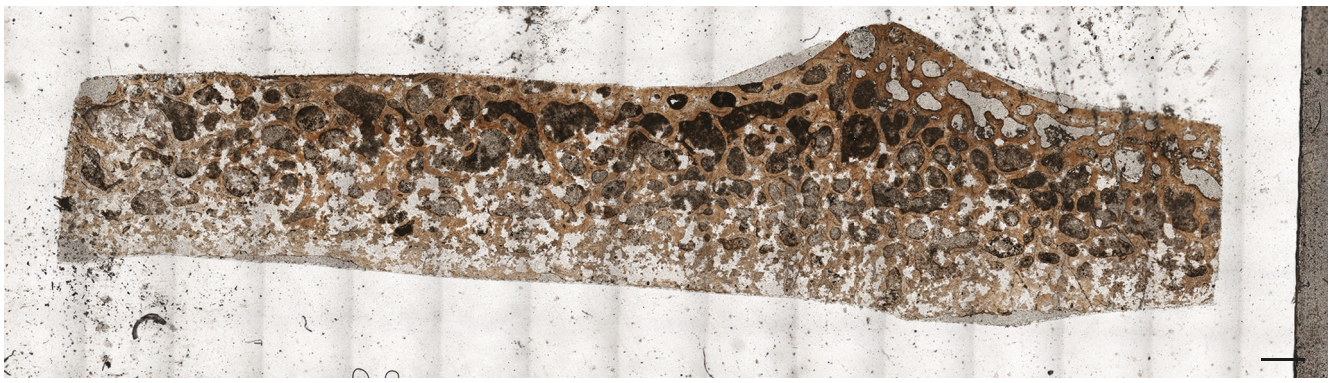

Appendix 12. — ZPAL V. 39/9. ?Costal bone, sectioned transversely in polarized light with quartz wedge. Scale bar: 1 mm.

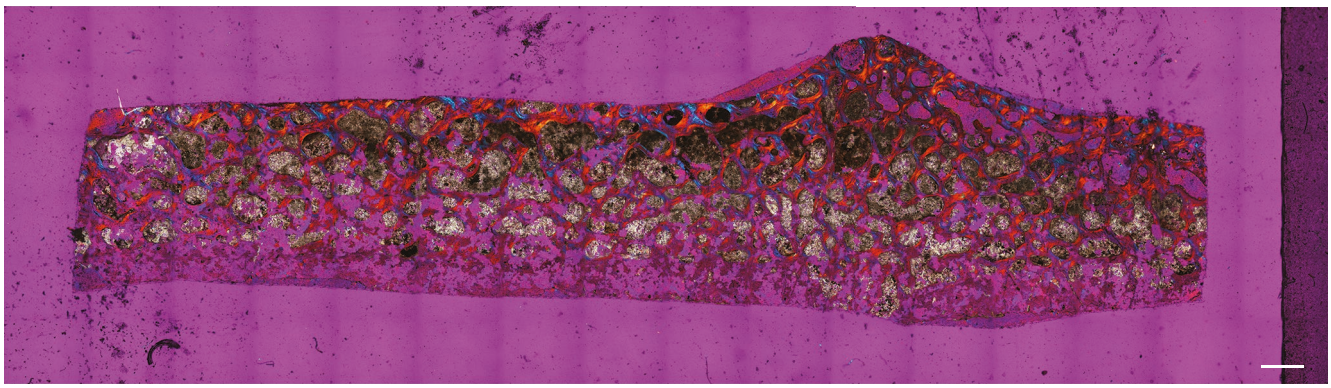

APPENDIX 13. — ZPAL V. 39/9. ?Costal bone, sectioned transversely in polarized light. Scale bar: 13 mm.

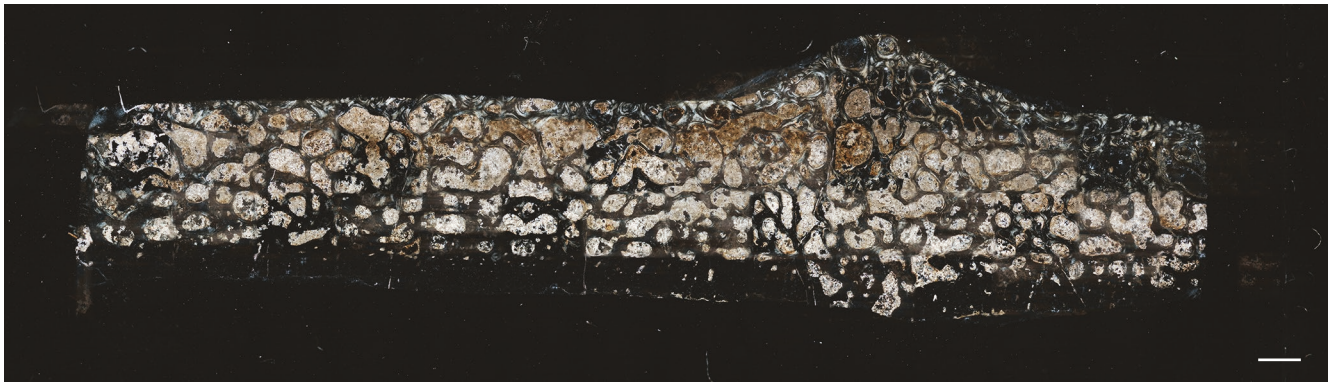

APPENDIX 14. — ZPAL V. 39/20. Posterior costal bone, sectioned transversely in normal light. Scale bar: 5 mm.

APPENDIX 15. — ZPAL V. 39/20. Posterior costal bone, sectioned transversely in polarized light with quartz wedge. Scale bar: 5 mm.

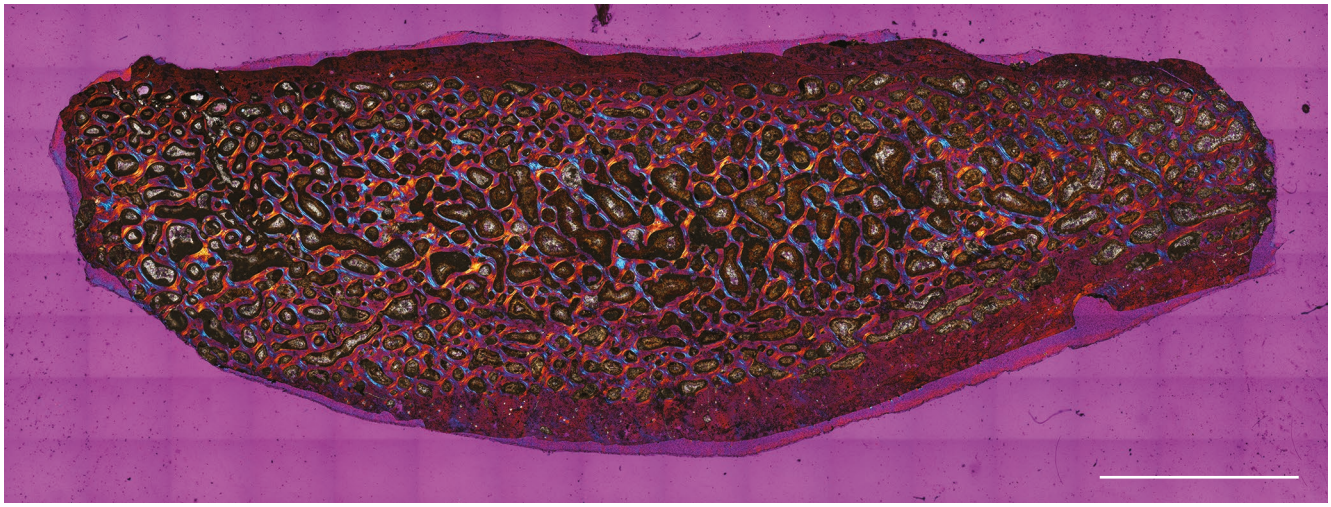

Appendix 16. — ZPAL V. 39/20. Posterior costal bone, sectioned transversely in polarized light. Scale bar: 5 mm.

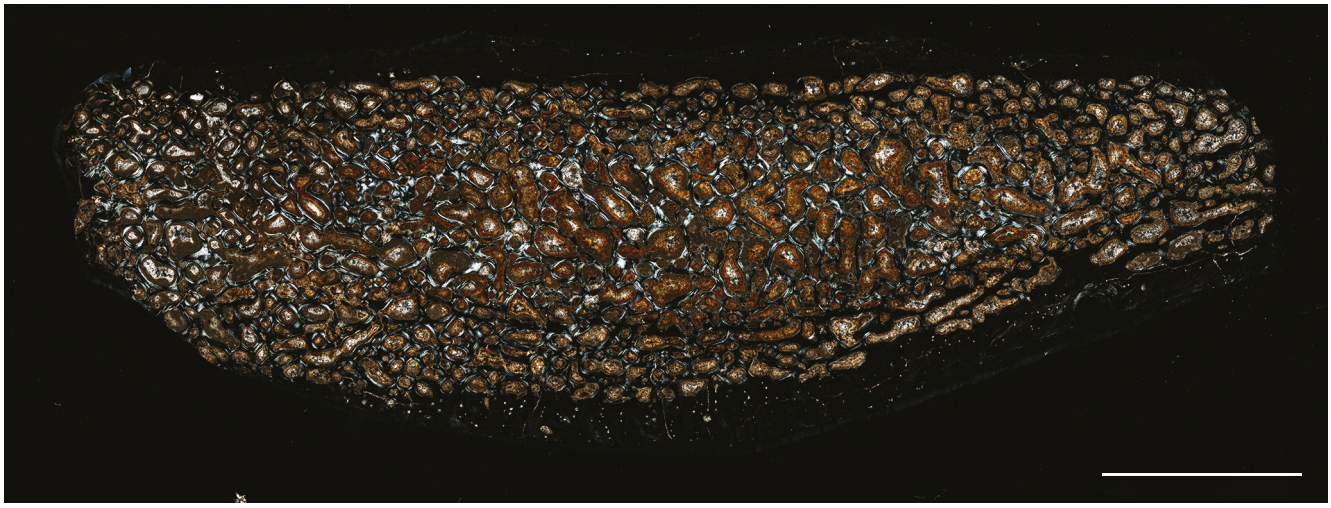

Appendix 17. — ZPAL V. 39/28. Carapace fragment sectioned transversely through costal in normal light. Scale bar: 5 mm.

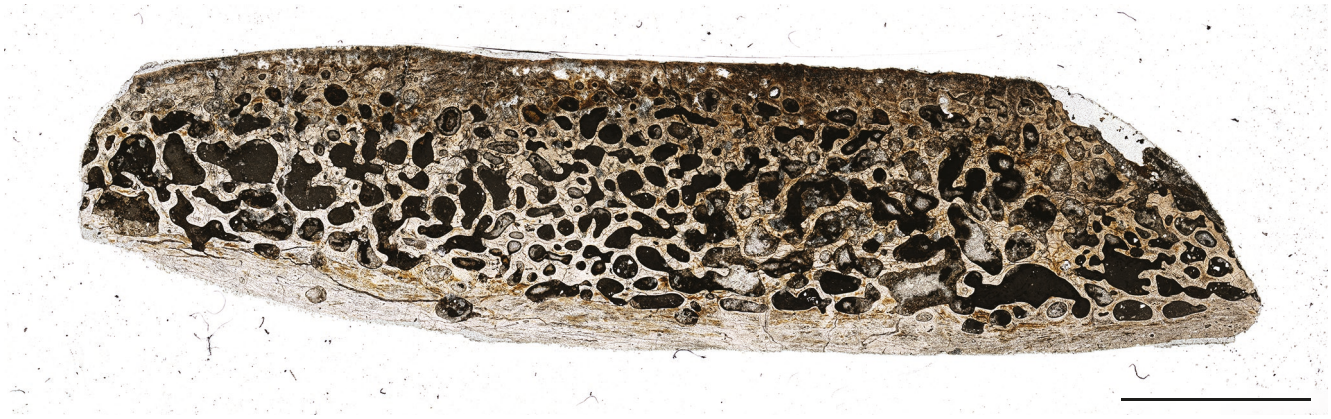

Appendix 18. — ZPAL V. 39/28. Carapace fragment sectioned transversely through costal in polarized light with quartz wedge. Scale bar: 5 mm.

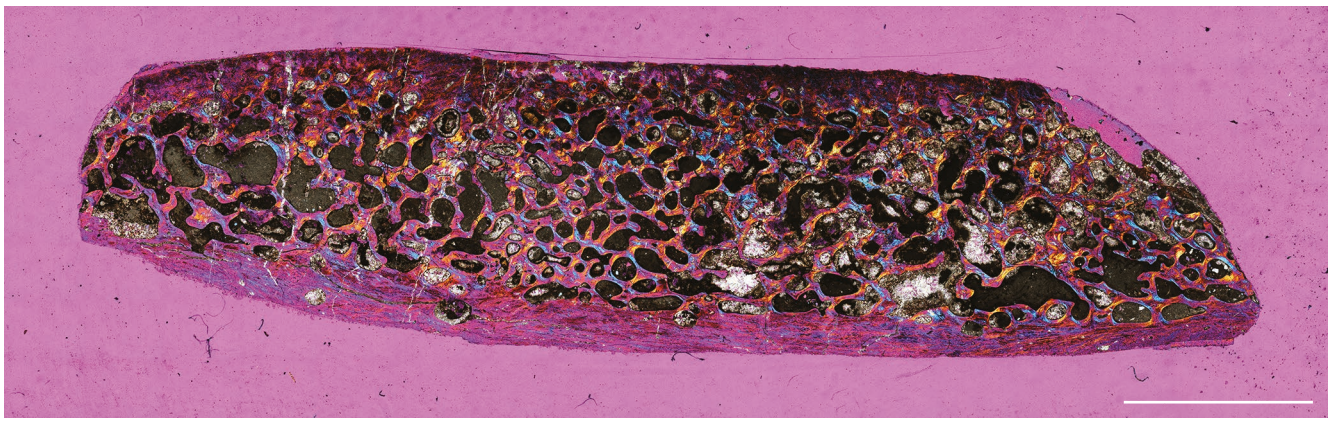

Appendix 19. — ZPAL V. 39/28. Carapace fragment sectioned transversely through costal in polarized light. Scale bar: 5 mm.

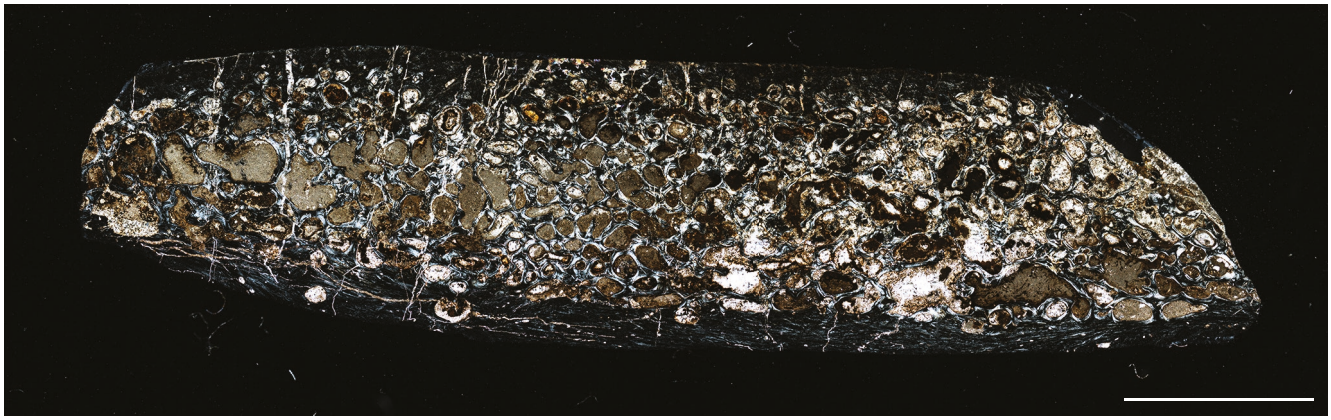

Appendix 20. — ZPAL V. 39/61. ?Ninth marginal and third supramarginal area (peripheral and costal, possibly supernumerary carapacial ossification), sectioned transversely (longitudinally along the costal) in normal light. Scale bar: 5 mm.

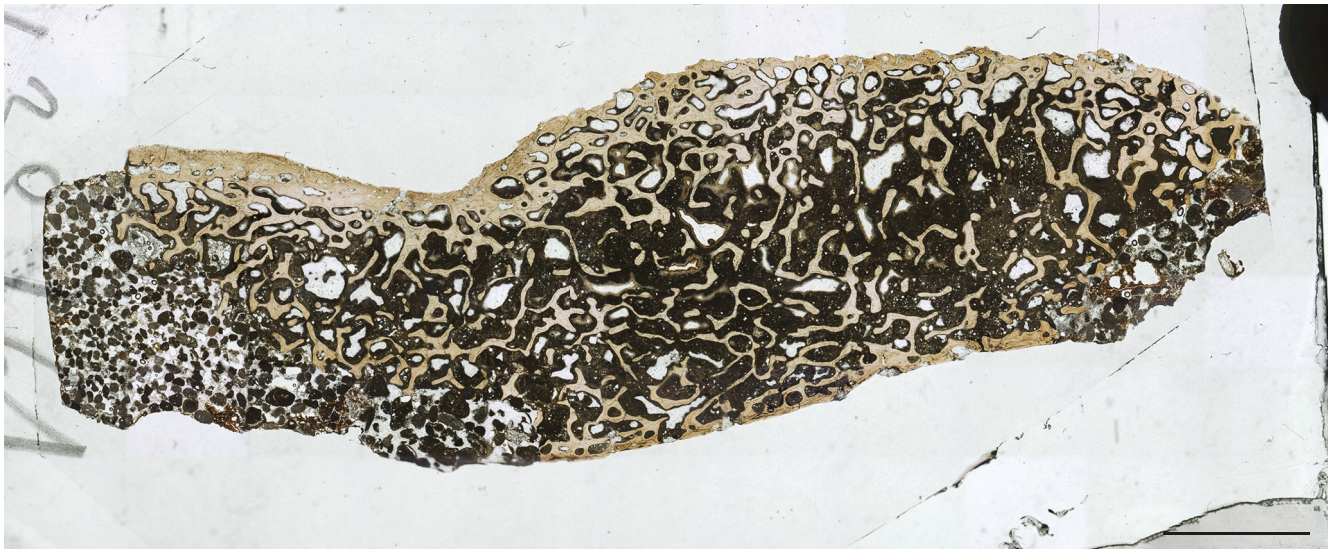

Appendix 21. — ZPAL V. 39/61. ?Ninth marginal and third supramarginal area (peripheral and costal, possibly supernumerary carapacial ossification), sectioned transversely (longitudinally along the costal) in polarized light with quartz wedge. Scale bar: 5 mm.

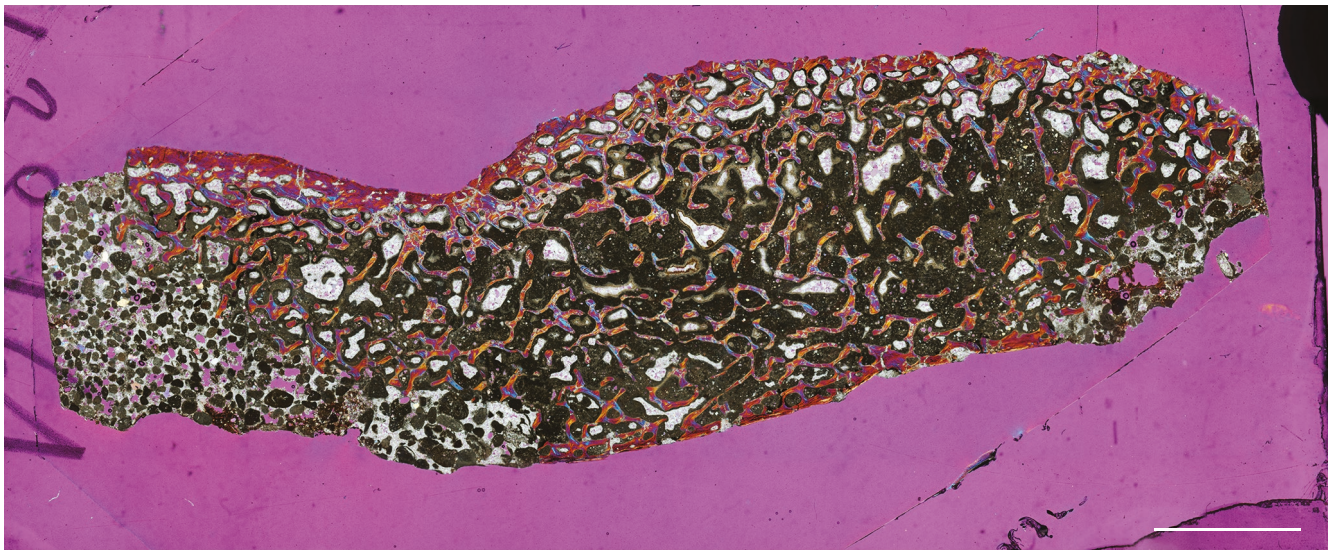

Appendix 22. — ZPAL V. 39/61. ?Ninth marginal and third supramarginal area (peripheral and costal, possibly supernumerary carapacial ossification), sectioned transversely (longitudinally along the costal) in polarized light. Scale bar: 5 mm.

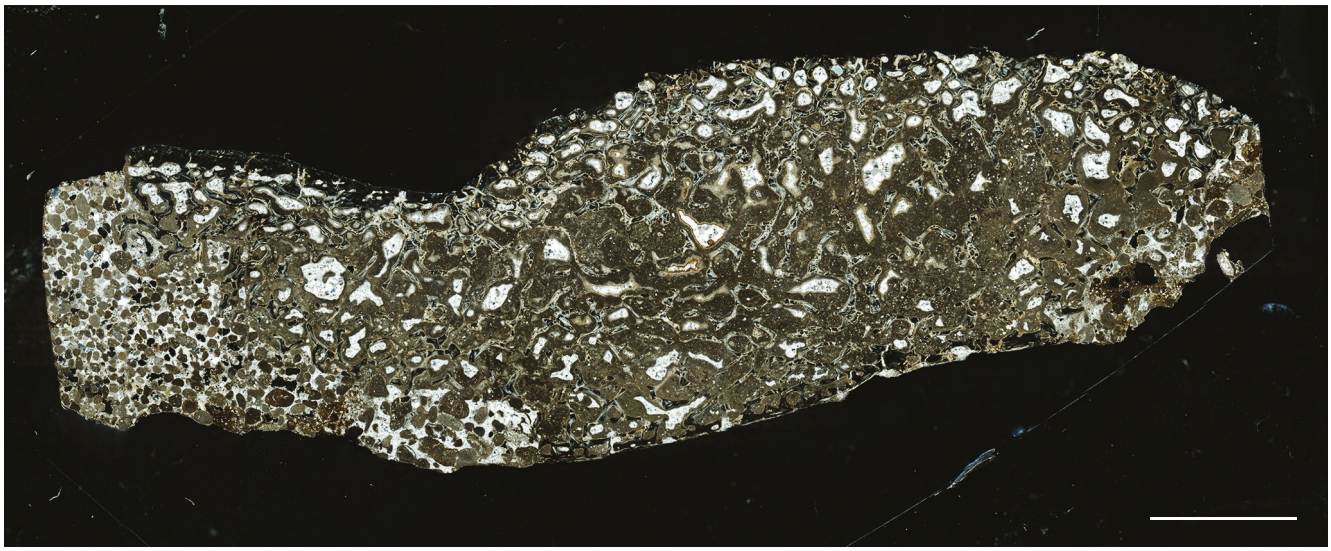

Appendix 23. — ZPAL V. 39/68. Posterior part of the ischium and plastron sectioned transversely through the caudal and intercaudal ossifications in normal transmitted light. Scale bar: 1 cm.

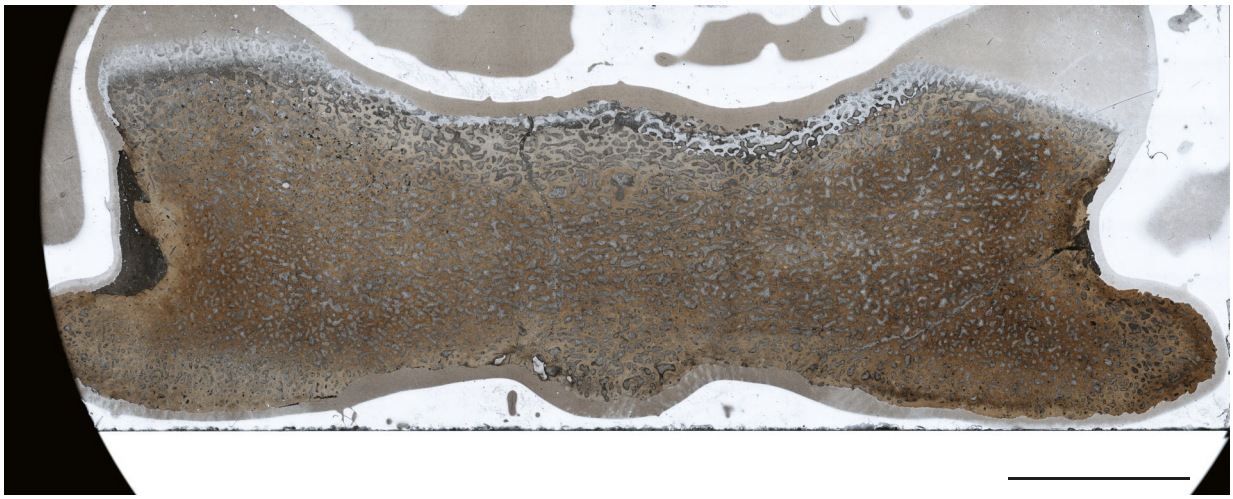

Appendix 24. — ZPAL V. 39/195. Plastral bone from the bridge region (?right first hyoplastron), sectioned longitudinally in normal light. Scale bar: 5 mm.

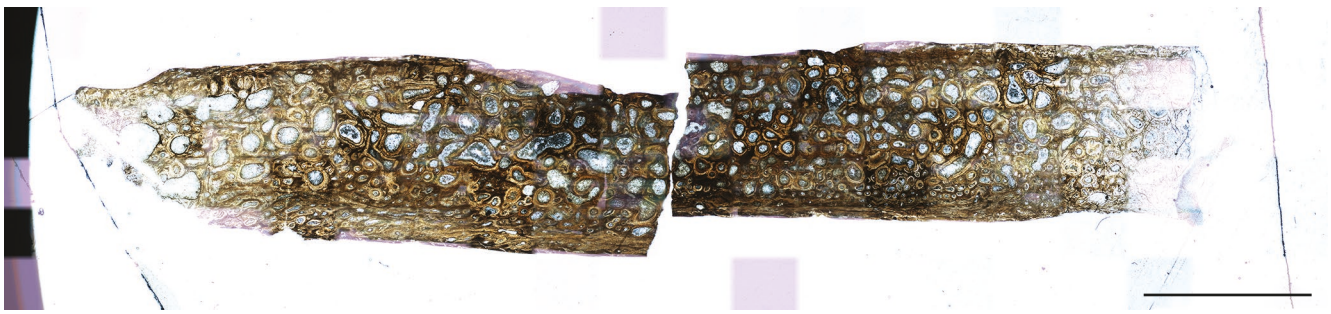

Appendix 25. — ZPAL V. 39/195. Plastral bone from the bridge region (?right first hyoplastron), sectioned longitudinally polarized light with quartz wedge. Scale bar: 5 mm.

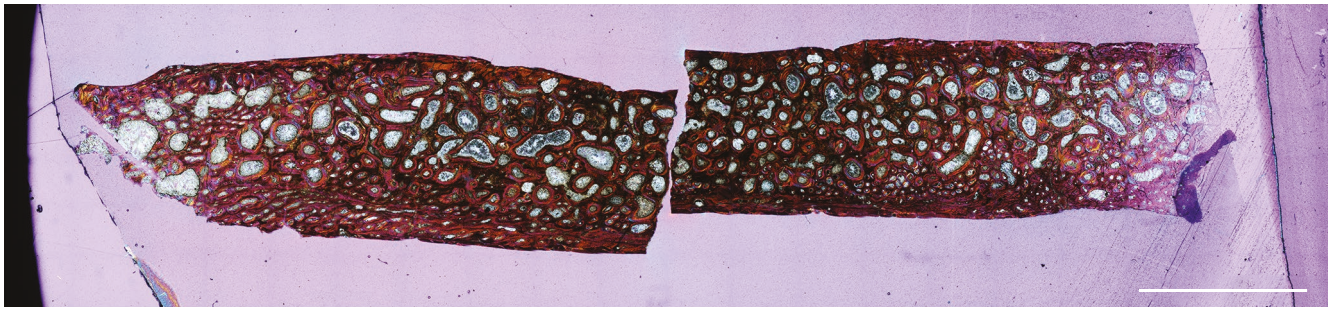

Appendix 26. — ZPAL V. 39/195. Plastral bone from the bridge region (?right first hyoplastron), sectioned longitudinally in polarized light. Scale bar: 5 mm.

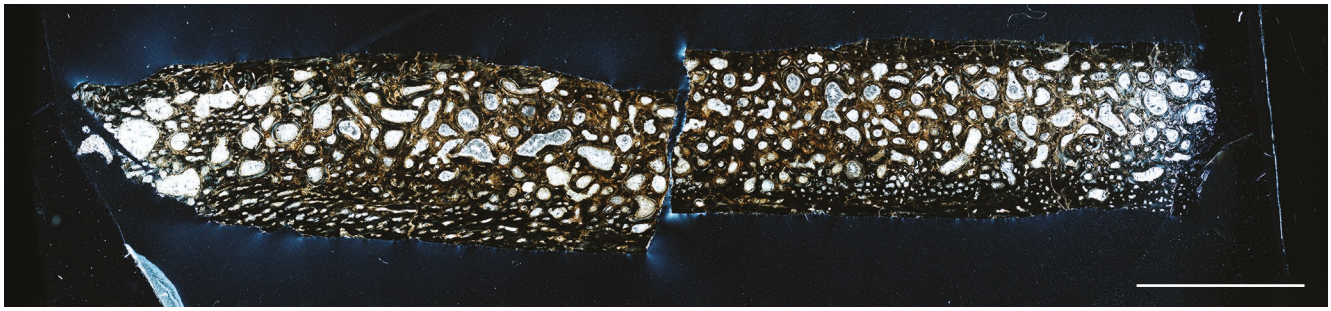

Appendix 27. — ZPAL V. 39/388. Anterior part of the plastron (gular and extragular projections), sectioned transversely in normal light. Scale bar: 1 cm.

Appendix 28. — ZPAL V. 39/392. ?Posterior peripheral, sectioned obliquely in normal light. Scale bar: 5 mm.

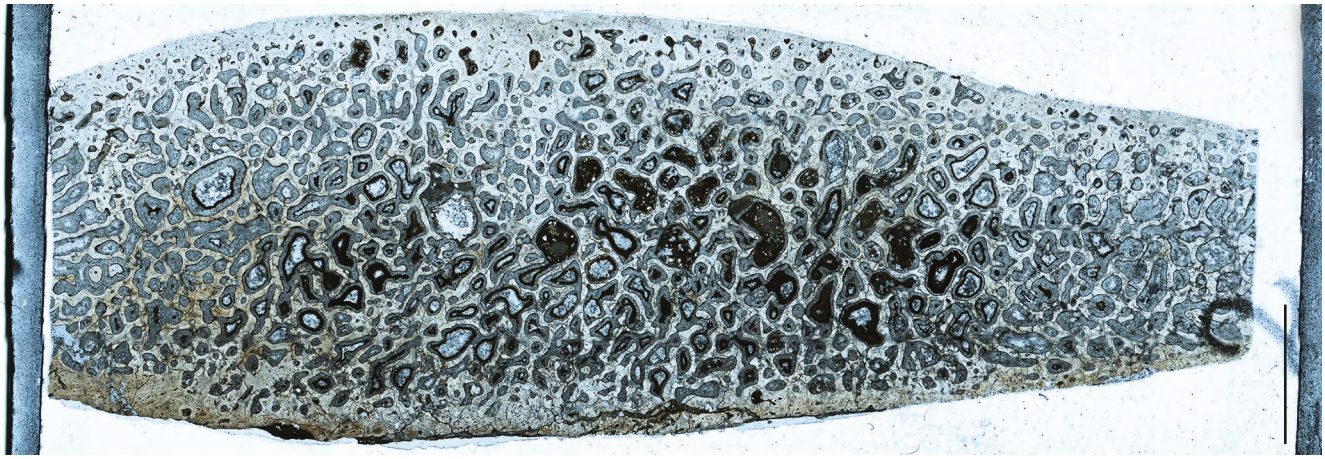

Appendix 29. — ZPAL V. 39/392. ?Posterior peripheral, sectioned obliquely in polarized light with quartz wedge. Scale bar: 5 mm.

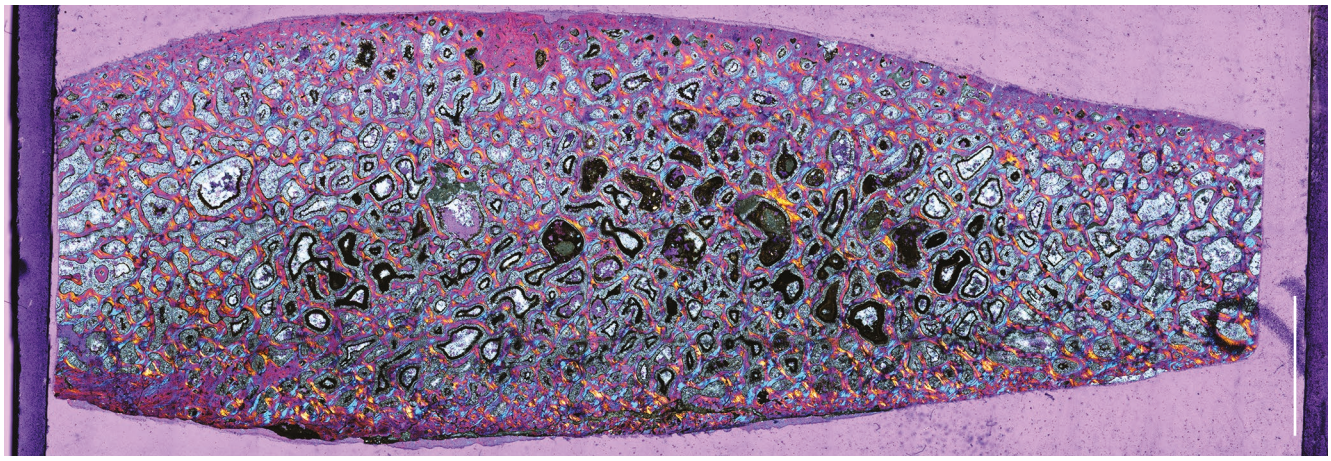

Appendix 30. — ZPAL V. 39/392. ?Posterior peripheral, sectioned obliquely in polarized light. Scale bar: 5 mm.

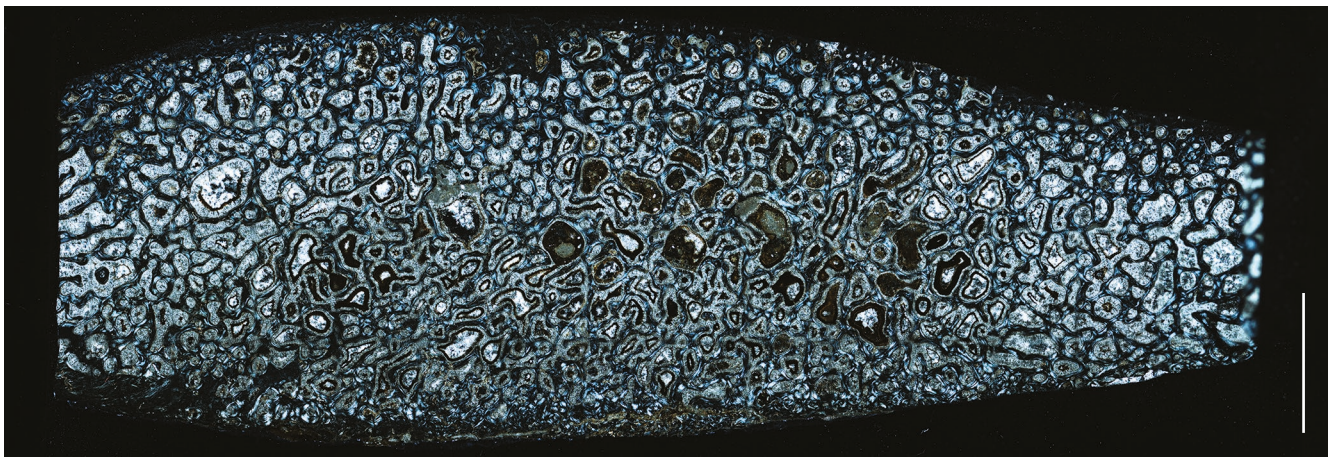

Appendix 31. — ZPAL V. 39/401. Hyoplastra and posterior process of the entoplastron, sectioned transversely in normal light. Scale bar: 5 mm.

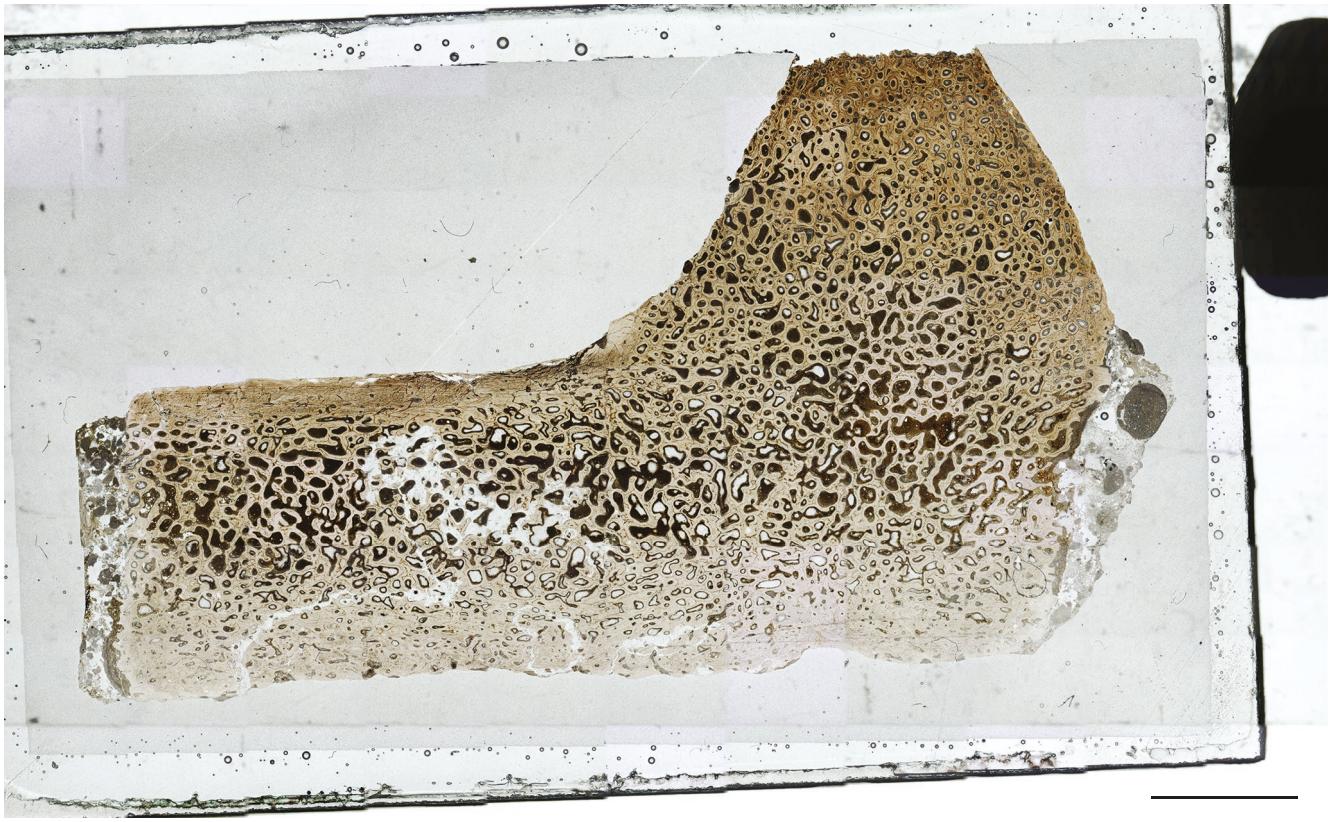

Appendix 32. — ZPAL V. 39/401. Hyoplastra and posterior process of the entoplastron, sectioned transversely in polarized light with quartz wedge. Scale bar: 5 mm.

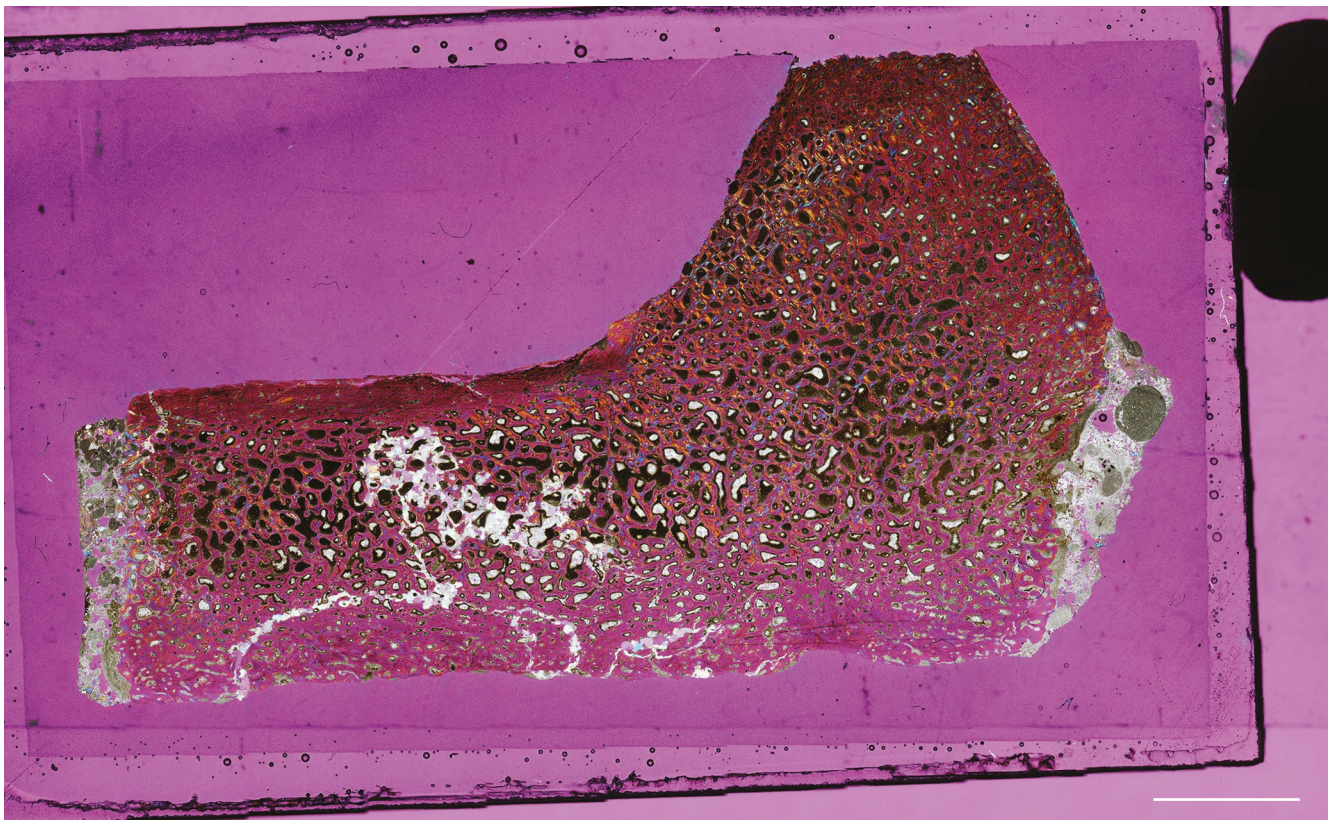

Appendix 33. — ZPAL V. 39/401. Hyoplastra and posterior process of the entoplastron, sectioned transversely in polarized light. Scale bar: 5 mm.

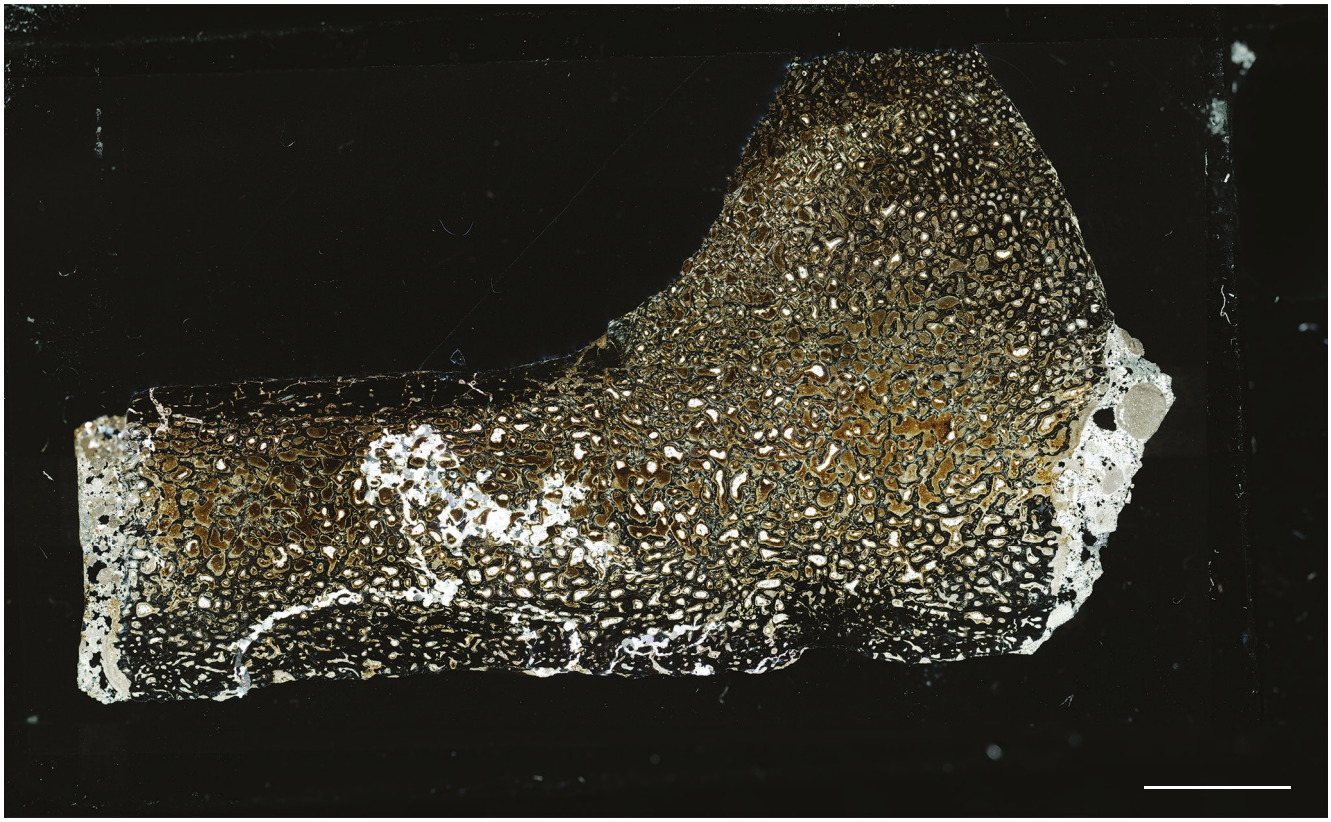

Appendix 34. — ZPAL V. 39/416. Neural bone, sectioned transversely in normal light. Scale bar: 1 mm.

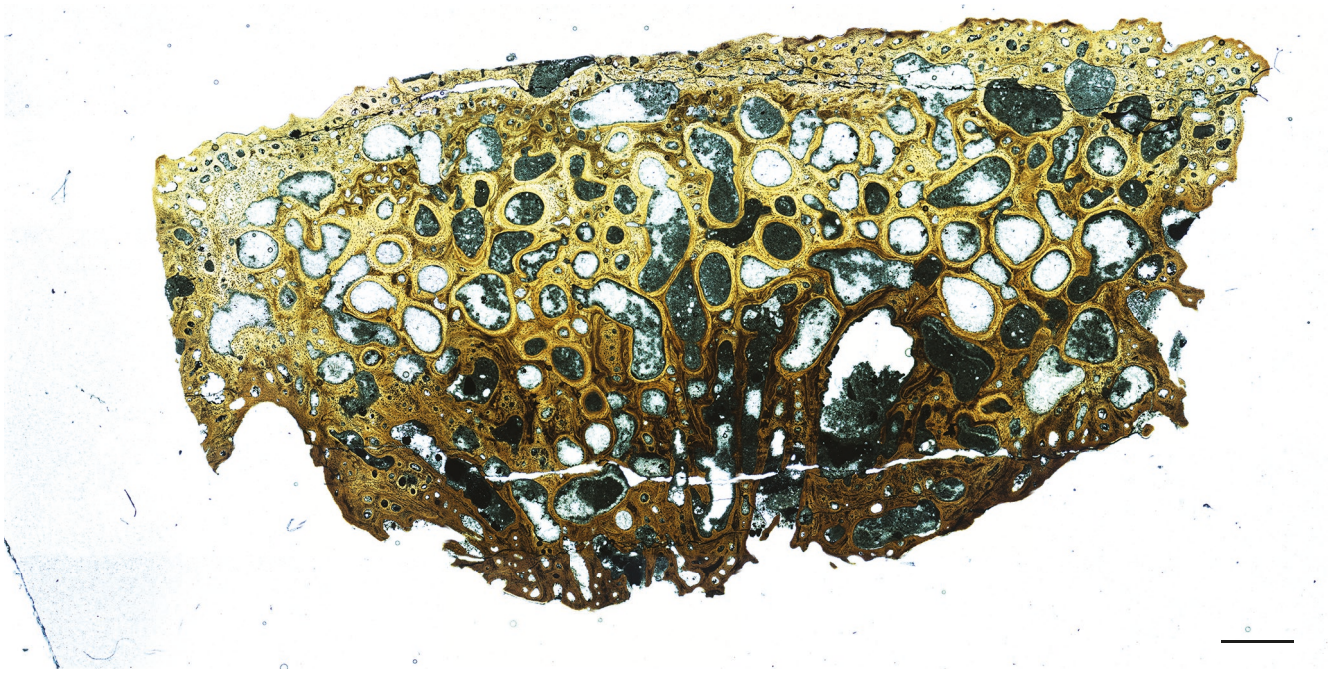

APPENDIX 35. — ZPAL V. 39/416. Neural bone, sectioned transversely in polarized light with quartz wedge. Scale bar: 1 mm.

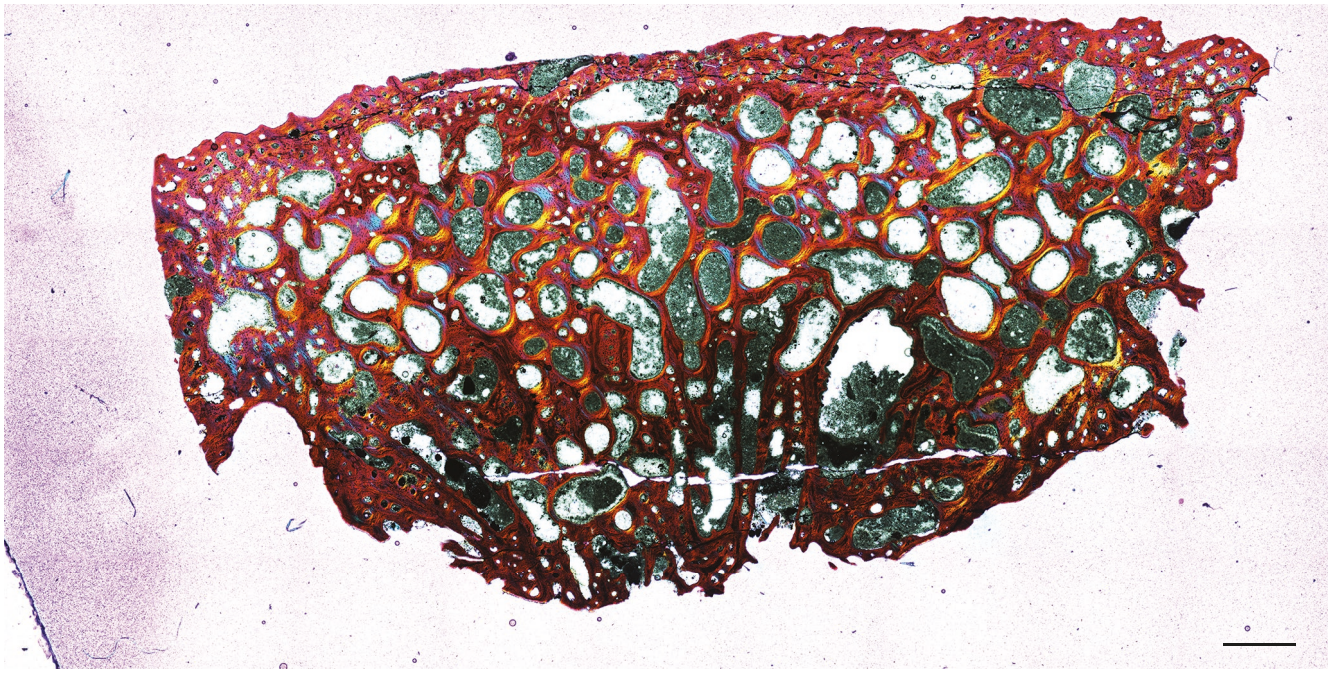

APPENDIX 36. — ZPAL V. 39/416. Neural bone, sectioned transversely in polarized light. Scale bar: 1 mm.

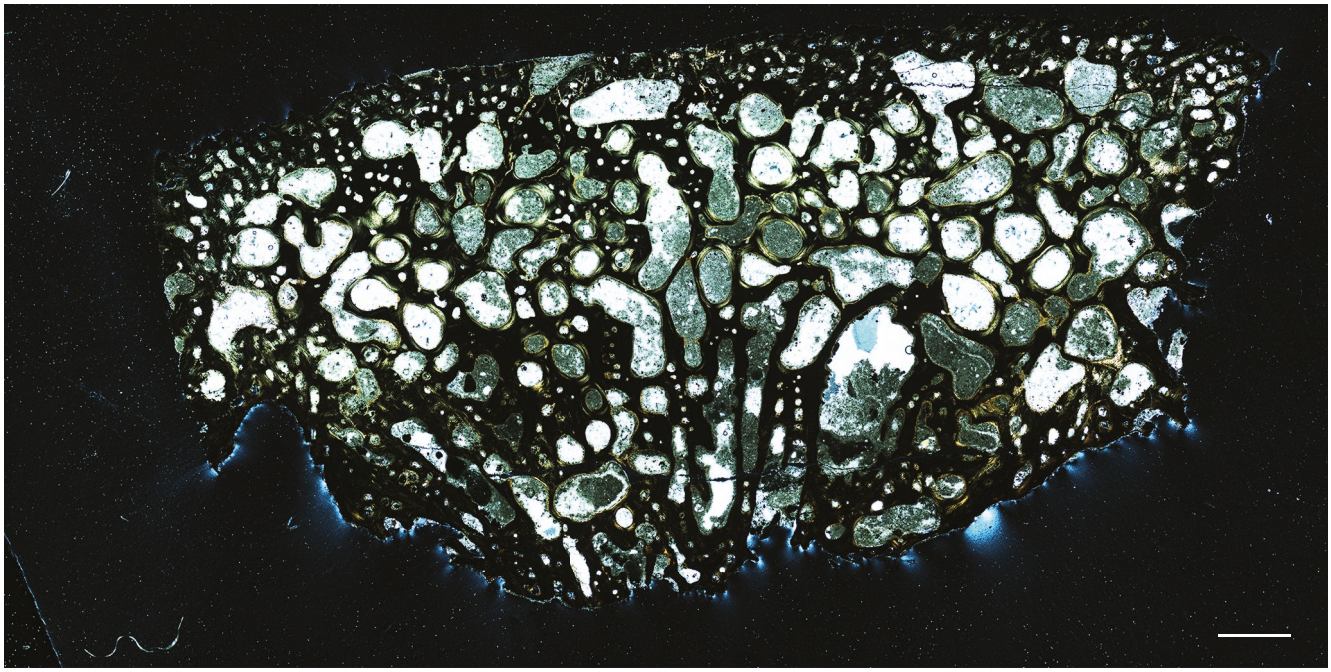

Appendix 37. — ZPAL V. 39/416. Neural bone, sectioned transversely. Close-up of the external cortex in normal light. Scale bar: 0.5 mm.

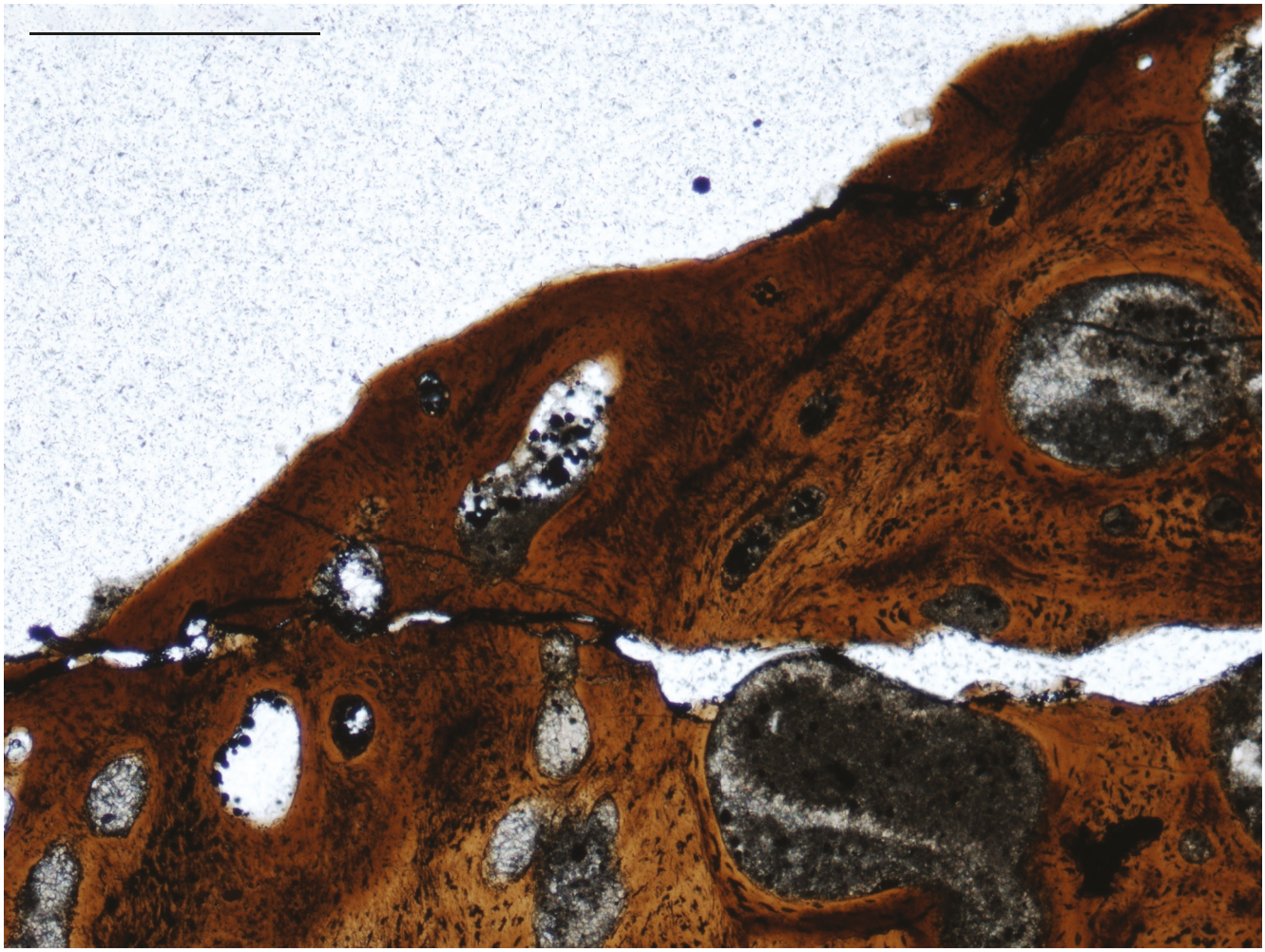

Appendix 38. — ZPAL V. 39/416. Neural bone, sectioned transversely. Close-up of the external cortex in polarized light. Scale bar: 0.5 mm.

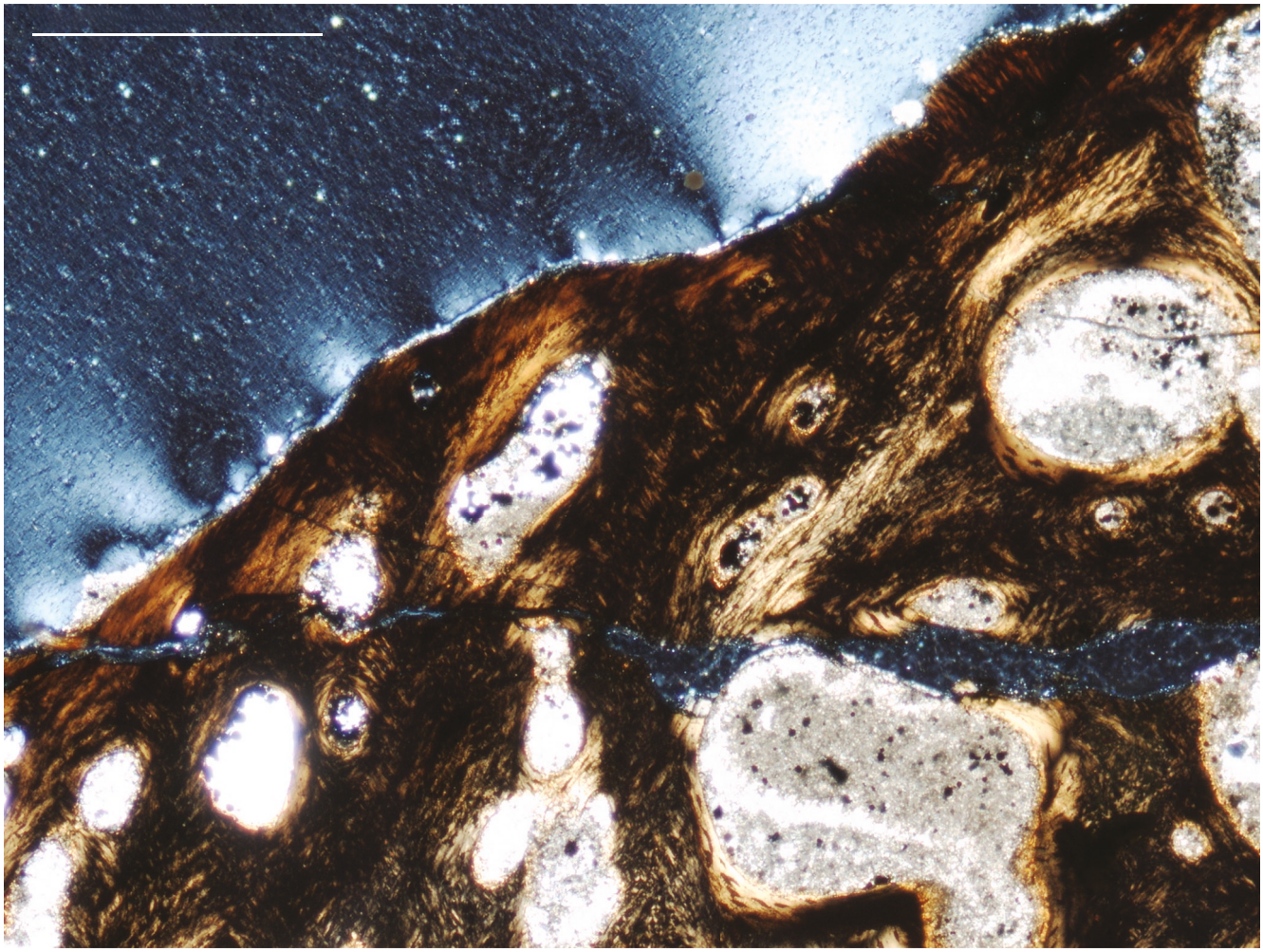

Appendix 39. — ZPAL V. 39/416. Neural bone, sectioned transversely. Close-up of the internal cortex in polarized light. Scale bar: 0.5 mm.

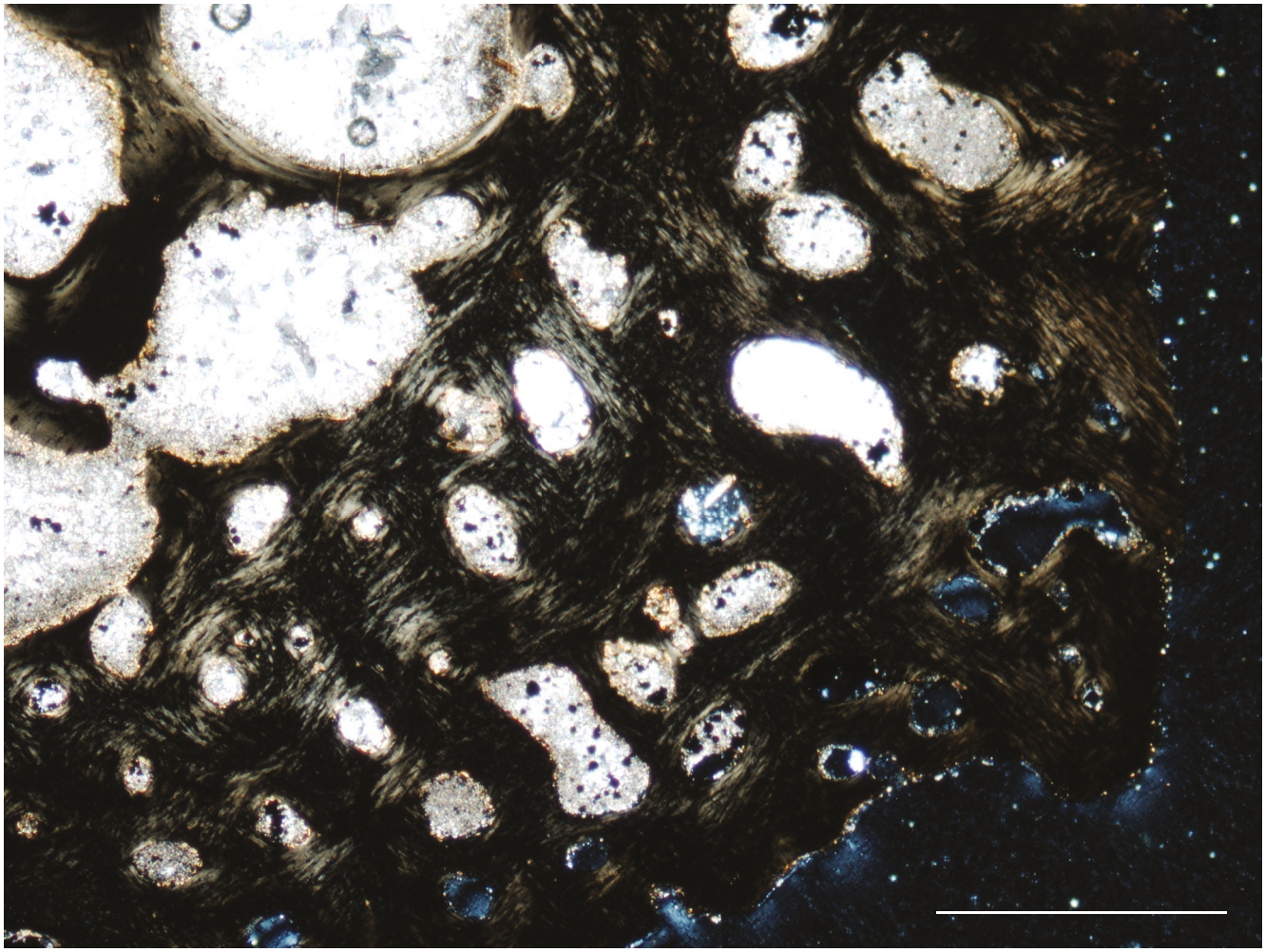

Appendix 40. — ZPAL V. 39/417. Supernumerary carapacial ossification (?third or fourth pleural boss), sectioned obliquely in normal light. Scale bar: 5 mm.

APPENDIX 41. — ZPAL V. 39/417. Supernumerary carapacial ossification (?third or fourth pleural boss), sectioned obliquely in polarized light with quartz wedge. Scale bar: 5 mm.

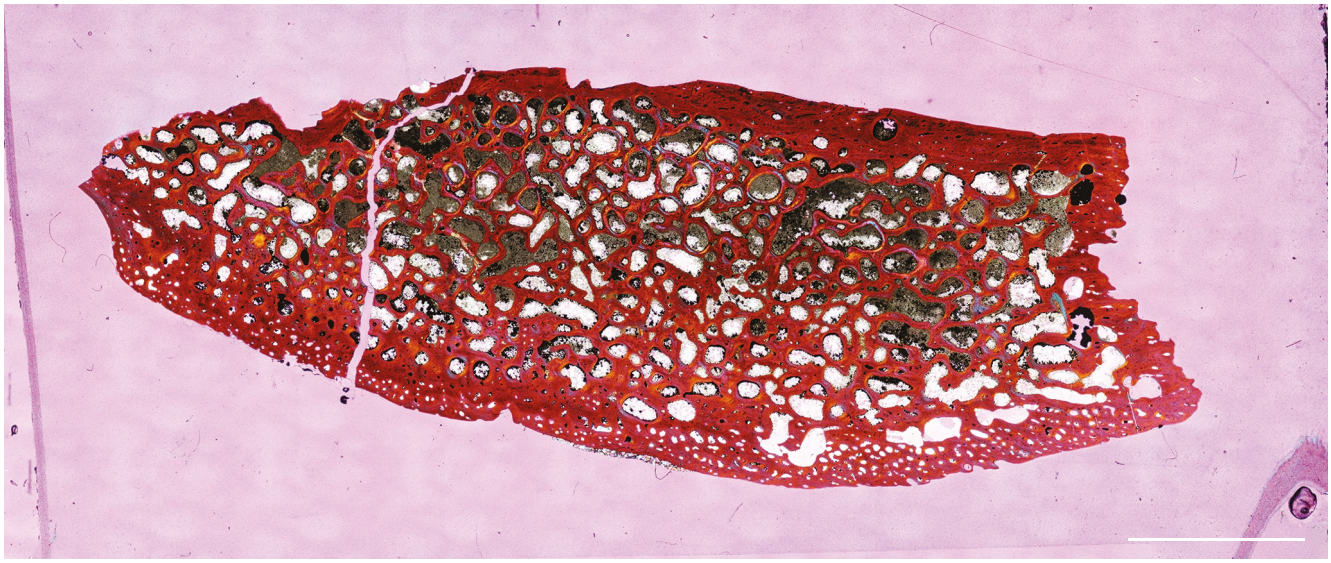

APPENDIX 42. — ZPAL V. 39/417. Supernumerary carapacial ossification (?third or fourth pleural boss), sectioned obliquely in polarized light. Scale bar: 5 mm.

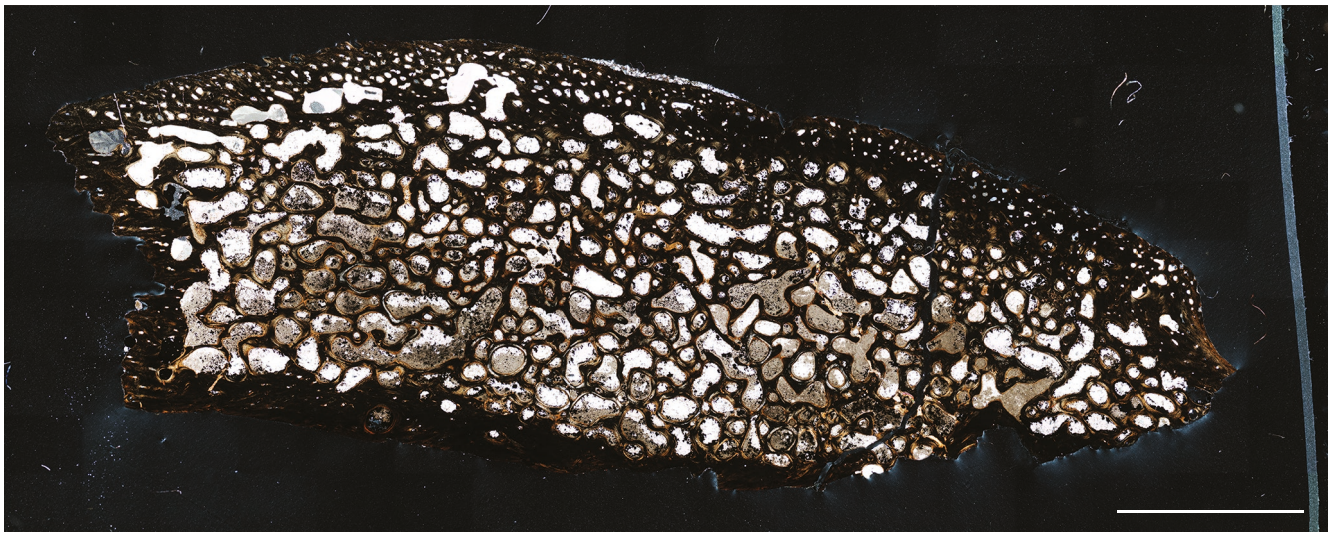

Appendix 43. — ZPAL V. 39/417. Supernumerary carapacial ossification (?third or fourth pleural boss), sectioned obliquely. Close-up of the external. Scale bar: 0.5 mm.

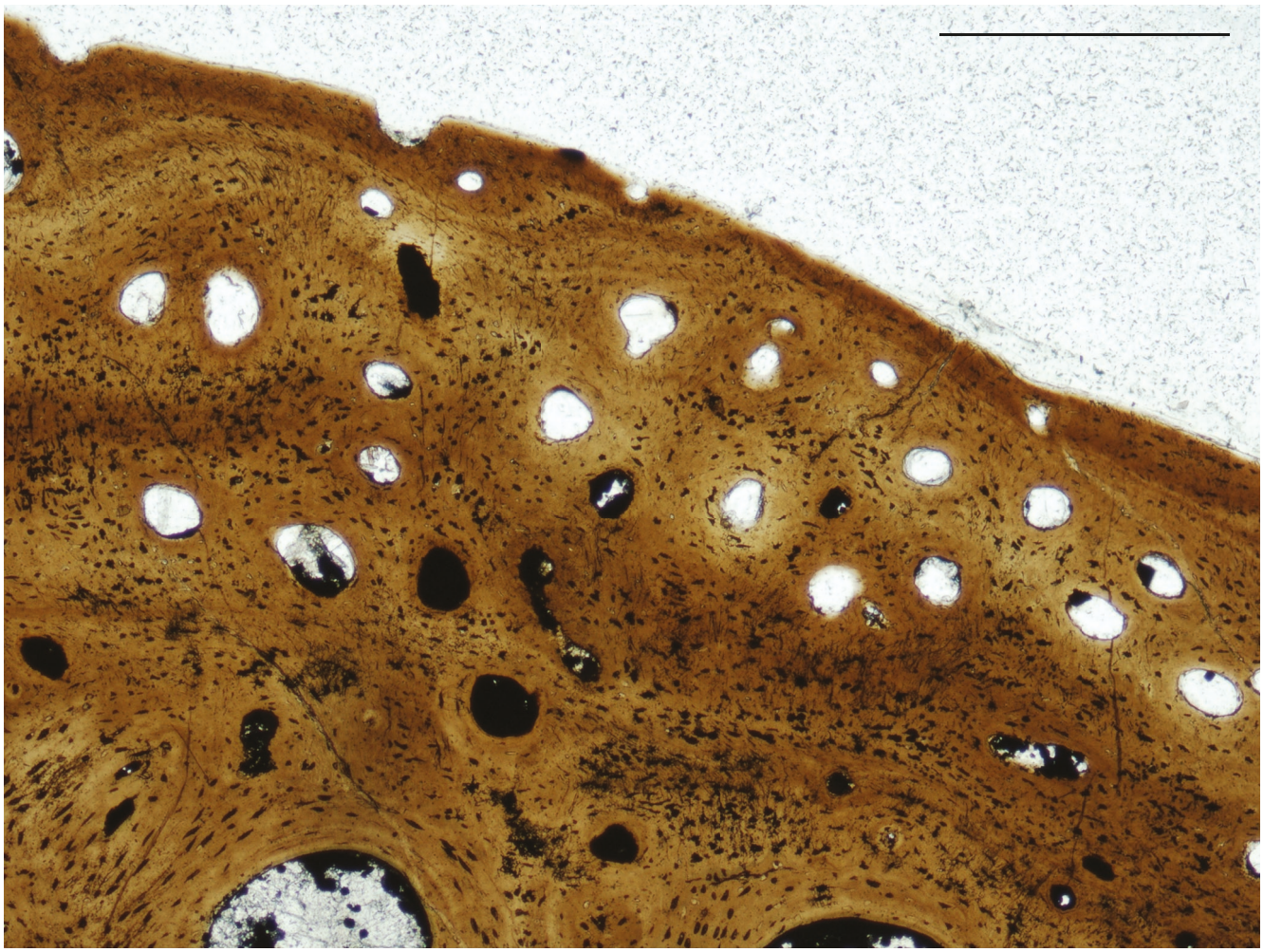

APPENDIX 44. — ZPAL V. 39/417. Supernumerary carapacial ossification (?third or fourth pleural boss), sectioned obliquely. Close-up of the external cortex in polarized light. Scale bar: 0.5 mm.

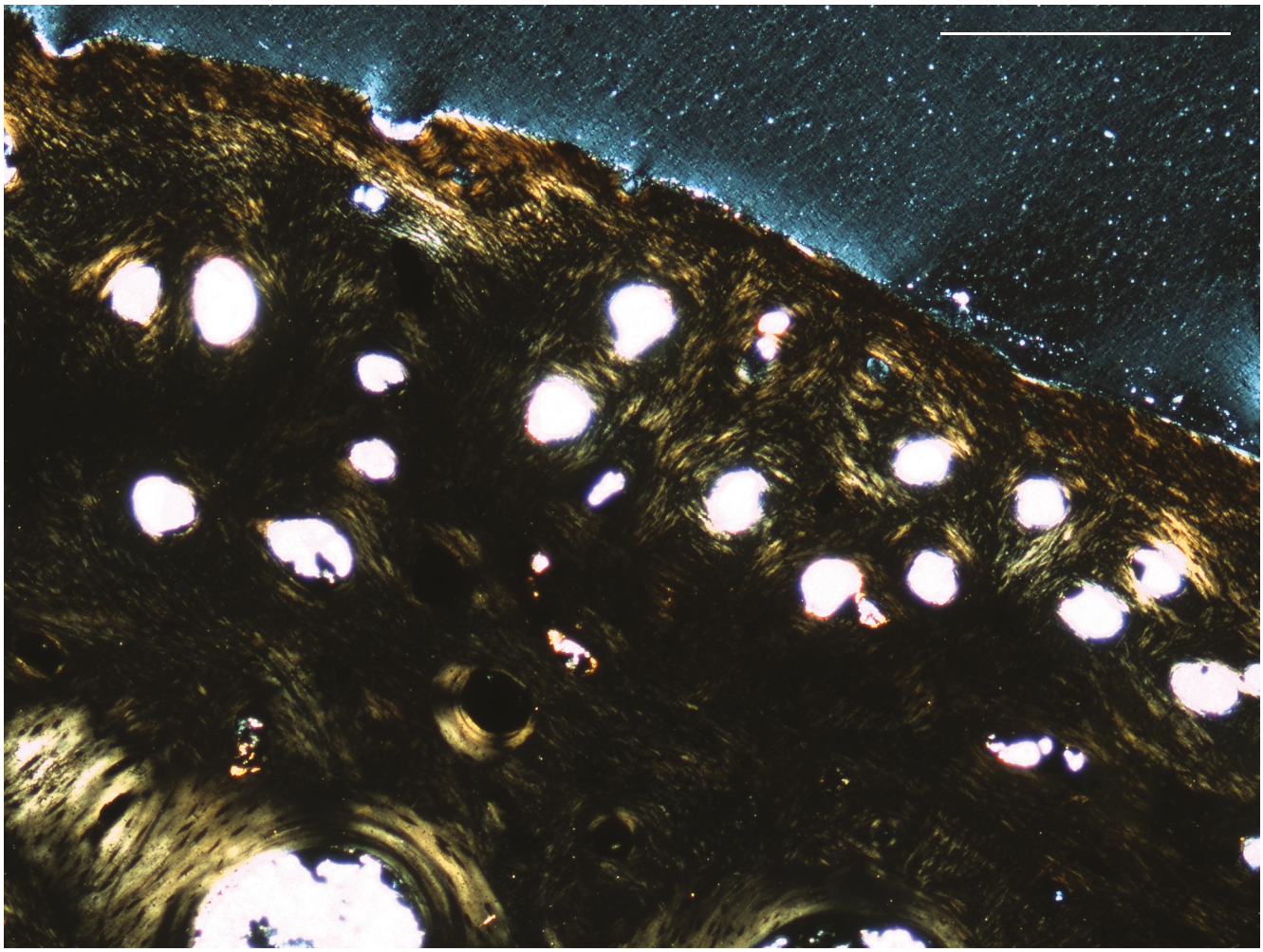

Appendix 45. — ZPAL V. 39/417. Supernumerary carapacial ossification (?third or fourth pleural boss), sectioned obliquely. Close-up of the visceral cortex in polarized light. Scale bar: 0.5 mm.

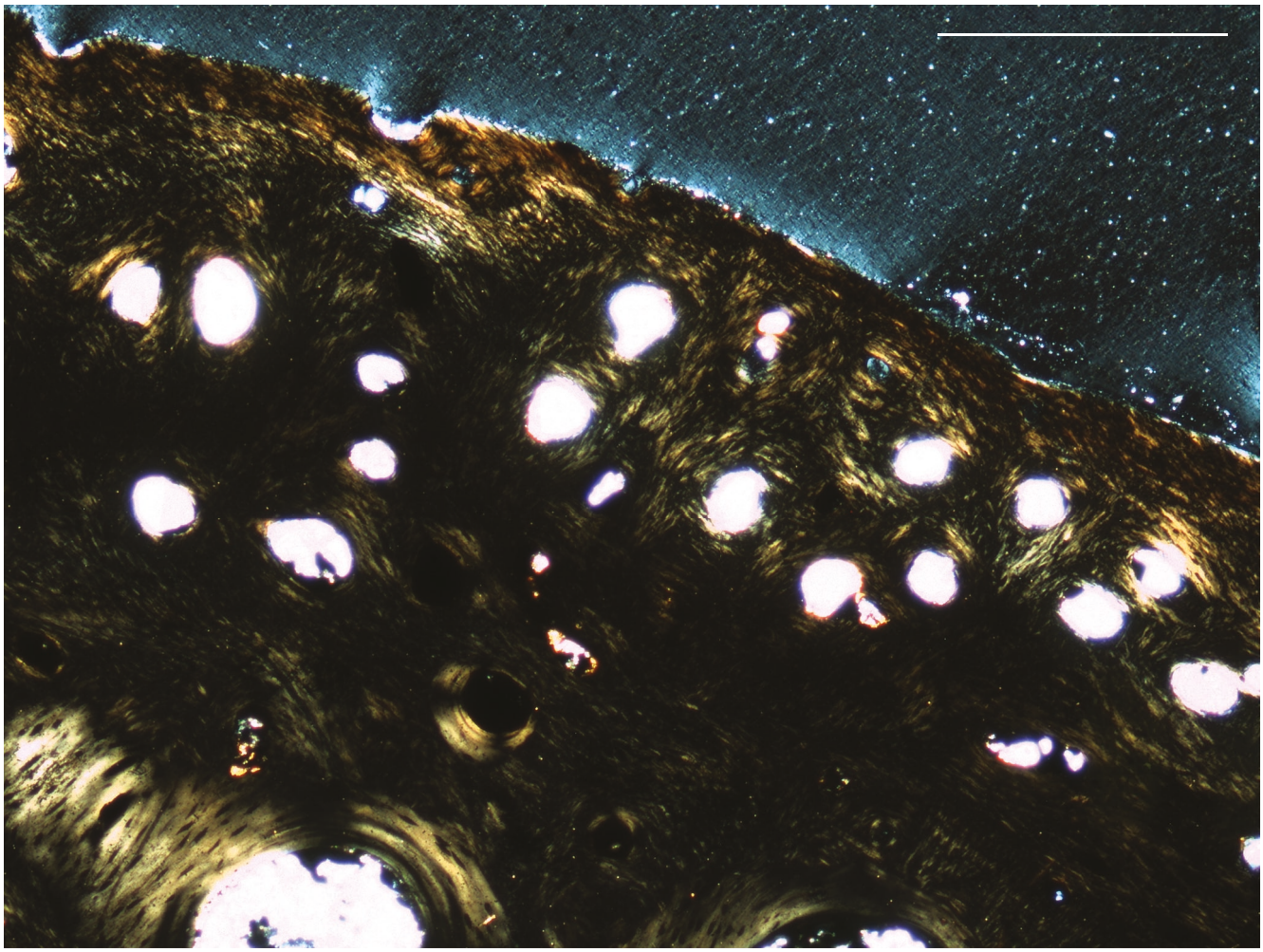

Appendix 46. — ZPAL V. 39/476. Plastral bone from the bridge region (?right hyoplastron), sectioned longitudinally in normal light. Scale bar: 5 mm.

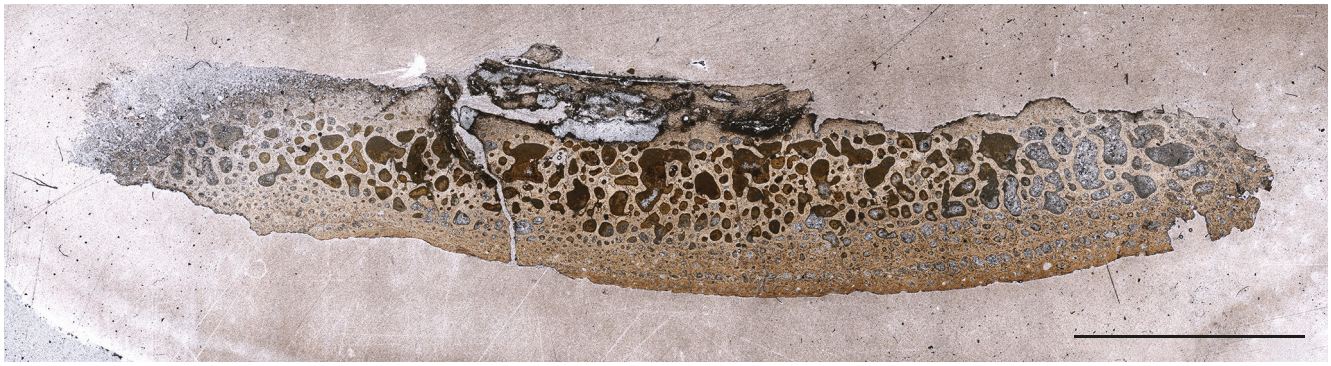

Appendix 47. — ZPAL V. 39/476. Plastral bone from the bridge region (?right hyoplastron), sectioned longitudinally in polarized light with quartz wedge. Scale bar: 5 mm.

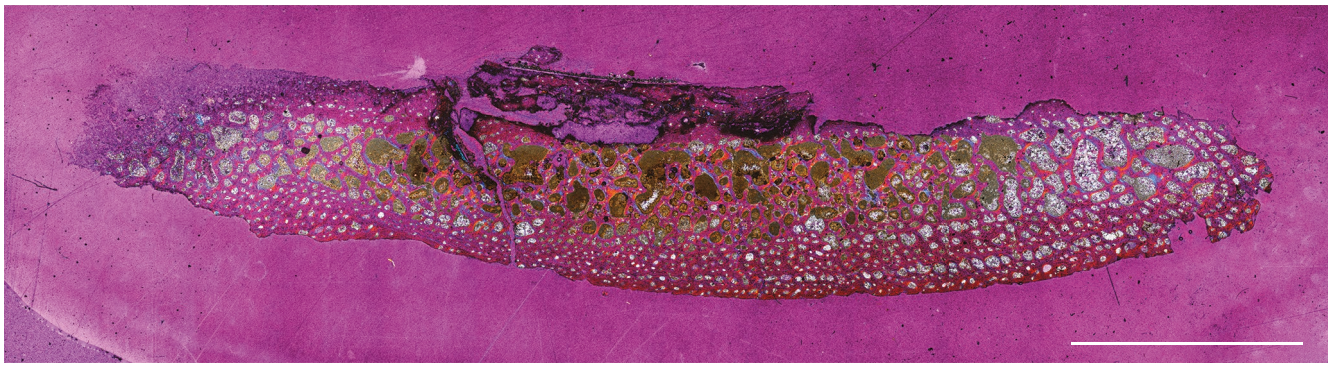

Appendix 48. — ZPAL V. 39/476. Plastral bone from the bridge region (?right hyoplastron), sectioned longitudinally in polarized light. Scale bar: 5 mm.

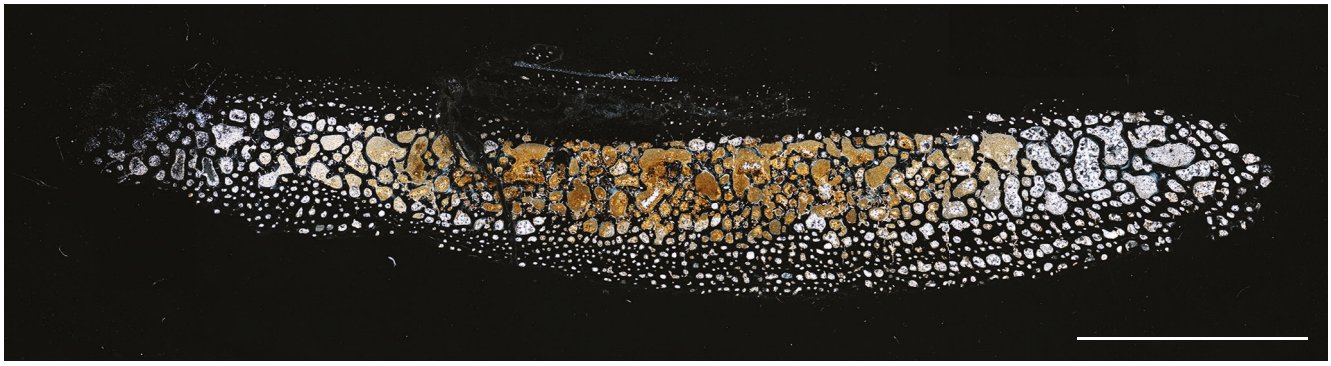

Appendix 49. — ZPAL V. 39/477. Costal bone, sectioned transversely in normal light. Scale bar: 5 mm.

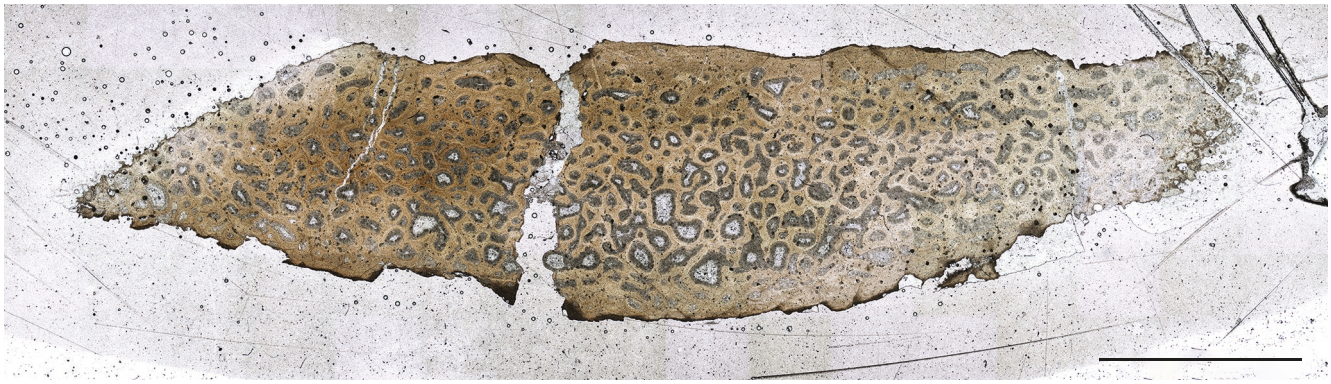

Appendix 50. — ZPAL V. 39/477. Costal bone, sectioned transversely in polarized light with quartz wedge. Scale bar: 5 mm.

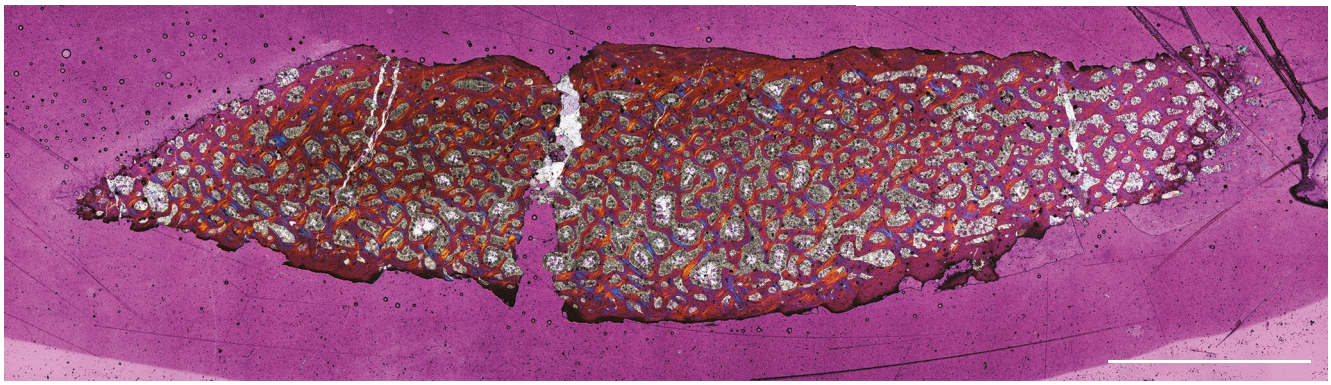

Appendix 51. — ZPAL V. 39/477. Costal bone, sectioned transversely in polarized light. Scale bar: 5 mm.

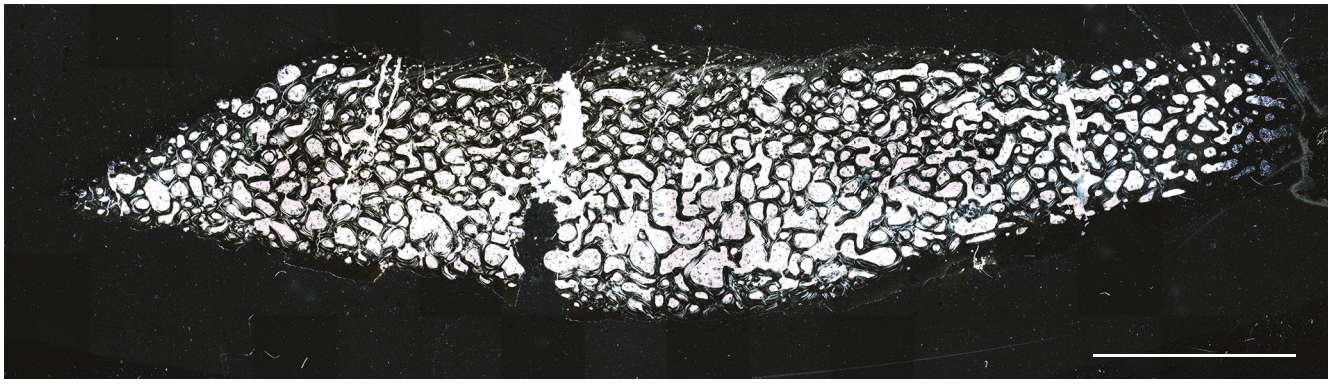

Appendix 52. — ZPAL V. 39/478. Neural bone, sectioned transversely in normal light. Scale bar: 5 mm.

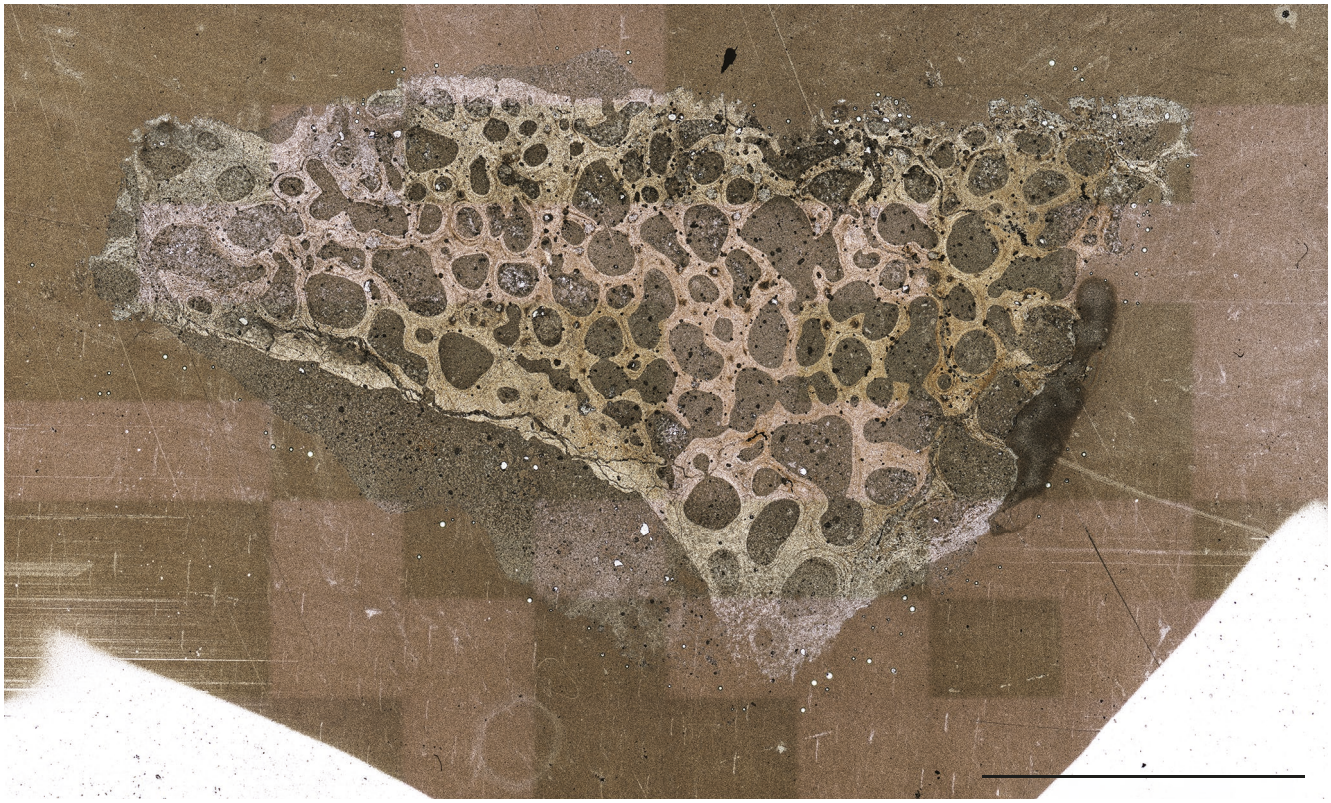

Appendix 53. — ZPAL V. 39/478. Neural bone, sectioned transversely in polarized light with quartz wedge. Scale bar: 5 mm.

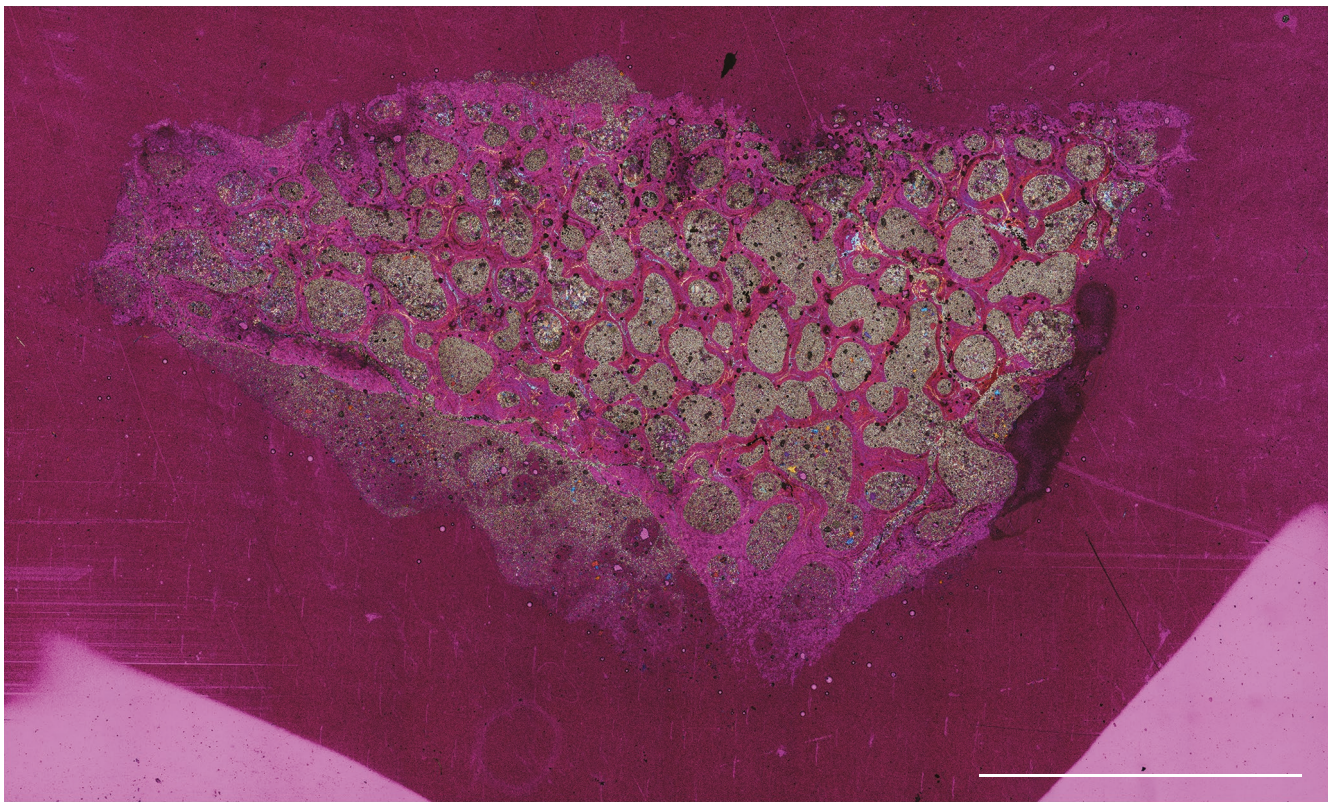

Appendix 54. — ZPAL V. 39/478. Neural bone, sectioned transversely in polarized light. Scale bar: 5 mm.

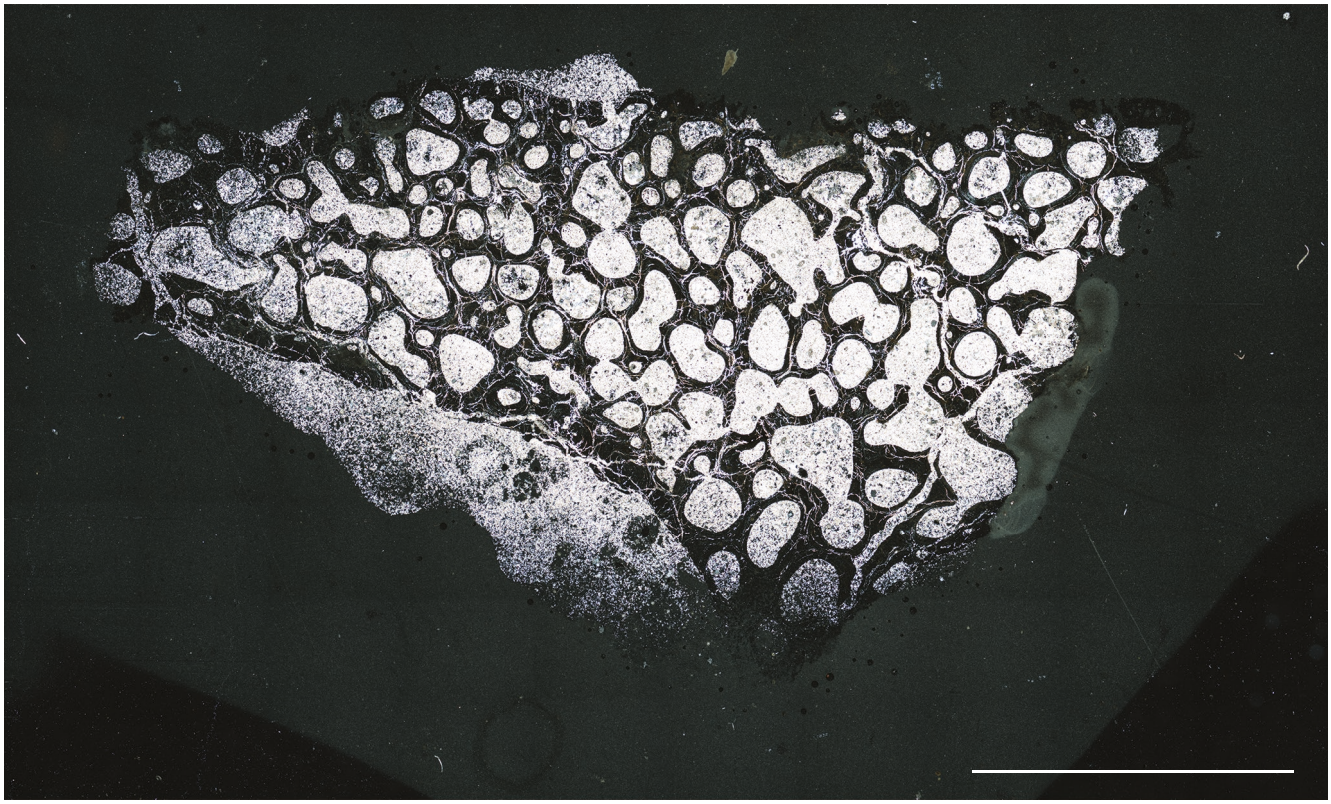

Appendix 55. — ZPAL V. 39/479. Costal bone, sectioned transversely in normal light. Scale bar: 5 mm.

APPENDIX 56. — ZPAL V. 39/479. Costal bone, sectioned transversely in polarized light with quartz wedge. Scale bar: 5 mm.

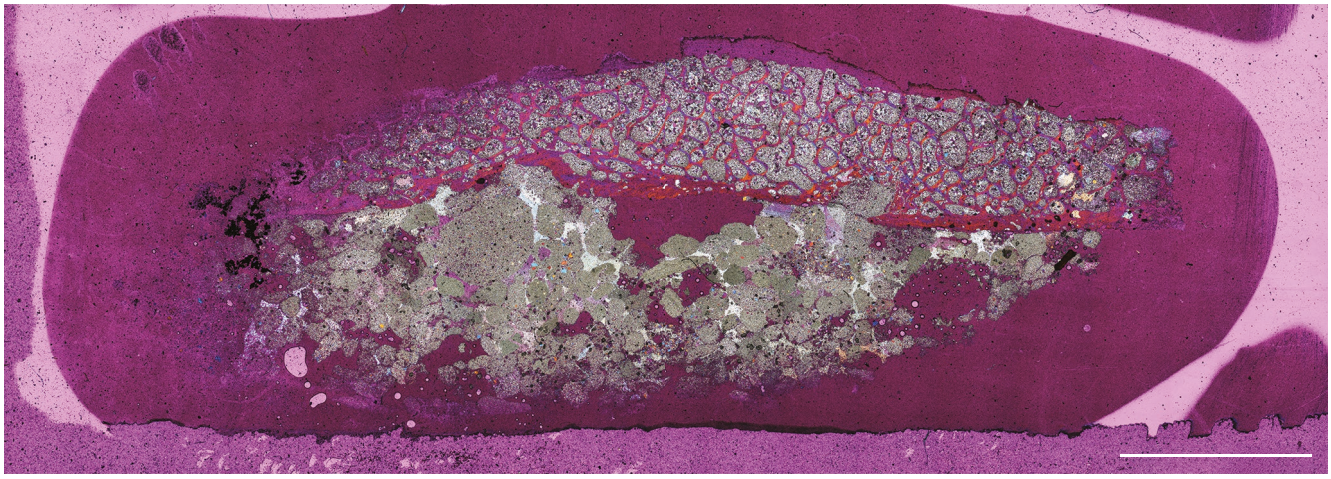

APPENDIX 57. — ZPAL V. 39/479. Costal bone, sectioned transversely in polarized light. Scale bar: 5 mm.

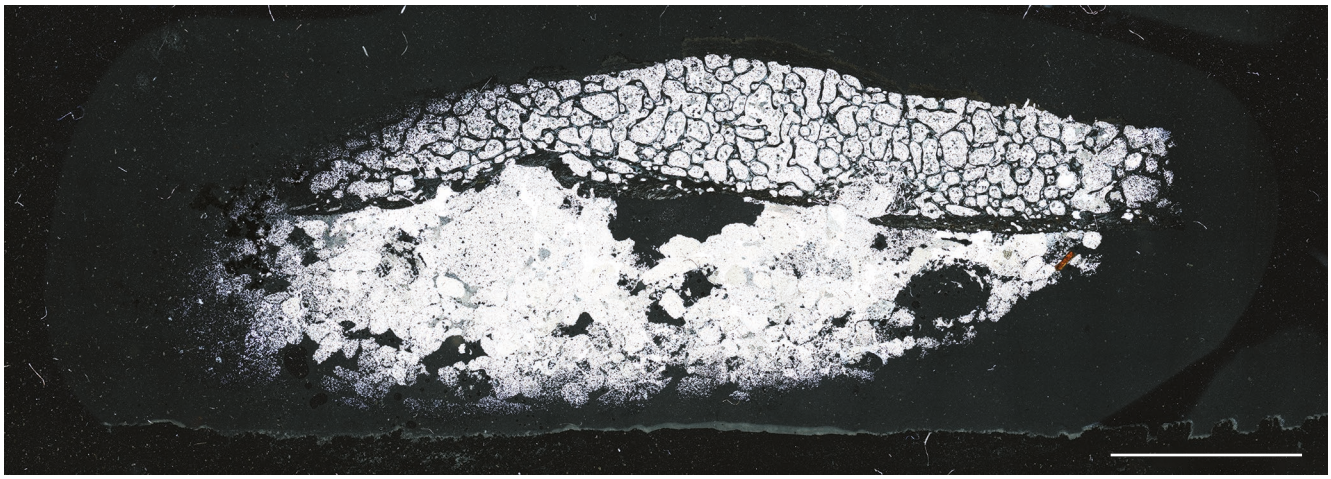

Appendix 58. — ZPAL V. 39/480. Distal part of a costal sectioned transversely in normal light. Scale bar: .0.1 cm

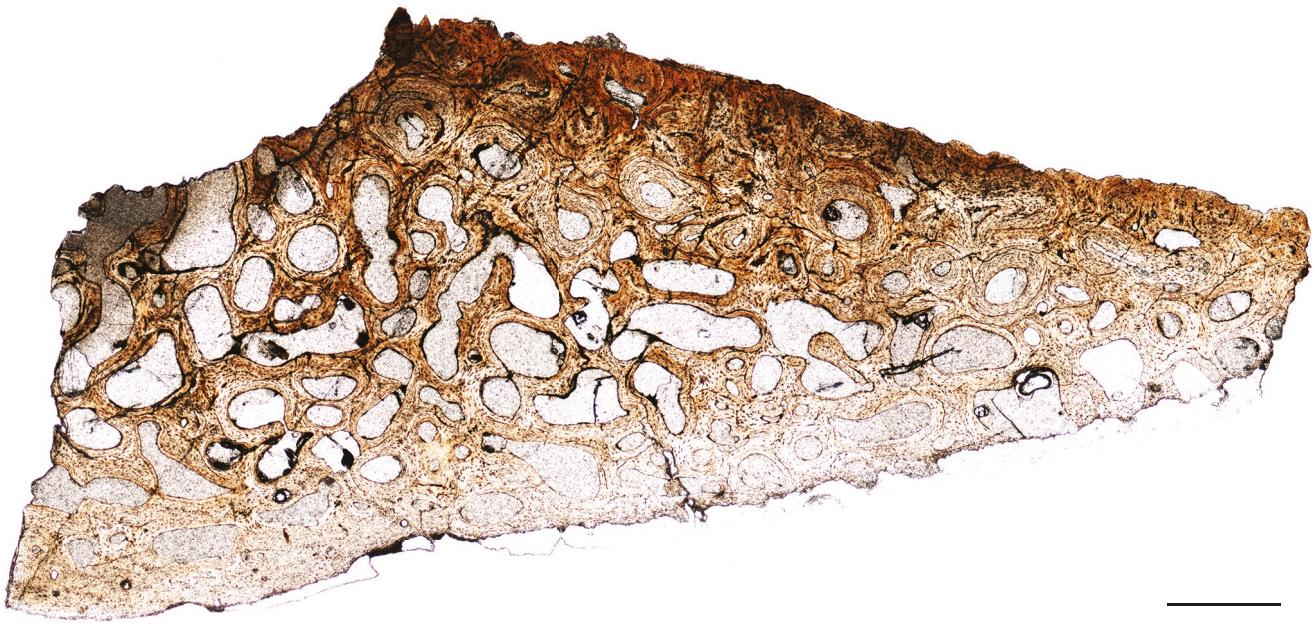

Appendix 59. — ZPAL V. 39/480. Distal part of a costal sectioned transversely in polarized light. Scale bar: 0.1 cm.

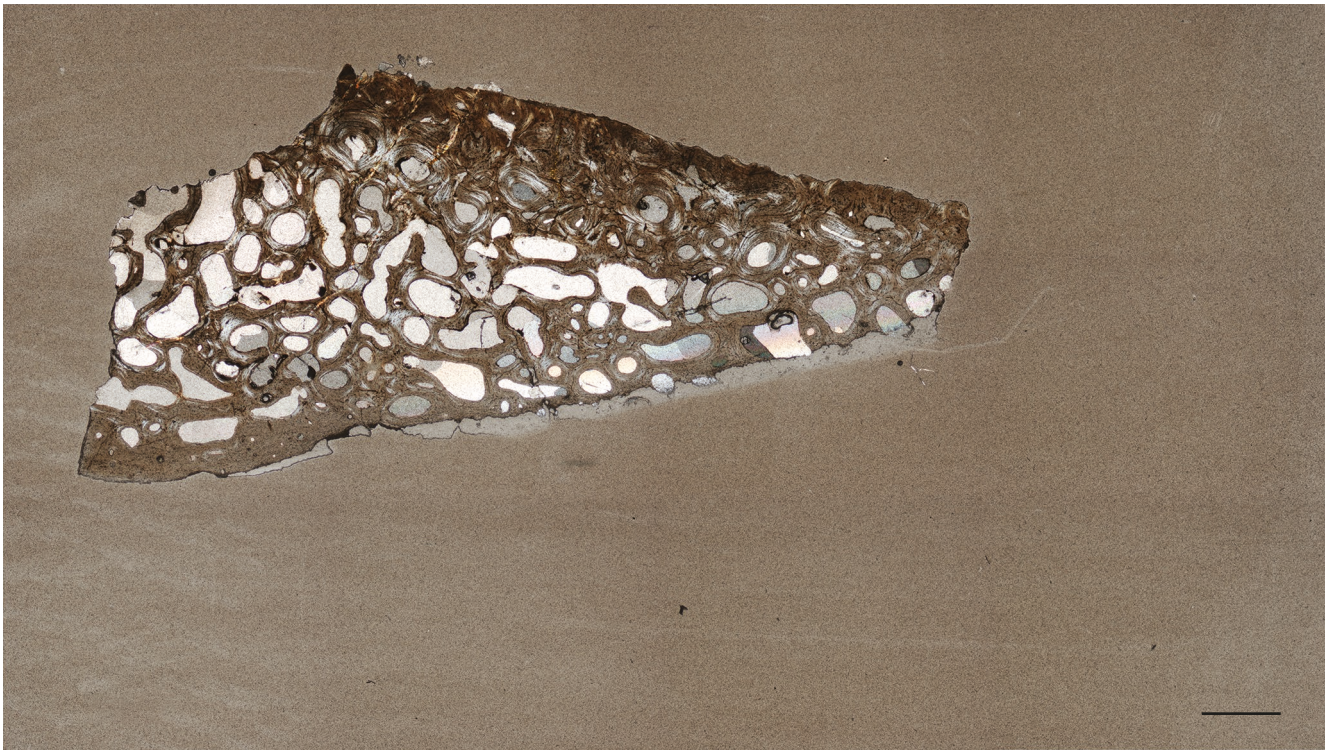

Appendix 60. — ZPAL V. 39/480. Costal sectioned longitudinally in normal light. Scale bar: 1 cm.

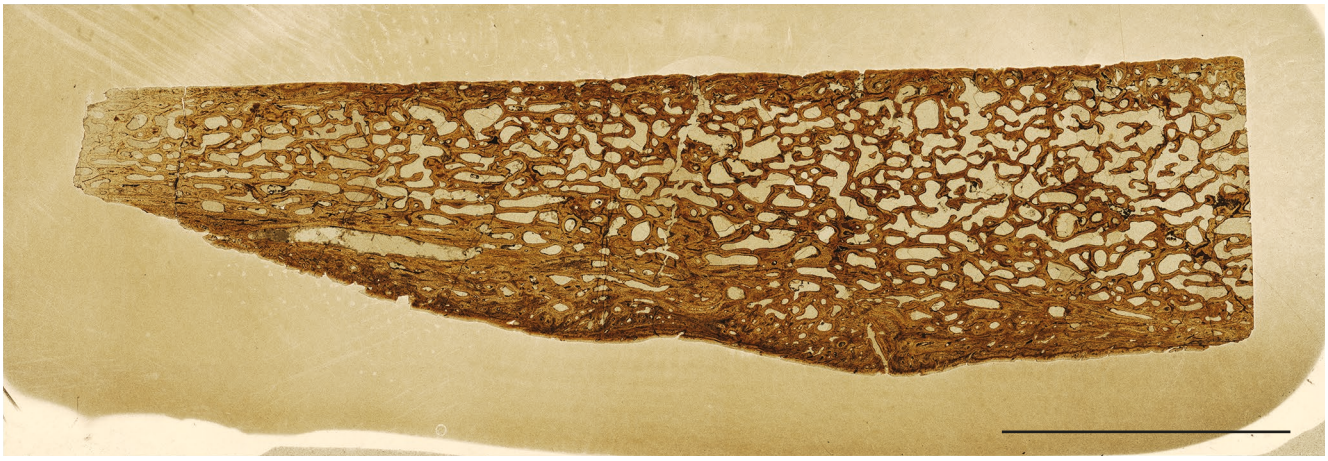

Appendix 61. — ZPAL V. 39/480. Costal sectioned longitudinally in polarized light. Scale bar: 1 cm.

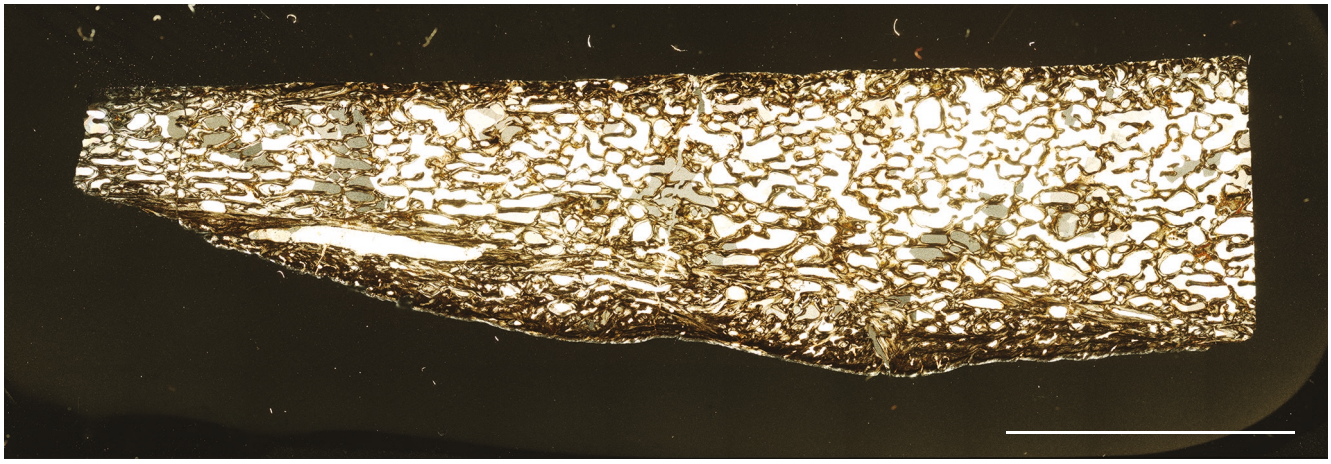

Appendix 62. — ZPAL V. 39/480. Costal sectioned longitudinally. Close-up of a canal-like structure in the external cortex in normal light. Scale bar: 0.1 cm.

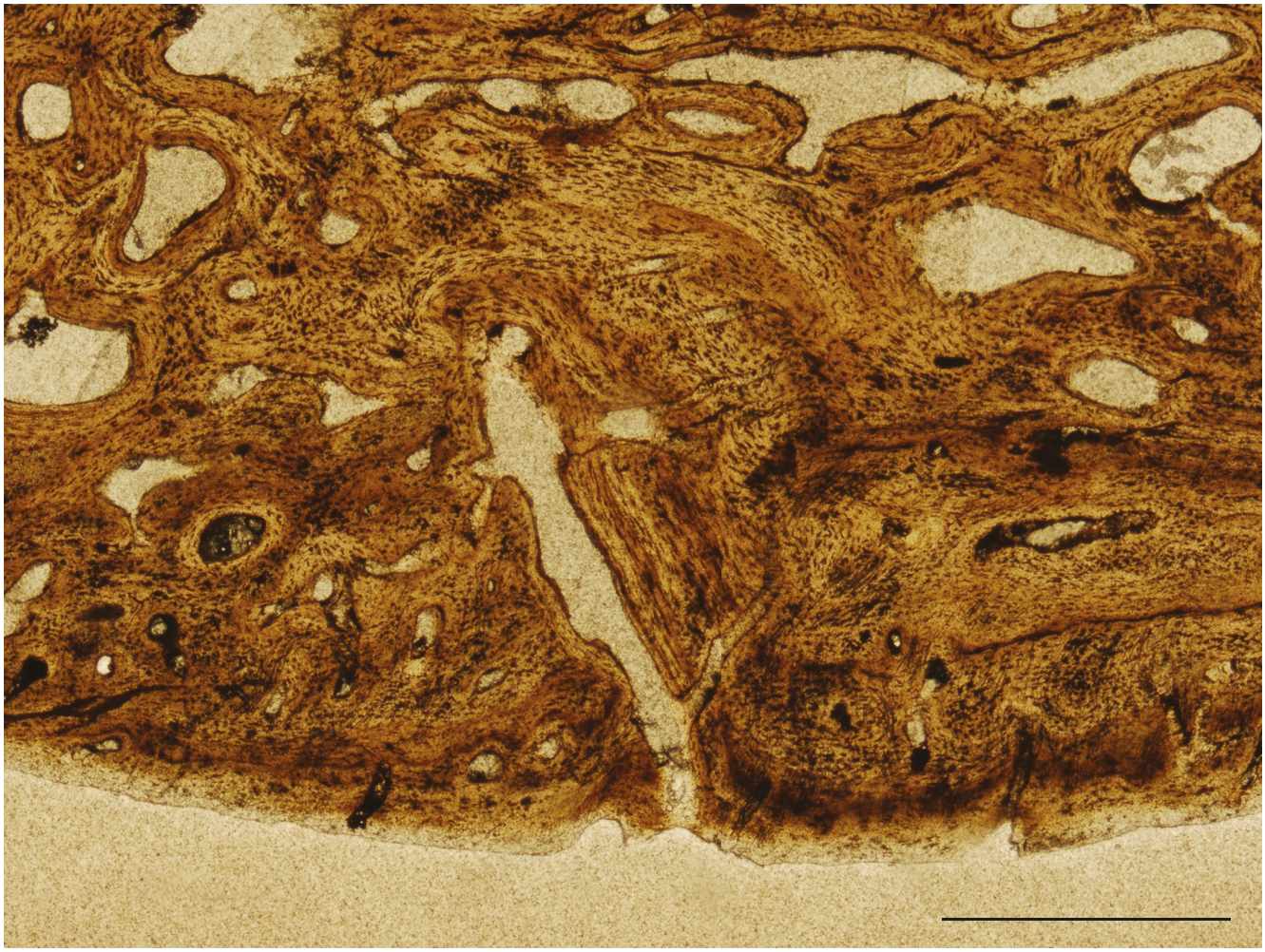

Appendix 63. — ZPAL V. 39/480. Costal sectioned longitudinally. Close-up of a canal-like structure in the external cortex in polarized light. Scale bar: 0.1 cm.

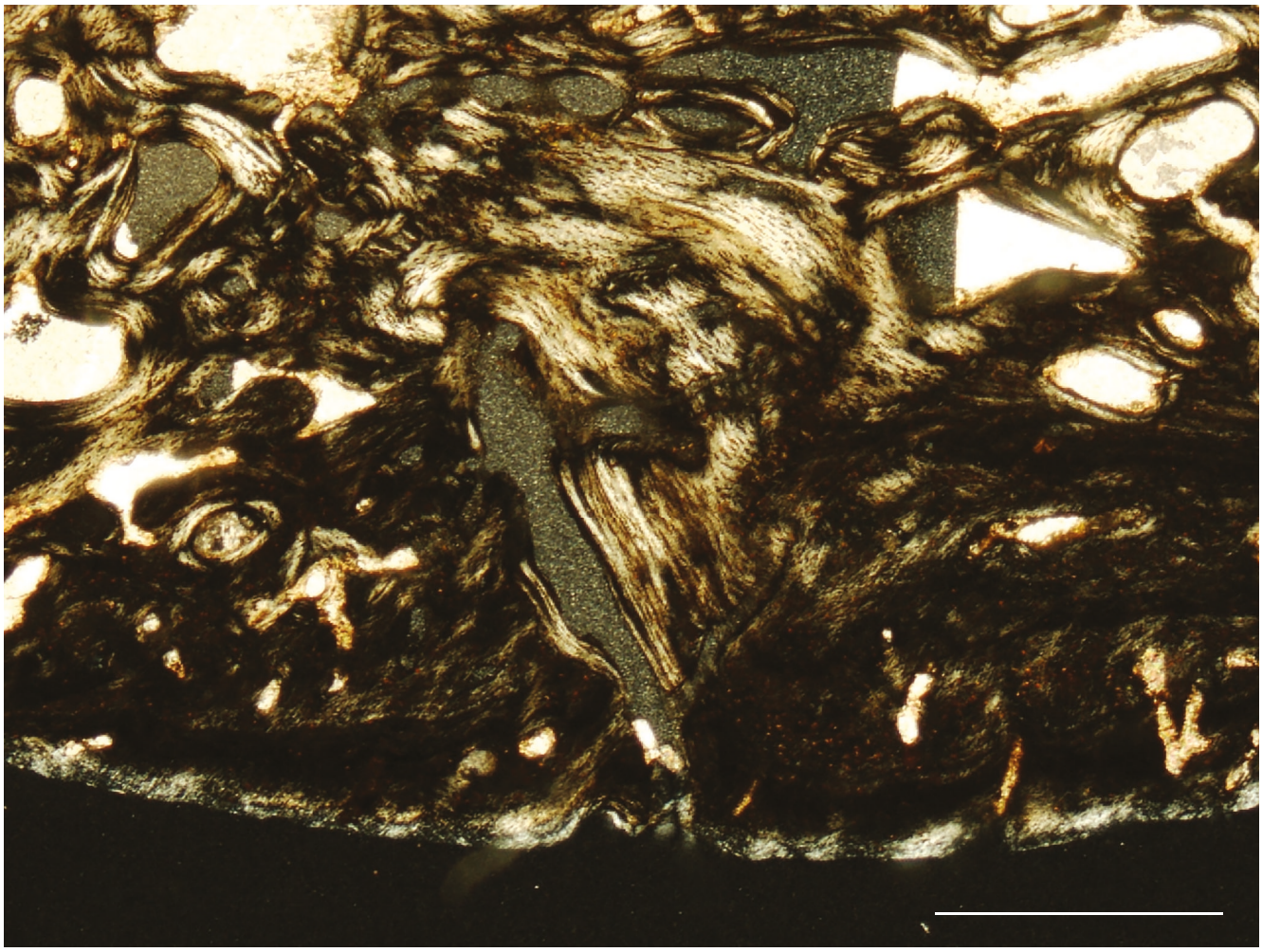

Appendix 64. — ZPAL V. 39/480. Costal sectioned longitudinally in normal light. Scale bar: 1 cm.

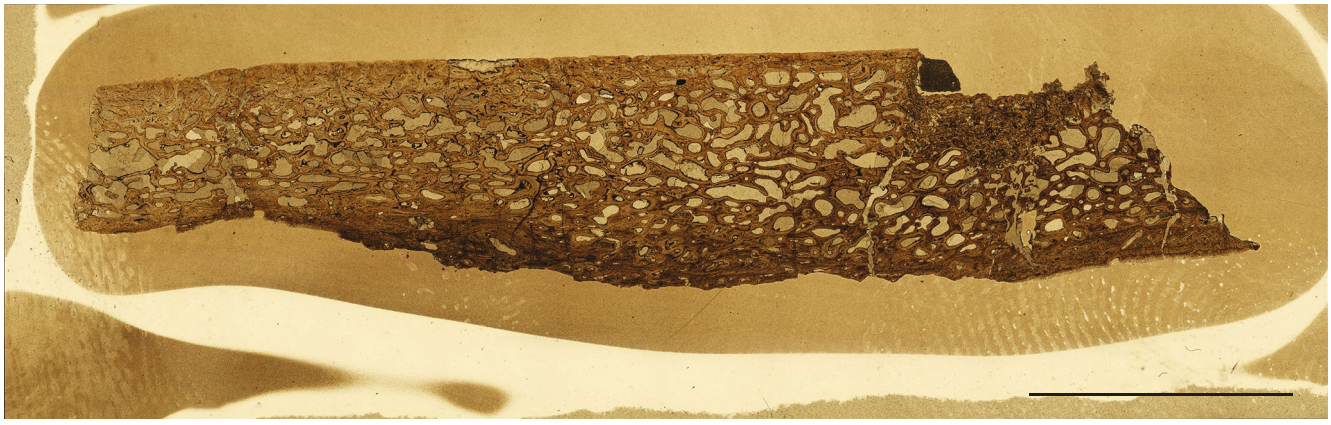

Appendix 65. — ZPAL V. 39/480. Costal sectioned longitudinally in polarized light. Scale bar: .1 cm

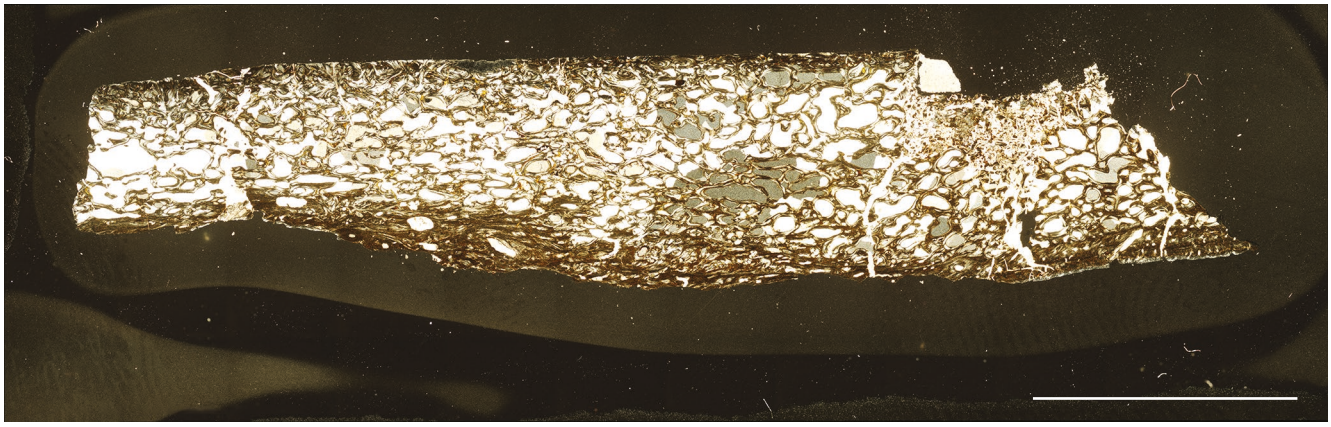

Appendix 66. — ZPAL V. 39/480. Costal sectioned transversely in normal light. Scale bar: 0.5 cm.

Appendix 67. — ZPAL V. 39/480. Costal sectioned transversely in polarized light. Scale bar: 0.5 cm.

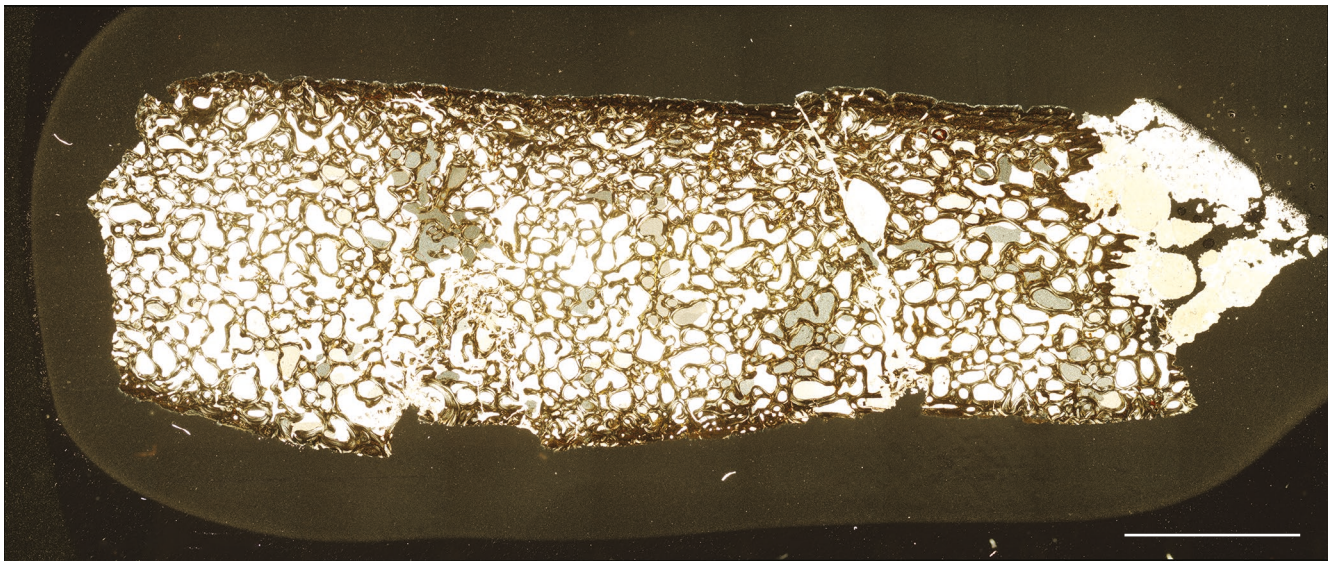

Appendix 68. — ZPAL V. 39/482. Anteroposterior section through the nuchal bone in normal light Scale bar: 0.1 cm.

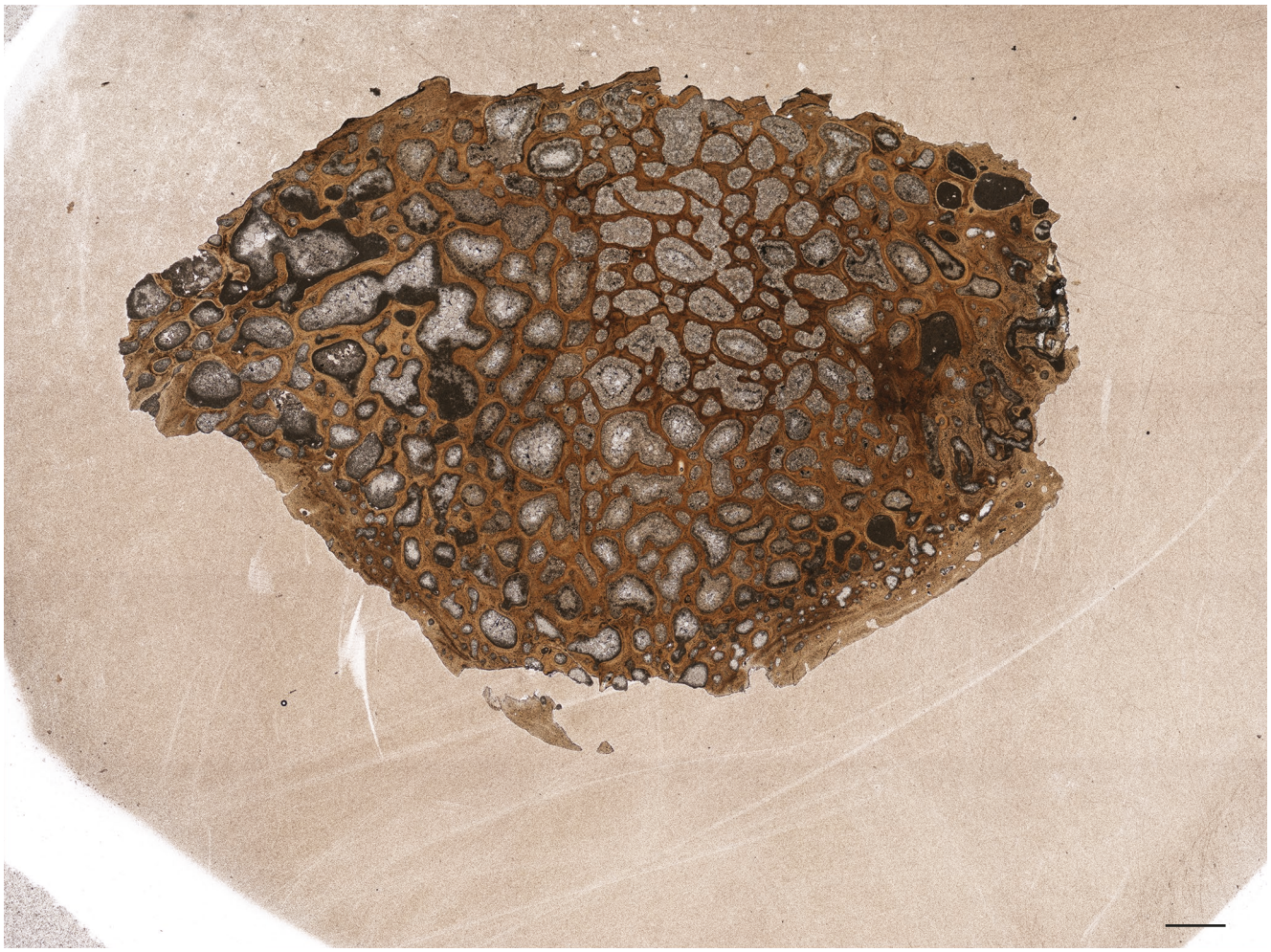

Appendix 69. — ZPAL V. 39/482. Nuchal region of the carapace, sectioned longitudinally through dermal ossifications (peripheral and supernumerary osteoderms) in normal light. Scale bar: 5 mm.